PROJECT ID: CE/…… -……/……

"INVESTIGATION OF FACTORS INFLUENCING THE SLOPE FAILURE ON ROAD: CASE STUDY "HUYE – NYAMAGABE ROAD"

DISSERTATION

Submitted by

NIYIGENA Eric (REG.NO: 221028015)

Under the Guidance of

Dr Mathieu NTAKIYEMUNGU

Submitted in partial fulfillment of the requirements for the award of

MASTER OF SCIENCE DEGREE

IN

HIGHWAY ENGINEERING AND MANAGEMENT

July 2025

COLLEGE OF SCIENCE AND TECHNOLOGY

SCHOOL OF ENGINEERING

P.O. Box: 3900 Kigali, Rwanda.

DEPARTMENT OF CIVIL ENVIRONMENTAL AND GEOMATICS ENGINEERING (CEGE)

DECLARATION

I, NIYIGENA Eric, with Reg. No 221028015 from University of Rwanda College of Science and Technology, School of Engineering; Department of Civil, Environmental and Geomatics Engineering, following studies of Master of Science in Highway Engineering and Management Programme, hereby declare that this work is of my original and has never been submitted for any academic award in any other University or Institution or anyone else where he/she had the same purpose.

Students Names: NIYIGENA Eric

Ref Number: 221028015

Signature:

Date: ……

CERTIFICATION

This research Thesis has been submitted with approval from the University supervisor (Main supervisor).

Main Supervisor Names: **Dr Mathieu NTAKIYEMUNGU**
Department of Civil, Environmental and Geomatics Engineering
University of Rwanda College of science and Technology

P.O. BOX 3900, KIGALI

Signature:.....

Date:.....

ACKNOWLEDGMENT

We thank **Dr. Mathieu NTAKIYEMUNGU** for the support and advices he kindly provided for the accomplishment of this work.

I would like also to thanks a lot my family: my wife, father, mother, brothers and sisters who supported me during my master studies through supports, encouraging me and giving me ideas.

I would like to thanks also RP-HUYE College and all the Lecturers who have taught us during this course.

ABSTRACT

This study examines the geotechnical factors contributing to slope instability along the Huye–Nyamagabe road in southern Rwanda. Comprehensive field investigations and laboratory tests were carried out to characterize the soil properties, while numerical simulations using GTS NX were employed to analyze slope behavior under seismic loading and stabilization measures using geogrid reinforcement and bench terrace in progressive steps. Slope stability was assessed using both the Bishop Method and the Strength Reduction Method (SRM), which revealed that most multi-layered and artificially cut slopes exhibited a Factor of Safety (FoS) below 1.35, indicating inherent instability. This instability is further exacerbated by the steep slope inclinations observed along the corridor

The seismic slope stability assessment involved both time history analysis and permanent deformation evaluation across varying Peak Ground Acceleration (PGA) levels. The findings indicated a progressive increase in displacement with higher seismic intensity: 0.030 m at 0.10g, 0.0595 m at 0.16g, and 0.066 m at 0.20g. Under static conditions, the slope demonstrated marginal stability with a low Factor of Safety (FoS) of 1.06. the road embankment fill material, which initially had a safety factor of 1.16, improved to 2.2 after reinforcement with geogrid.

Rainfall and seismic loading significantly affect slope stability. Rainfall infiltration raises pore-water pressure, reducing the factor of safety from 1.504 to 1.068 at 45 mm/hr (Partha Pratim Boruah V. R., 2025). Vegetation, such as vetiver grass, improves stability by reducing displacement by about 36%. Seismic vibrations also generate excess shear stresses and pore pressures, triggering landslides (Partha Pratim Boruah J. T., 2024). Hence, integrating rainfall and seismic effects is vital for accurate slope stability assessment

The study highlights the substantial impact of seismic activity on slope failure, emphasizing the need for mitigation measures that address both soil strength and earthquake-induced stresses. These insights will inform future slope stabilization and road safety enhancements in Rwanda's hilly regions.

Keywords: Slope stability, GTS Nx software, direct shear test, property of soil, bearing capacity of soil, seismic and permanent deformation.

LIST OF SYMBOLS AND ACRONYMS

FoS: Factor of Safety

PGA: Peak Ground Acceleration

GTS NX: Geo-Technical Software by MIDAS IT for Finite Element Analysis

DCP: Dynamic Cone Penetration

CBR: California Bearing Ratio

MC: Moisture Content

LL: Liquid Limit

PL: Plastic Limit

PI: Plasticity Index

GWT: Ground Water Table

SSR: Shear Strength Reduction

DEM: Digital Elevation Model

UCS: Unconfined Compressive Strength

kN/m^3: Kilonewton per cubic meter (unit of soil density)

kPa: Kilopascal (unit of pressure or stress)

τ: Shear Stress

σ: Normal Stress

φ: Friction Angle

c: Cohesion

Δ: Displacement

List of tables

LIST OF FIGURES

TABLE OF CONTENTS.

CHAP I: GENERAL INTRODUCTION.

1.1 BACKGROUND OF STUDY.

Slope failures threaten infrastructure, especially in areas with complex geology, heavy rainfall, or seismic activity, In Rwanda's Southern Province, the Huye–Nyamagabe road has faced repeated slope instabilities, These failures have disrupted transport, damaged property, and posed safety risks, This study investigates the geotechnical causes of slope failure along this corridor.

It uses field data, lab testing, and numerical modeling with MIDAS GTS NX, The goal is to assess soil properties, simulate failure mechanisms, and analyze seismic and rainfall effects.

Rwanda is a hilly, densely populated country covering an area of 26,338 km^2. The government is divided into three agro-ecological zones (AEZs) based on topography, elevation, and climate: Highlands, Midlands, and Lowlands, occupying 17%, 32%, and 38% of the territory, respectively. Escarpments, marshes, islands, and lakes constitute the remaining 13% of the country. The soils in Rwanda are generated by physicochemical weathering of basic schistose, quartzite, gneiss, granite, and volcanic rocks, leading to a varied biophysical environment across short distances due to the complexity of topography and parent materials (REMA, 2018).

The heavy rainfall in 2022 and 2023 resulted in significant damage, including the destruction of 20 national roads,57 district road sections, and 48 bridges, as well as the loss of lives, destruction of houses, damage to crops, and infrastructure, such as classrooms, health facilities, churches, administrative buildings, transmission lines, and factories. The impact was widespread, affecting various districts and highlighting the vulnerability of the region to such weather events (MININFRA, 2018)

Rwanda has 25 national Road Huye-Nyamagabe Road is among them identified NR 10 (HUYE-NYAMAGABE-KITABI-BUHINGA) on the list of road classifications from RTDA (Rwanda Transportation Development Agency), a national road is an international road that connects Rwanda with neighboring countries; a road that connects Districts or that connects a District with the City of Kigali, Road that provides access to an area of touristic significance and to other facilities of national or international significance from **LAW N° 042/2023 OF 02/08/2023 GOVERNING LAND AND WATERWAYS TRANSPORT**.

Rwanda is a landlocked country; road transport is the most commonly used means of transport. The road transport network of any country plays an important role in its economy, and the physical condition of its civil engineering infrastructure is critical. Highways and rural roads would damage or deteriorate without adequate and appropriate maintenance of cut slope and Embankments, resulting in higher vehicle running costs, increase the number of accidents, affect transport service efficiency and reduce life span of the road.

An exposed ground surface that stands at an angle with the horizontal is called an unstrained slope. The slope can be natural or manmade, if the ground surface is not horizontal, a component of gravity will tend to move the soil downward if the component of gravity is large enough, slope failure can occur. The driving force overcomes the resistance from the shear strength of the soil along the rupture surface. The slope failure can cause enormous damage to property and human lives, in many cases civil engineers are expected to make calculations to check the safety of natural slopes, slop of excavation, and compacted embankments this check involves determining and comparing the shear stresses developed along the most likely rupture surface with the shear strength of the soil this process is called slope stability analysis the most likely to slide is the one which having the minimum safety factor (ongcheezen, 2005)

For the assessment of slope stability, it is important to characterize all the different types of uncertainties related to the geotechnical design properties and calculation models in which the properties are used and consider the design (LARSSON, 2018).

1.2 PROBLEM STATEMENT

Huye-Nyamagabe road as a national road of 53.3 km plays great importance in transportation to facilitate the movement of people, goods, and services from Huye to Nyamagabe in economic Growth the road networks of Huye to Nyamagabe contribute to economic growth by enhancing trade and commerce. Improved accessibility attracts investments, stimulates employment opportunities, and supports the overall economic development of a region or country.

Slope failure was observed on the **Huye-Nyamagabe city road** of 26 km after heavy rain The figure shows the failure of the stone pitch on the slope at Nkungu near Nyamagabe city where as Figure 1-1 and 1-2 photo shows the failure occurs on the slope at Karambi cell, Kigoma sector.

Figure 1- 1 The Failure of Road Huye-Nyamagabe at Nkungu near Nyamagabe Town

Figure 1- 2 The failure of road Huy heavy rains in Karambi cell, Kigoma sector in Huye district(NKURUNZIZA, 2024).

Figure 1- 3 The Failure of a road in Rwanda western/Province Rutsiro District

(Editorial, 2020)

1.3 OBJECTIF OF THE PROJECT.

1.3.1 Main Objectives of Project

The main objectives of this research are to develop geotechnical parameters and investigate factors influencing slope failure on the road: "**HUYE – NYAMAGABE ROAD"** by using numerical modeling techniques.

1.3.2 Specific Objectives:

- To review and investigate the current practice for protecting cut slope and fills slope suitable construction techniques at Huye-Nyamagabe road
- To Evaluate the mechanical characteristic of soil
- To evaluate slope stability and permanent deformation using MIDAS GTS NX software
- To propose the improvement for the construction technique for slope protection by considering the climate effect
- To propose optimized construction techniques and slope protection measures considering the impacts of climate change

1.3 RESEARCH QUESTIONS

In this study, the following questions will be answered:

1. What are the geotechnical properties of soils and rocks present along the slope section?

2. How do seismic forces and rainfall infiltration influence slope stability in this region?
3. What is the failure mechanism observed in the slope under static and dynamic conditions?
4. What are the suitable remedial measures to mitigate future slope failures?

1.4 SCOPE AND LIMITATIONS

This study focuses on a specific slope failure section along the Huye–Nyamagabe road corridor, where three boreholes were investigated. Laboratory tests were limited to samples collected from the site, and GTS NX modeling was based on assumed conditions in the absence of full rainfall and groundwater data. The permanent deformation and seismic analyses are focused on 2D slope cross-sections.

CHAP II: LITERATURE REVIEW

2.1 INTRODUCTION

This chapter presents a critical review of literature relevant to slope stability analysis, geotechnical characterization techniques, and advanced numerical modeling approaches applicable to hilly terrains. The discussion focuses particularly on challenges encountered in the Southern Province of Rwanda, such as rainfall-induced and earthquake-induced failures, while highlighting the practical role of MIDAS GTS NX and field methods like Dynamic Cone Penetration (DCP) testing in quantifying slope vulnerability. The chapter also provides insight into the interpretation of geotechnical data for use in FEM-based modeling frameworks.

2.2 SLOPE FAILURE MECHANISMS

Slope failures occur when the driving forces acting on soil or rock masses exceed the resisting forces, leading to downward movement. Types of slope failure include rotational slips, translational slides, debris flows, and wedge failures.

2.2.1 Major Factors Causing slope failures

2.2.1.1 High Slope Angle (Steep Inclination)

(Shiferaw, 2021)The analysis model was conducted by simultaneously decreasing the slope height and slope angle while keeping the soil parameters constant. The results indicated that a reduction in slope angle leads to an almost linear increase in the factor of safety, whereas a reduction in slope height increases the factor of safety at a parabolic rate. The influence of slope height reduction on the factor of safety was more significant for clay soils, while the reduction in slope angle had a greater effect on the factor of safety in sandy soils. However, in this particular analysis, only one type of soil sandy clay was considered. The calculated factor of safety values for various slope heights are presented in Table 2-1.

Table 2- 1 Slope Angle, Height, and Factor of Safety Analysis

Slope h_t (m)	**H**	**V/H (tan α)**	**FoS**
12	20.0	0.6	1.151

12	25.0	0.48	1.3855
12	30.0	0.4	1.6028
12	35.0	0.3429	1.8047
9	15.0	0.6	1.2546
9	18.75	0.48	1.5019
9	22.5	0.4	1.7233
9	26.25	0.3429	1.9299
6	10.0	0.6	1.4433
6	12.5	0.48	1.713
6	15.0	0.4	1.9315
6	17.5	0.3429	2.1485
3	5.0	0.6	1.9494
3	6.25	0.48	2.2387
3	7.5	0.4	2.4882
3	8.75	0.3429	2.7344

(Partha Pratim Boruah J. T., 2024) According to rainfall-induced landslides are among the most frequent geohazards globally, with infiltration rapidly reducing matric suction and soil shear strength. The authors note that intense or prolonged rainfall saturates the slope, increases pore-water pressure, and significantly lowers the factor of safety. Vegetation, especially vetiver grass with deep root systems, is found to enhance slope stability by slowing infiltration and reinforcing soil. Studies reviewed in the paper show that rainfall-triggered failures typically initiate at the slope toe and progress upward. Additionally, numerical and experimental research confirms that rainfall intensity, duration, and slope angle are critical factors influencing deformation behavior. Therefore, understanding the interaction between rainfall characteristics and phreatic surface movement is vital in assessing rainfall-induced slope failure mechanisms.

(Partha Pratim Boruah V. R., 2025) demonstrated that rainfall significantly reduces slope stability through both infiltration and pore-water pressure buildup. Their numerical simulation revealed that the factor of safety (FoS) dropped from 1.504 to 1.068 as rainfall intensity increased from 0 mm/hr to 45 mm/hr. Prolonged rainfall also caused the phreatic line to rise substantially, reaching nearly halfway up the slope after 24 hours of infiltration. Moreover, the critical slip surface was shown to migrate upward with increased rainfall duration. Vegetation played a stabilizing role; for example, slopes reinforced with vetiver grass exhibited

approximately 36% less horizontal displacement compared to bare slopes under the same rainfall conditions. In addition, the maximum horizontal displacement rose from 0.004 m to 0.014 m under 12-hour rainfall as intensity increased. These findings confirm that rainfall intensity, duration, and vegetation cover are critical in influencing slope deformation behavior.

2.2.1.2 Earthquake or vibration effects.

(Partha Pratim Boruah J. T., 2024) highlighted that seismic loading plays a significant role in slope instability, especially in earthquake-prone regions. Earthquake shaking increases shear stresses and generates excess pore-water pressure, leading to soil liquefaction and brittle failure. The review explains how seismic waves cause sudden deformation in soil masses, particularly in slopes with saturated or weak materials. Case studies from recent earthquakes (e.g., Jiuzhaigou, Wenchuan) demonstrate widespread landslides triggered by ground shaking. The authors emphasize that cracks and fissures created during earthquakes often facilitate subsequent rainfall infiltration, compounding the slope's vulnerability. Finite element and pseudo-static analyses reveal that displacement is highly dependent on slope geometry, soil type, and seismic acceleration. The paper recommends integrating seismic behavior with deformation analysis for more accurate stability predictions under earthquake conditions.

The study by (Partha Pratim Boruah V. R., 2025) also highlighted the destabilizing effect of seismic loading on slopes, especially when combined with weak soil conditions. Under a seismic acceleration of 0.2g, the factor of safety was observed to decrease from 1.40 to 1.06, indicating a high risk of failure. As peak ground acceleration (PGA) increased, slope displacements also rose, with maximum displacement reaching 0.038 m under a 0.3g load. The critical acceleration threshold was identified at approximately 0.16g, below which the slope remained stable. Finite element analysis confirmed that slope displacement increased quadratically with PGA. Furthermore, when rainfall was combined with seismic loading, the resulting slope displacement was more than three times higher than that of dry static conditions. This combined effect led to a full slope collapse in the simulation, as shown in Figure 9 of the study. These results underscore the importance of multi-hazard analysis when assessing slope stability in seismically active and high-rainfall regions.

2.3 SLOPE STABILITY ASSESSMENT METHODS

2.3.1 Slope Stability Analysis Limits Equilibrium

Limit Equilibrium Methods: These methods assess the stability of a slope by comparing the forces driving potential slope failure (e.g. gravity, water pressure) to the forces resisting failure (e.g. soil strength). Common limit equilibrium methods include:

2.3.1.1 Bishop's Method

(Engineers®, 2003)The Simplified Bishop Method, developed by Bishop in 1955, is based on the following key assumptions:

1. The interslice forces acting on the slice are assumed to be horizontal.
2. A circular slip surface is assumed for the slope.
3. The forces are summed in the vertical direction to establish the equilibrium equation.
4. The Mohr-Coulomb equation and the definition of the safety factor are then used to determine the forces acting on the base of each slice.
5. Finally, the moments are summed up around the center of the circular slip surface to obtain the expression of the factor of safety.

$$F_n = \frac{\Sigma\left[\frac{ć\,\Delta x+(W+P\,Cos\;\cos\beta-u\,\Delta X\sec\alpha)\tan\emptyset'}{m_\alpha}\right]}{\Sigma W\sin\alpha-\frac{\Sigma M_p}{R}} \quad \ldots\ldots\ldots\ldots\ldots\ldots 2.1$$

up around the center of the circular slip surface to obtain the expression of

Where Δx is the width of the slice, and mα is defined by the following equation

$$m_\alpha = Cos\,\alpha + \frac{Sin\alpha\;\tan\emptyset'}{F} \quad \ldots\ldots\ldots\ldots\ldots\ldots 2.2$$

β: inclination from horizontal of the top of the slice (degrees)

Ć: cohesion intercept for Mohr-Coulomb diagram plotted in terms of total effective stress, σ' (F/L^2)

M_P = moment produced by the force P about the center of the circle (FL)

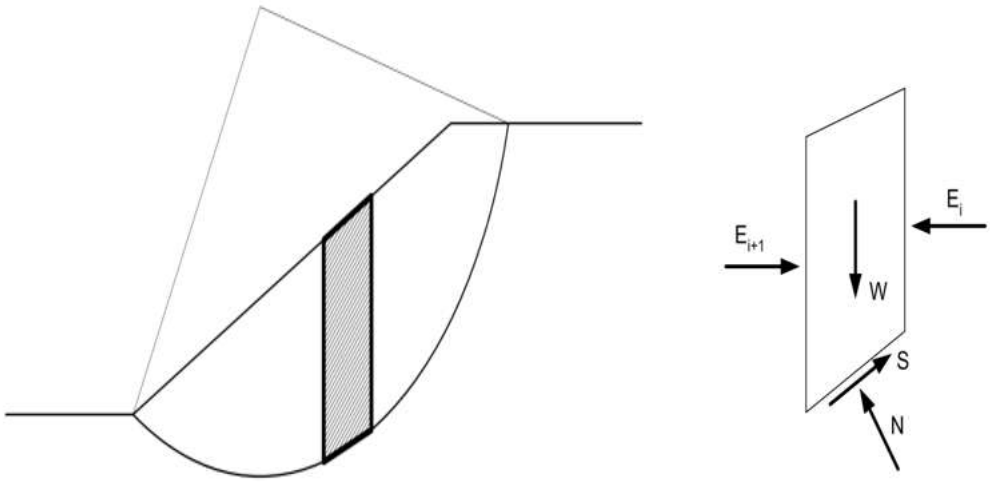

Figure 2- 1 Slope and typical slice types

2.3.1.2 Ordinary Method of Slices

The method of slices for slope stability analysis can be explained using Figure 2.2 In this figure, AC represents the trial failure surface, and the soil above this surface is divided into several vertical slices. The width of each slice does not have to be the same.

Considering a unit length perpendicular to the cross-section, the forces acting on a typical (nth) slice are shown in Figure 2.2. The forces include:

Wn: The weight of the slice.

Nr and **Tr:** The normal and tangential components of the reaction force R, respectively.

Pn and Pn+1: The normal forces acting on the sides of the slice.

Tn and Tn+1: The shearing forces acting on the sides of the slice.

For simplicity, it is assumed that the pore water pressure is zero.

The forces Pn, Pn+1, Tn, and Tn+1 are difficult to determine. However, an approximate assumption can be made that the resultants of Pn and Tn are equal in magnitude to the resultants of Pn+1 and Tn+1, and that their lines of action coincide. This assumption allows for a simplified analysis of the forces acting on the slice.

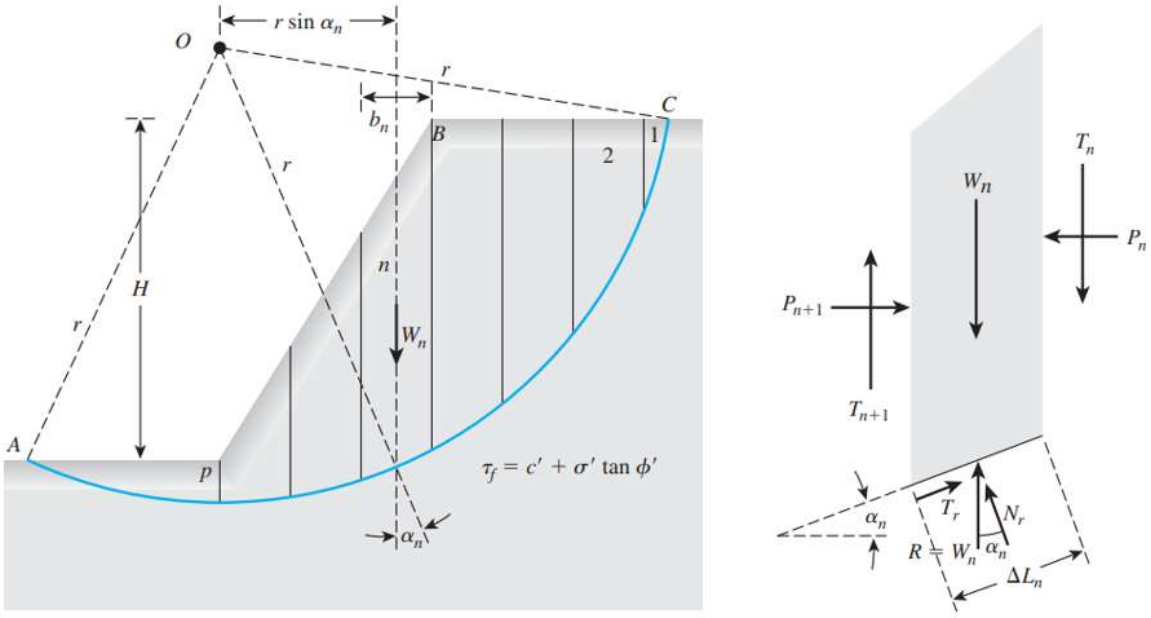

Figure 2- 2 Stability analysis by the ordinary method of slices: (a) trial failure surface; (b) forces acting on nth slice

(DAS, 2010)

For equilibrium consideration,

$$N_r = W_n \operatorname{Cos} \alpha_n \quad \ldots 2.3$$

The resisting shear force can be expressed as:

$$T_r = \tau_d(\Delta L_n) = + \frac{\tau_{f(\Delta L_n)}}{F_S} = \frac{1}{F_S}[\acute{c} + \sigma' \tan \emptyset'] \Delta L_n \ldots\ldots 2.4$$

$$\frac{N_r}{\Delta L_n} = \frac{W_n \operatorname{Cos} \alpha_n}{\Delta L_n} \ldots\ldots\ldots 1.5$$

For equilibrium of the trial wedge ABC, the moment of the driving force about O equals the moment of the resisting force about O, or

$$\sum_{n=1}^{n=p} W_n \, r \operatorname{Sin} \alpha_n = \sum_{n=1}^{n=p} \frac{1}{F_S} \left(\acute{c} + \frac{W_n \operatorname{Cos} \alpha_n}{\Delta L_n} \tan \emptyset'\right)(\Delta L_n)(r) \ldots\ldots\ldots\ldots 2.6$$

$$F_S = \frac{\sum_{n=1}^{n=p} (\acute{c} \Delta L_n + W_n \operatorname{Cos} \alpha_n \tan \emptyset r)}{\sum_{n=1}^{n=p} W_n \operatorname{Sin} \alpha_n} \ldots\ldots\ldots\ldots\ldots 2.7$$

2.3.1.3 Slope Stability Analysis Finite Element Method

(LANE, 1999)In the **soil model** including the dilation angle ø. The dilation angle affects the volume change of the soil during yielding and can vary from negative (initial volume decrease) to positive (dilation) to zero (constant volume).

Using an associated flow rule (where ø = ϕ) has some theoretical advantages, but tends to over-predict dilation compared to observed behavior, leading to overly conservative failure load predictions.

For slope stability analysis, the choice of dilation angle is less critical. A compromise value of ø = 0 (non-associated flow rule with zero volume change) is used in this study, as it allows the model to provide reliable factors of safety and reasonable predictions of failure surface location and shape.

The other key soil parameters are the effective cohesion c' and friction angle ϕ', which are modeled using the Mohr-Coulomb failure criterion, a widely used approach for representing soil strength.

$$\mathbf{F = \frac{\sigma'_1+\sigma'_3}{2}\ Sin\ \emptyset' - \frac{\sigma'_1-\sigma'_3}{2} - c'cos\emptyset'} \ \mathbf{.....2.8}$$

where σ'_1 and σ'_3 are the major and minor principal effective stresses. The failure function F can be interpreted as follows

F<0 stresses inside failure envelope (elastic)

F=0 stresses on failure envelope (yielding)

F > 0 stresses outside failure envelope (yielding and must be redistributed)

The elastic parameters E' and ὐ refer to Young's modulus and Poisson's ratio of the soil. If a value of Poisson's ratio is assumed (typical drained values lie in the range 0,2 < ὐ < 0,3), the value of Young's modulus can be related to the compressibility of the soil as measured in a one-dimensional oedometer (e.g. Lambe & Whitman, 1969):

$$E = \frac{(1+ὐ)(1-2ὐ)}{m_v(1-ὐ)} \text{.....2.9}$$

where m_v is the coefficient of volume compressibility. Although the actual values given to the elastic parameters have a profound influence on the computed deformations before failure, they have little influence on the predicted factor of safety in slope stability analysis

(C.VENKATRAMAIAH, 2006) A 'finite slope' is one with a defined base and top surface, with a limited height. The inclined faces of various earth structures, such as dams, embankments, and

excavations, are all examples of finite slopes. Analyzing the stability of these slopes is of critical importance in geotechnical engineering.

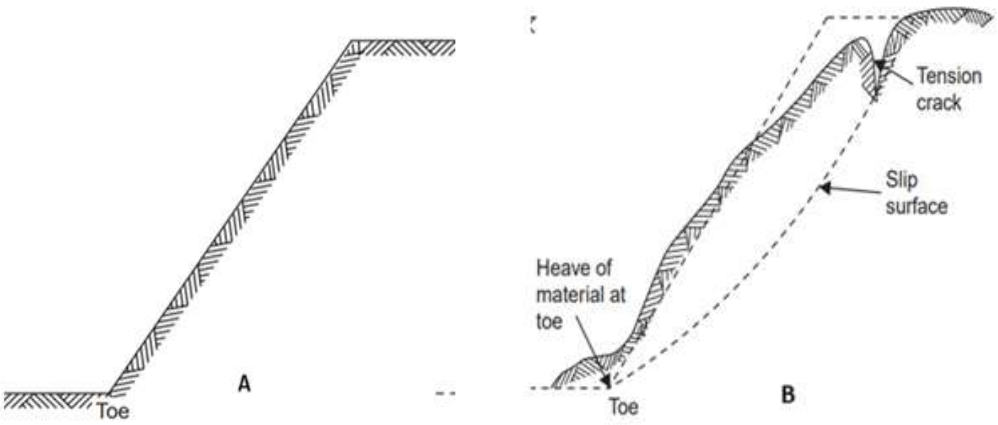

Figure 2- 3 a) Slope in cohesive material, (b) Slip surface of a slope in cohesive material

The following important methods will be considered:

(i) Total stress analysis for purely cohesive soil:

(ii) Total stress analysis for cohesive-frictional soil–the Swedish method of slices

(iii) Effective stress analysis for conditions of steady seepage, rapid drawdown, and immediately after construction

(iv) Effective stress analysis by Bishop's method

(v) Friction circle method

(vi) Taylor's method

2.3.2 Total Stress Analysis for a Purely Cohesive Soil

Analysis based on total stresses, also known as '$\varphi = 0$ analysis', assesses an embankment's stability immediately after its construction. This approach assumes that the soil has not had sufficient time to drain, and the shear strength parameters used are based on the undrained strength concerning total stresses. These undrained shear strength parameters can be obtained from either of two test methods:

a) Unconfined compression test

b) Undrained triaxial test without pore pressure measurements

Let AB be a trial slip surface (a circular arc of radius r) as shown in Fig. 2.4

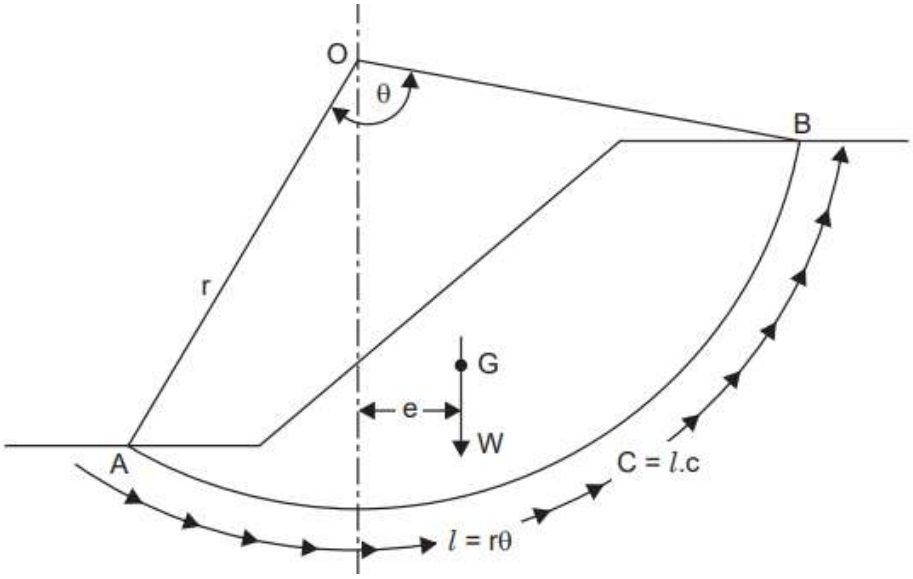

Figure 2- 4 Total stress analysis for a purely cohesive soil

Let W be the weight of the soil within the slip surface and G the position of its centre of gravity. The shearing strength of the soil is c, since φ = 0°.

Taking moments about 0, the center of rotation: **W.e. = c.l.r = c.r.θ.r = cr^2.θ**, for equilibrium (incipient failure).

Factor of safety, $F = \frac{\text{Restraining moment}}{\text{sliding moment}} = \frac{C.r^2.\theta}{W.e}\pi r^2$ 2.9

Here: W.e is dependent on the cohesion mobilized which will be less than the maximum soil cohesion. The exact position of G is not required and it is only necessary to ascertain the position of the line of action of **W**. This may be obtained by dividing the sector into a set of vertical slices and taking moments of area of these slices about any convenient vertical axis.

2.4 SLOPE STABILITY NUMERICAL METHOD OF MODELING

To study the influence of unit weight γ on FOS, the unit weight values have been chosen from 15 to 30 kN/m^3 while the internal friction angle and the cohesion have been selected from as 15˚ and 15 kPa, respectively Table 2.2 shows the effect of unity weight on FoS.

Table 2- 2 showing the effect of unity weight on the factor of safety

model number	unit weight (KN/m^3)	Internal friction angle (^{0})	cohesion (Kpa)	factor of safety
1	15	15	15	2.411
2	16	15	15	2.295
3	18	15	15	2.173
4	20	15	15	2.044
5	22	15	15	1.956
6	24	15	15	1.884
7	26	15	15	1.822
8	28	15	15	1.769
9	30	15	15	1.724

(SHLASH, 2020)

In Table 2.3 the values showed that as the soil's unit weight raise, FOS values decrease. The weight of the soil could explain this reduction as the unit weight increases, weight of soil as the main derivative force behind the failure, increases. Therefore, increasing unit weight causes the slope to become more unstable leading to a reduction in the FOS. Clayey and silty sands represent the value between 17-32 kN/m^3 of unite weight (Alexandria, September 1986).

The following Table 2.3 provides the minimum NYSDOT (New York State Department of Transportation) required Factors of Safety if a geotechnical designer has enough information to adequately define soil profile, slope geometry, soil shear strength, and pore water pressure in a slope stability model:

Table 2- 3 Minimum Required Factors of Safety – Slope Stability Analysis

GEOTECHNICAL ELEMENTS	FS	LRFD
Embankment side slope	1.25	-
Embankment end slope	1.30	-
Cut slope	1.50	-
Landslide remediation	1.25	-
Bridge or wall structure on slope*	1.50	0.65

Minor wall with minimal impact slope*	1.30	0.75

*Load factor of 1 (manual, 2014).

GTS NX (Geotechnical and Tunnel System) is a 3D finite element software developed for the analysis of soil and rock behavior under various geotechnical conditions. It supports complex modeling, including terrain generation, bedding plane insertion, and simulation of slope stability.

GTS NX (Geo-Technical System NX) is a cutting-edge finite element analysis (FEA) software created by MIDAS IT, purpose-built for use in geotechnical and underground engineering. It offers a robust and intuitive environment for modeling intricate soil-structure interactions and conducting analyses related to slope stability, foundation performance, tunnel construction, and seismic ground movement. (Griffiths, 1999).

GTS NX is extensively utilized by engineers and researchers because of its capability to simulate realistic subsurface conditions. It accurately represents complex behaviors such as nonlinear soil response, stratified ground layers, pore water pressure influence, and time-dependent processes like consolidation and creep. The software supports a variety of analysis types including static, dynamic, seepage, consolidation, and coupled analyses within a single, integrated platform (IT, 2023):

GTS NX offers a wide range of advanced functionalities, including:

- Support for both 2D and 3D finite element modeling
- Implementation of advanced soil behavior models such as Mohr-Coulomb, Hardening Soil, and Cam-Clay
- Automated tools for mesh creation and refinement
- Slope stability evaluation through the shear strength reduction (SSR) technique
- Capabilities for seismic and time history analysis
- Interface elements for simulating structural components like retaining walls, piles, and anchors

(Arjun Tirkey, 2023)conducted a finite element analysis using MIDAS GTS NX to assess slope stability under various conditions natural, rainfall, and reinforced across weathered soil, weathered rock, and bedrock. A 2D slope model (50m height, 55m width) was used. The study

revealed that Factor of Safety (FOS) decreased with increasing slope height and increased with higher friction angles and optimized soil nailing reinforcement Table 2.4 shows the shear parameters used in modeling and table 2.5 it shows the variation of nail diameter against factor of safety.

Table 2- 4 Soil Properties Used in MIDAS GTS NX

Parameter	Weathered Soil	Weathered Rock	Bed Rock
Cohesion (kPa)	8	40	98
Friction Angle (°)	20	25	37
γ (kN/m³)	19.8	23	24

Table 2- 5 Variation of FOS with Diameter of nail

Sl. No.	**Dia. of nail (m)**	**Initial stress**	**Rain SRM 1**	**SRM with nails**
1	0.012	1.00625	1.0082	1.0082
2	0.016	1.0125	1.0125	1.0289
3	0.02	1.01563	1.05664	1.09375
4	0.025	1.0125	1.0125	1.01563

(Arjun Tirkey, 2023).

2.5 FUNDAMENTALS OF PERMANENT DEFORMATION ANALYSIS

2.5.1 Pseudo static Analysis.

(J. Michael Duncan, 2014) The pseudo-static procedure is one of the earliest methods used to analyze the seismic stability of slopes. In this approach, the earthquake loading is represented by a static force, calculated as the soil weight multiplied by a seismic coefficient (k or k_s). This pseudo-static force is then used in a conventional limit equilibrium slope stability analysis. Most commercial slope stability software can accommodate the use of a seismic coefficient.

The seismic coefficient can be thought of as an acceleration, expressed as a fraction of the acceleration due to gravity (g), the earthquake produces that. However, this pseudostatic force acts in only one direction, whereas actual earthquake accelerations act for a short time and can change direction, sometimes even stabilizing the soil rather than destabilizing it. The term "pseudostatic" is somewhat misleading, as the approach is actually a static analysis that would be more accurately called "pseudodynamic." Nonetheless, the pseudostatic terminology is widely used in geotechnical literature.

The vertical components of the earthquake accelerations are typically neglected in the pseudostatic method, and the seismic coefficient usually represents a horizontal force. Incorporating the seismic coefficient and pseudostatic force into limit equilibrium slope stability analyses is relatively straightforward from a mechanics perspective, as the pseudostatic force is treated as a known force that is included in the various equilibrium equations.

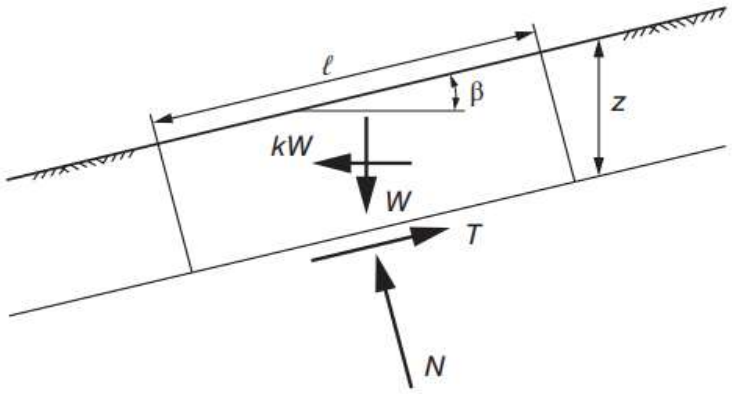

Figure 2- 5 Derivation of the equation for the factor of safety of an infinite slope with a seismic force (kW)—total stress analyses

Resolving forces perpendicular to the slip plane.

$$N = W\cos\beta - k\,W\sin\beta \ldots\ldots\ldots\ldots\ldots\ldots\ldots\ldots\ldots\ldots 2.10$$

Resolving forces parallel to slip plane

$$T = W\sin\beta - k\,W\cos\beta \ldots\ldots\ldots\ldots\ldots\ldots 2.11$$

Weight of sliding block

$$W = \gamma\ell z\cos\beta \ldots\ldots. 1.12$$

Substituting (3) in (1)

$$N = \gamma\ell z\cos^2\beta - k\gamma\ell z\cos\beta\sin\beta \ldots \ldots\ldots\ldots\ldots 2.13$$

$$T = \gamma\ell z\cos\beta\sin\beta - k\gamma\ell z\cos^2\beta \ldots \ldots\ldots\ldots\ldots 2.14$$

For the stresses on the slip plane:

$$\sigma = \frac{N}{\ell} = \gamma z \cos^2\beta - k\gamma z \cos\beta \sin\beta \ldots\ldots, \ldots\ldots\ldots 2.15$$

$$\tau = \gamma z \cos\beta \sin\beta + k\gamma z \cos^2\beta \ldots\ldots\ldots\ldots\ldots\ldots 2.16$$

Finally, for the factor of safety (total stresses)

$$F = \frac{S}{\tau} = \frac{C+\sigma \tan\emptyset}{\tau} = \frac{c+(\gamma z \cos^2\beta - k\gamma z \cos\beta \sin\beta)\tan\emptyset}{\gamma z \cos\beta \sin\beta + k\gamma z \cos^2\beta} \ldots\ldots\ldots\ldots\ldots\ldots\ldots 2.17$$

PSEUDOSTATIC SCREENING ANALYSES

Reference	Reference Acceleration, a_{ref}	Acceleration Multiplier, a/a_{ref}	Strength Reduction Factor	Minimum Factor of Safety	Tolerable Displacement
Seed (1979)	0.75g (M ≈ 6½)	0.133	0.85	1.15	Approx. 1 m
Seed (1979)	0.75g (M ≈ 8¼)	0.167	0.85	1.15	Approx. 1 m
Hynes-Griffin and Franklin (1984)	PGA_rock (M ≤ 8.3)	0.5	0.8	1.0	1 m
Bray et al. (1998)	PGA_rock	0.75	Recommend using conservative (e.g., residual) strengths	1.0	0.30 m for landfill covers; 0.15 m for landfill base sliding
Kavazanjian et al. (1997)	PGA_soil	0.17 if PGA accounts for amplification	0.8a	1.0	1 m
Kavazanjian et al. (1997)	PGA_soil	0.5 for free-field PGA determined	0.8a	1.0	1 m

NCHRP 12-70 (2008) FHWA (2011)	PGA_soil	0.2–0.5 (PGA includes site amplification effects)	0.8	1.0	5 cm or less
Bray and Travasarou (2009)	Spectral accel., Sa (5% damped at specified period)	Depends on slope height and displacement	1.0 Median or "best estimate"	Varies	Varies

Figure 2- 6 Suggested Methods for Performing Pseudo-Static Screening Analyses

2.5.2 Sliding Block Analysis/Newmark method

Newmark (1965) proposed a relatively simple deformation analysis based on a rigid sliding block model. In this approach, the displacement of a soil mass above a slip surface is modeled as a rigid block sliding on a plane. When the acceleration of the block exceeds a yield acceleration (ay), the block begins to slip along the plane. Any acceleration above the yield acceleration causes the block to slip and impart a relative velocity to the block. The block continues to move even after the acceleration falls below the yield acceleration until its relative velocity drops to zero. This stick-slip pattern of motion continues until the accelerations remain below the yield acceleration. To compute the displacements, the accelerations over the yield acceleration are integrated twice - first to obtain velocities, and then to obtain displacements. This can be done numerically, given an acceleration-time history and the yield acceleration. Upslope movements are typically neglected, with all displacements assumed to be in one direction.

The yield acceleration (ay) used in the sliding block analysis is typically determined from limit equilibrium slope stability analyses. This yield acceleration is often expressed as a seismic yield coefficient ($k_y = a_y/g$), which represents the seismic coefficient that would produce a factor of safety of unity in a pseudo-static slope stability analysis. The specific slip surface assumed in the limit equilibrium analysis determines both the seismic yield coefficient and the mass of soil used in the sliding block computations**.**

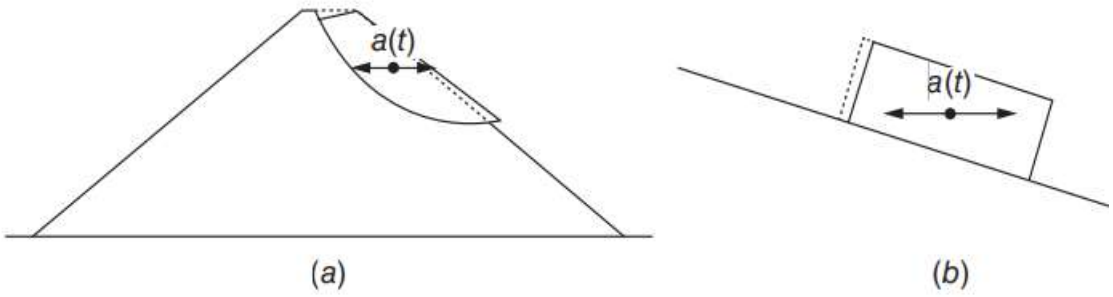

Figure 2- 7 Actual slope and (b) sliding block representation used to compute permanent soil displacements in a slope subjected to earthquake shaking

(B.NADI, 2014) It considers a simple sine motion acceleration time history, as shown in Fig. 2.7. The model assumes that permanent deformation begins when the earthquake-induced accelerations acting on a slide mass exceed the yield resistance on the slip surface, quantified by the seismic yield coefficient (ky) (refer to (1) in Fig. 2.7 a). At this point, the slide mass breaks away from the underlying slope and slides at a constant acceleration equal to ky (refer to (2) in Fig. 2.7 a). During this sliding, the velocity of the ground is greater than the velocity of the slide mass (Fig. 3b). Sliding continues until two conditions are met : (1) accelerations fall below ky and (2) the velocity of the slide mass and the underlying ground coincide (refer to (3) in Fig. 2.7b). The permanent displacement during each slip interval is determined by double-integrating the shaded regions of the acceleration time history, and the total permanent deformation is shown in the displacement plot in Fig. 2.8.

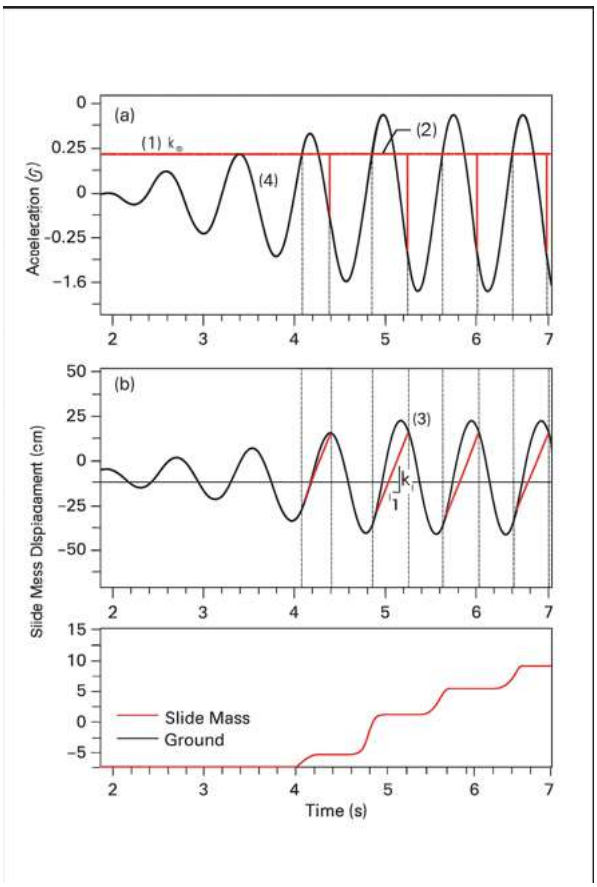

Figure 2- 8 Newmark's rigid -block procedure for calculating Earthquake-induced permanent deformation (simple sine motion).

2.6 PERMANENT DEFORMATION ANALYSIS

Deformation Caused by Seismic loading, rainfall on slope stability

(Boruah, 27 June 2024) The factor of safety (FOS) obtained by analyzing the combined effect of rainfall seepage and seismic shaking is 70% of the FOS obtained by analyzing rainfall seepage alone. This highlights the importance of considering the combined effect of rainfall seepage and seismic shaking for slope stability (C.- Y. Chen & Wu, 2019).

Studies using limit equilibrium method (LEM) and finite element method (FEM) have investigated the effects of dynamic loads, such as earthquakes and heavy rainfall, on slope behavior in Southwest China. The findings suggest that slope instability is ultimately caused by permanent structural damage due to earthquakes or ground motions, as well as secondary damage due to heavy rainfalls.

Researchers have developed numerical models using finite difference methods to estimate the dynamic response of reinforced flexible earth slopes affected by earthquakes and rainfall, including the pore pressure and tensile stress distributions in the reinforcement.

A formula has been developed to determine the sliding distance of mudflow-like landslides induced by earthquakes and rainfall, which can be used for prevention and control measures.

A study on a specific landslide along the Bâsca Rozilei River found that the safety factor was 1.17-1.32, with static displacements of 0.4 - 4 m and dynamic displacements up to 8-60 m. The groundwater effect was found to reduce the safety factor and increase the displacement.

Another study on the Zhoujiashan landslide in Tianshui, China, revealed that under low-to-moderate seismic conditions (0.1- 0.3 g), the slope deformed and had decreased safety, but did not suffer overall damage. However, under stronger seismic conditions (0.6 g), the slope liquefied, resulting in overall damage and deformation.

The effect of the coupling between earthquakes and rainfall on slope stability is much greater than the effect of either factor individually, and the slope toe is always the most unstable factor regardless of the coupling conditions.

(Boruah, 27 June 2024) studies have examined the response of unsaturated slopes to post-earthquake rainfall, the stability of mine waste dump slopes under rainfall conditions, the importance of vegetation type in slope stability, and the effectiveness of Geosynthetic Cementitious Composite Mats (GCCMs) in reinforcing soil slopes under seepage and rainfall conditions. Researchers have also investigated three-dimensional slope stability analysis, finding that the safety factor increases with decreasing slope height and angle, and that the 3-dimensional safety factor is generally 10-20% higher than the 2-dimensional safety factor for the same problem (S. Kumar et al., 2023).

CHAP III. METHODOLOGY

3.1 INTRODUCTION

This chapter outlines the methodology adopted to analyze slope stability and investigate contributing factors to slope failure along the Huye–Nyamagabe road. It includes descriptions of the study area, procedures for data collection and laboratory testing, and the modeling techniques employed using MIDAS GTS NX.

3.2 STUDY AREA DESCRIPTION

The study area 250 X 250 m located along the Huye–Nyamagabe road in the Southern Province of Rwanda. The terrain in this region is hilly and mountainous, characterized by steep slopes, high rainfall, and deeply weathered soil and rock formations. Several landslides have been reported along this corridor, especially during the rainy season, making it a critical area for geotechnical investigation.

3.3 DATA COLLECTION

The process of slope design starts with dividing the geotechnical model for the proposed slope into geotechnical domains with similar geological, structural and material property characteristics. For each domain, potential failure modes are assessed and designs at the respective scales (bench, inter-bench, overall) are based on the required acceptance levels (FOS) against instability.

3.3.1 Slope inclination determination

Slope inclination measurements were carried out on-site using a handheld clinometer. The instrument was carefully aligned parallel to the slope surface to determine the angle of inclination relative to the horizontal. Readings were taken by sighting along a straight reference object, such as a ranging rod or staff. At each measurement point, the observer positioned the clinometer at the base of the slope and aimed it toward the top edge. Multiple readings were collected along the slope profile to improve accuracy and account for terrain irregularities. The average inclination was calculated from these readings, revealing slope angles ranging between 33° and 42°. These measured values were subsequently used to construct the slope geometry in AutoCAD and imported into MIDAS GTS NX for numerical modeling and analysis.

3.3.2 Field sampling and testing.

In material characterization, various geotechnical tests were performed in accordance with the procedures outlined for each respective test. The process began with careful attention to the sampling method and sample size. Samples were collected directly from existing slope failure zones or by excavating trial pits along the affected ground. Soil samples were taken from each identifiable layer along the slope profile. The sample size varied depending on the test requirements, as specified in Table 3.1 for disturbed samples, while undisturbed samples were collected using cylindrical tubes with dimensions of 8 cm diameter by 30 cm height. Visual inspection was conducted to assess the physical condition of the materials, and detailed observations were made regarding the location and soil profile of the selected site, which is situated in the Southern Province along the Huye–Nyamagabe road in Rwanda. Laboratory tests were then conducted on the collected materials based on relevant standards, to obtain key parameters for geotechnical characterization and numerical modeling using slope stability software figure 3.1 show the method used to get undisturbed sample for laboratory tests while table 3.1 shows the amount of sample used for disturbed test analysis.

Table 3- 1 Disturbed sample quantities from the site

Test	**Minimum quantity(kg)**
CBR	40
Particle above 20 mm (coarse gravel and above)	10
Particle less 20 mm (medium gravel and below)	2
Particle less 6 mm (fine gravel and below)	0.5
Hydrometer test –particle size less than 2 mm (coarse sand and below)	0.25
Atterberg tests	0.5

(Look, 2007)

Figure 3- 1 Sampling an undisturbed sample slided portion of a road Huye-Nyamagabe road

Figure 3- 2 DCP Test performing on two difference area of slided area

3.3.2.1. Sieve Analysis Test (BS 1377 Part 2:1990)

The grain size distribution of the soil was determined using the wet sieving method to ensure proper separation of fine particles. This test provides important information on soil classification and grading, which is essential for geotechnical design and slope stability assessment. The percentage retained on each sieve was calculated. A grain size distribution curve was plotted to classify the soil and assess its grading, for data sheet and graphs of test pits check appendix2.

Equipment Used

Standard set of sieves (ranging from 75 mm to 75 µm)

- ✓ Mechanical sieve shaker check figure 3.3
- ✓ Oven (105 °C ± 5 °C)
- ✓ Weighing balance (accuracy ±0.01 g)
- ✓ Water container and wash bottle
- ✓ Brushes and trays

Figure 3- 3 Sieve shaker and sieve mesh used in grading analysis

Test Procedure

- ✓ A representative soil sample was soaked in water and washed through a 75 µm sieve to remove fine particles.
- ✓ The material retained on the sieve was oven-dried at 105 °C ± 5 °C until constant weight was achieved.
- ✓ The dried soil was placed on a stack of sieves with decreasing mesh sizes and shaken using a mechanical sieve shaker for uniform separation.
- ✓ The weight of soil retained on each sieve was measured, and the percentage retained and percentage passing were calculated.
- ✓ A grain size distribution curve was plotted to classify the soil and assess its grading characteristics.

3.3.2.2. Direct Shear Test (BS 1377 Part 7:1990)

Shear strength parameters were evaluated using the direct shear test on undisturbed sample. The sample was placed in a split shear box under a known normal stress. Horizontal force was applied until failure occurred along a predefined plane. The peak shear stress at failure was recorded. Shear strength was calculated using the formula 3.1, for the results and check appendix-3:

$$\tau = c + \sigma \times \tan(\varphi) \quad \ldots\ldots\ldots\ldots\ldots\ldots\ldots\ldots\ldots\ldots\ldots\ldots 3.1$$

where τ is shear strength, σ is normal stress, c is cohesion, and φ is angle of internal friction.

Tools and Equipment

- ✓ Direct Shear Apparatus: Main machine for applying horizontal shear and vertical normal loads check the figure 3.6 of equipment.
- ✓ Shear Box: Split box that holds the soil specimen and creates the predefined failure plane.
- ✓ Loading Frame: Applies vertical load (normal stress) through calibrated weights or a load cell.
- ✓ Proving Ring / Load Cell: Measures the applied shear force.

- ✓ Dial Gauges: Record horizontal displacement and vertical deformation during shearing.
- ✓ Weights: Used to apply specific normal stresses.
- ✓ Sample Trimming Tools: Cutters, spatulas, and straightedges to prepare specimens to size.
- ✓ Balance: Measures mass of soil samples for moisture content determination.
- ✓ Oven: Dries samples at 105 ± 5 °C to determine water content.
- ✓ Porous Stones & Filter Papers: Placed above and below the specimen to allow drainage and prevent soil loss.
- ✓ Calipers / Vernier Scale: Measures specimen dimensions accurately.
- ✓ Data Recording Sheets / Computer Interface: For logging applied loads, displacements, and failure readings.

A. Sample Preparation

- ✓ Collect soil from the test location and air-dry.
- ✓ Sieve soil to remove oversized particles (>2 mm for fine soils).
- ✓ Forn Remold the soil specimen to the desired moisture content and density, matching field conditions.
- ✓ For undisturbed sample the sampler was used to get the sample from sampling tools as per figure 3.4 and figure 3.5
- ✓ Prepare a square specimen of dimensions typically 60 mm of diameter × 20 mm of thickness (or per equipment specifications).
- ✓ Place the specimen in the shear box with a porous stone and filter paper at the top and bottom

Figure 3- 4 Putting the sample in the sampler for direct shear and unit weight determination

Figure 3- 5 after sample preparation and shear box apparatus

Figure 3- 6 direct shear testing equipment

3.3.2.3. California Bearing Ratio (CBR) Test (AASHTO T 193-99)

The CBR test was used to estimate the soil's bearing capacity for pavement and subgrade design. Compacted soil specimens were soaked (if required), and a plunger was penetrated into the sample at a constant rate. Load readings were recorded at 2.5 mm and 5.0 mm depths. The CBR was calculated using the formula 3.2:

$$CBR = \frac{P}{Ps} X\ 100 \ldots\ldots\ldots\ldots 3.2$$

where **P** is the measured load and $\mathbf{P_s}$ is the standard load at the same penetration.

3.3.2.4. Atterberg Limits Test (BS 1377 Part 2:1990)

This test was conducted to classify fine-grained soils based on their plasticity. The liquid limit (LL) was determined using the Casagrande apparatus, and the plastic limit (PL) by rolling soil threads. The plasticity index (PI) was calculated using the formula 3.3, application of formular you can check appendix 2:

$$PI = LL - PL \ldots\ldots\ldots\ldots\ldots 3.3$$

These parameters helped assess the soil's shrink-swell potential and workability.

Tools & Equipment

- ✓ Casagrande liquid limit apparatus check the figure 3.7 the used apparatus
- ✓ Grooving tool
- ✓ Glass plate
- ✓ Spatula
- ✓ Containers

- ✓ Balance
- ✓ Oven

Procedure

Liquid Limit:

- ✓ Place soil paste in Casagrande cup.
- ✓ Cut a groove in the center.
- ✓ Rotate the cup until the groove closes for 25 blows.
- ✓ Repeat for multiple water contents and plot flow curve.

Plastic Limit:

- ✓ Roll soil thread on a glass plate until it crumbles at 3 mm diameter.
- ✓ Record corresponding water content

Figure 3- 7 Casagrande apparatus to perform liquid limit (LL)

3.3.2.5. Moisture Content Test (BS 1377 Part 1:1990)

The water content of soil samples was determined to assess their natural moisture condition. Samples were oven-dried at 105°C for 24 hours. The moisture content (w) was calculated using formular 3.2b application and results obtained check appendix 4:

$W = (W_w / W_d) \times 100\ \%$.....3.3b.

where W_w is the weight of water lost and W_d is the dry weight. This test helped evaluate soil saturation and in-situ strength.

3.3.2.6. Dynamic Cone Penetration (DCP-CBR Equipment):

This test was used to estimate soil strength parameters for weathered and soft rock layers where laboratory results were unavailable was performed as per figure 3.2.

Estimation of Shear Strength from DCP Results

DCP testing provides penetration resistance data that can be empirically related to soil strength. From the measured DCP index (DCPI) or average penetration rate, denoted as DN (in mm/blow), California Bearing Ratio (CBR) was estimated using:
The following equations are used:

For DN > 2 mm/blow: (Kleyn, 1983)

$\mathrm{CBR} = 410\ \mathrm{DN}^{-1.27}$.....3.4

For DN ≤ 2 mm/blow:

$CBR = (66.66 \times DN^2) - (330 \times DN) + 563.33$ (Livneh, 1987)…….….3.5

For cohesive soils, undrained cohesion (Cu) was derived as:

Cu = 0.3 × CBR (Powell & Quarterman, 1988) ……..3.6

For frictional soils, the internal friction angle (φ) was approximated as:

φ = 27.1 + 0.3 × CBR (Livneh & Livneh, 1994)……3.7

These estimated parameters were input into the MIDAS GTS NX modeling environment to define soil behavior at various depths, application of formulars and obtained figure check appendix 1:.

3.3.3 Climate change effect on the road embankment

In order to simulate the effect of rainfall on slope stability, a uniformly distributed load representing rainwater pressure was applied on the slope surface in the MIDAS GTS NX

environment. Based on meteorological data obtained from Mateo-Rwanda for the Simbi station in Nyamagabe District, the maximum daily rainfall recorded was 29.7 mm. This rainfall depth was converted into an equivalent pressure using the hydrostatic formula:

$P = \gamma_w \times h = 9.81\ kN/m^3 \times 0.0297\ m = 0.291\ kN/m^2$ …….3.8

This pressure was applied vertically (in the Y-direction) as a Uniformly Distributed Load (UDL) on the top surface of the slope in the 2D model. The load was assigned under Load Set-1 with constant magnitude across the slope profile. The inclusion of this rainfall load reflects the influence of short-term heavy rainfall on slope behavior, particularly in inducing pore pressure increase and reducing effective stress in surface soils.

3.4 CONSTRUCTION OF MODEL

3.4.1 Contours generation in QGIS

Inclination Angle from DEM in QGIS to AutoCAD, the 2D contour lines were generated in QGIS using the Layer → Add Layer → Add Raster Layer function, based on the Digital Elevation Model (DEM) data of Rwanda. The contour interval was set to 10 meters. To extract the study area, the DEM was clipped using Raster → Extraction → Clip Raster by Mask Layer. These outputs effectively represent the terrain features and validate the model's ability to capture realistic slope behavior, while Figure 3.3 presents the generated contour lines for the selected area.

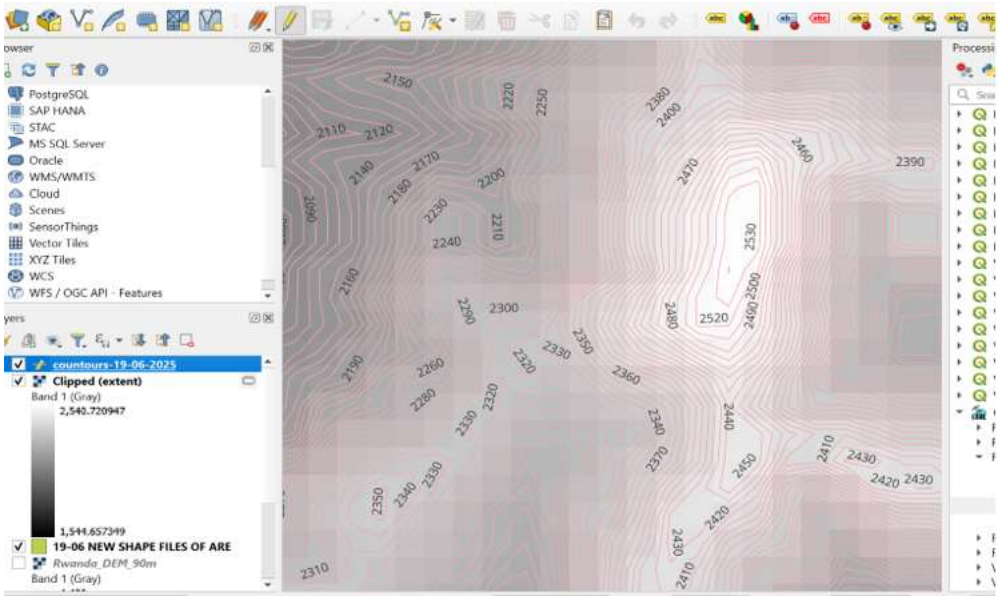

Figure 3- 8 Contours created with their elevations

3.4.2 Creation and importing of elevation data in form of grids

The elevation data was organized into a 50×50 grid and imported into MIDAS GTS NX using the "Make Face" function to generate the terrain surface, as illustrated in Figure 3.4. The material behavior in the model was simulated using the Mohr-Coulomb failure criterion, selected for its simplicity and suitability for representing common soil and rock behavior. As outlined in Table 3.2, this model relies on two primary parameters—cohesion (c) and internal friction angle (ϕ) both derived from site investigations. Table 3.3 provides the specific parameter values used and explains the rationale for choosing the Mohr-Coulomb model over more advanced constitutive models. The defined material properties were assigned to the model through the interface shown in Figure 3.5.

Table 3- 2 type of material uses to be used in the analysis in GTS Nx modeling

Type	**Description**
Mohr-Coulomb	Basic soil/rock model using c, φ, E, ν. Good for slope analysis.
Linear Elastic	For solid materials with no plastic deformation.
Hoek-Brown	Nonlinear model for intact and jointed rock.
Drucker-Prager	An alternative to Mohr-Coulomb, good for soft soils.

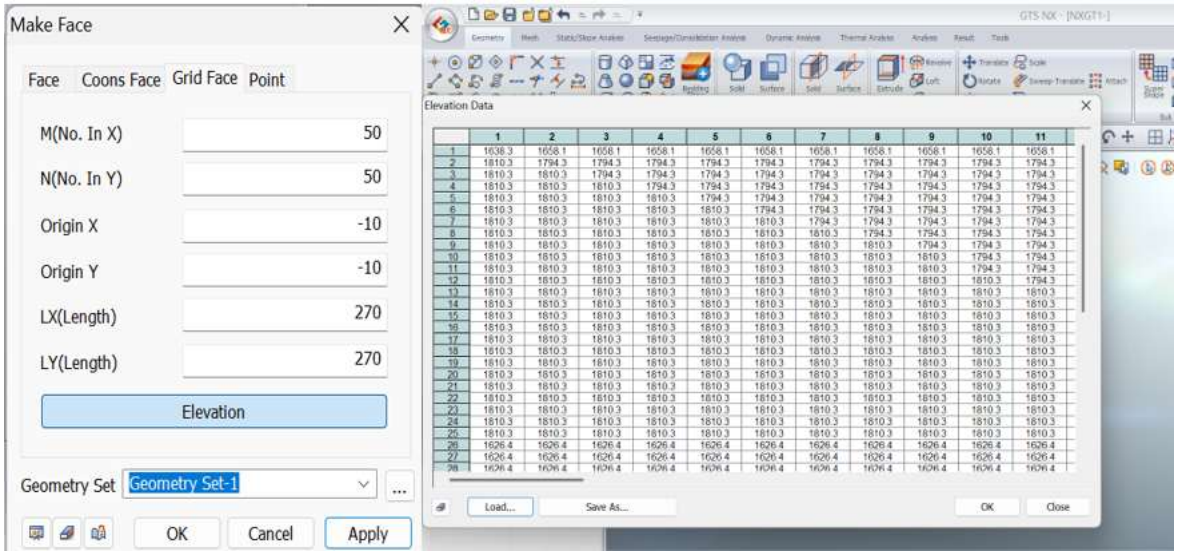

Figure 3- 9 The prepared excel grid in the excel sheet is imported in the GTS NX Software

Table 3- 3 the properties of the material inserted in model

No.	Name	Type	γ (Unit Weight)	c (Cohesion)	φ (Friction Angle)	E (Modulus)	ν (Poisson)
1	Weathered Soil	Mohr-Coulomb	16.48	17.6	26.6	30000	0.25
2	Soft Rock	Mohr-Coulomb	18	18.2	29.4	80000	0.30

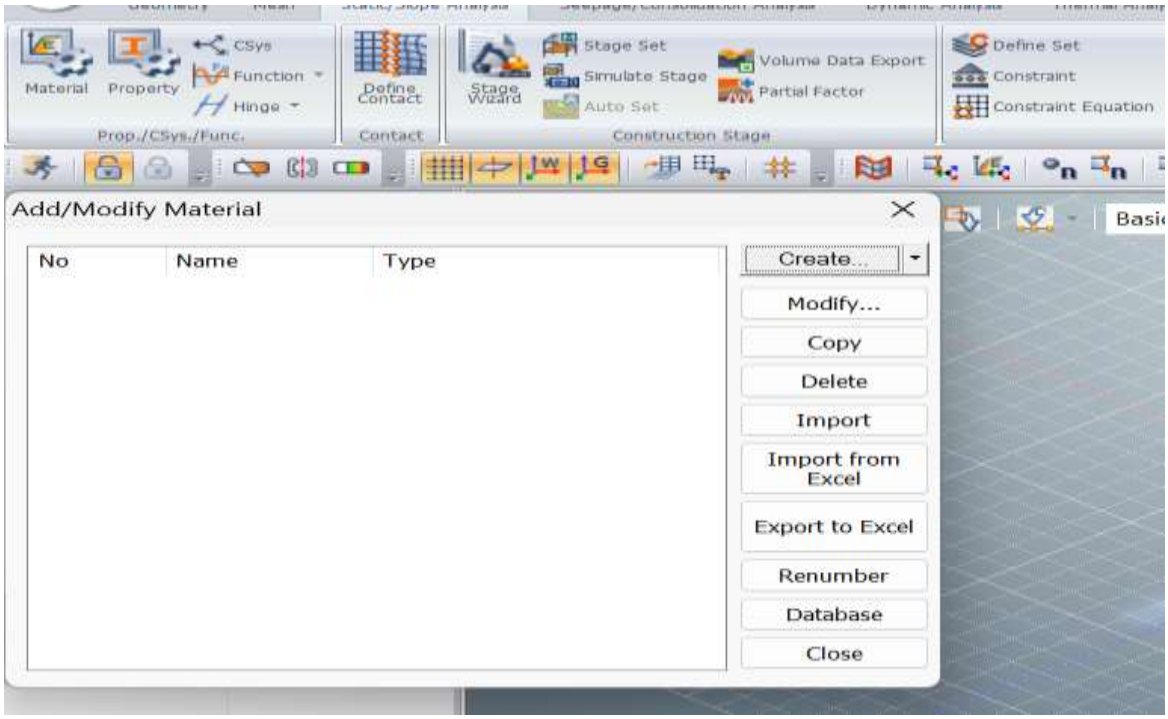

Figure 3- 10 The interface used for inserting the material

Two strata layers (weathered soil, soft rock) were interpolated based on borehole/test pits depths and converted into elevation grid files, these strata were then generated using the Terrain Geometry Maker tool and assembled into a 3D solid, The Mohr-Coulomb material model was selected for all layers, using parameters derived from laboratory test and DCP data. Created surface from the elevation and two layers created as shown in figure 3.6, Geometry > Divide > Solid.

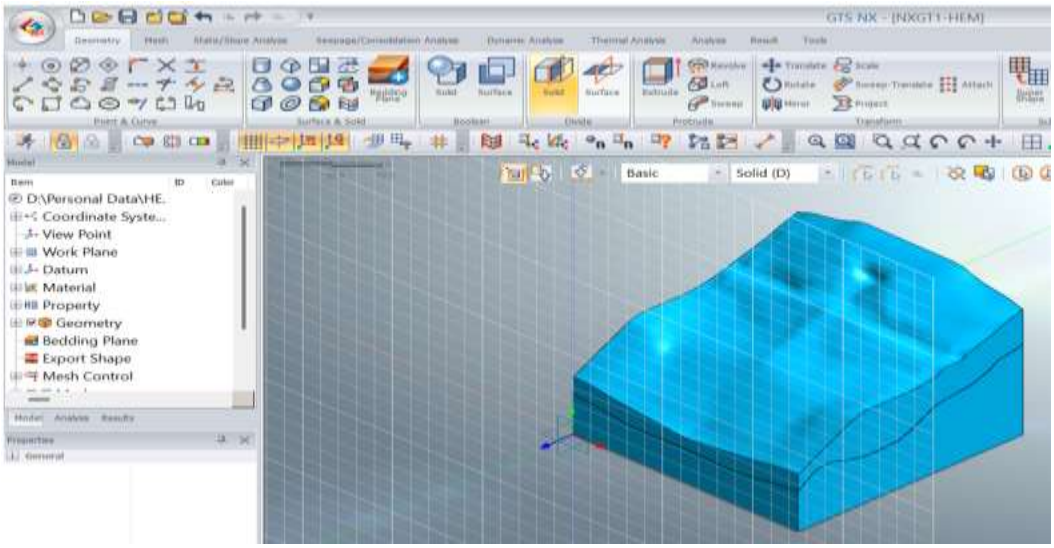

Figure 3- 11 Two layers generated by using the 50X50 grid

3.4.3 Description of Strength Reduction Method (SRM)

In this study, the Strength Reduction Method (SRM) was applied in MIDAS GTS NX to evaluate the global stability of the slope, as illustrated in Figure 3.7. SRM is a widely used numerical technique in finite element analysis that allows the failure mechanism to emerge naturally from the stress–strain behavior of the soil, rather than relying on predefined failure surfaces, as in traditional limit equilibrium methods. In GTS NX, SRM is implemented using the Shear Strength Reduction (SSR) technique, which progressively reduces the shear strength parameters cohesion (c) and internal friction angle (ϕ) until the model reaches a failure state. This failure condition is typically indicated by either non-convergence of the numerical solution or the development of excessive plastic deformation within the soil mass:

$\tau = c + \alpha \tan(\phi)$……...3.9

In SSR, this transformed to:

$T_{reduced} = \frac{c}{F} + \delta . \tan(\frac{\emptyset}{F})$ …….3.10

or mor accurately (and commonly in software):

$C_{reduced} = \frac{C}{F}$ $\tan \emptyset$ reduced $\frac{(\tan\emptyset)}{F}$ ……...3.11

The model is analyzed iteratively by incrementally increasing F until the system fails to converge (plastic strain localizes), indicating global instability.

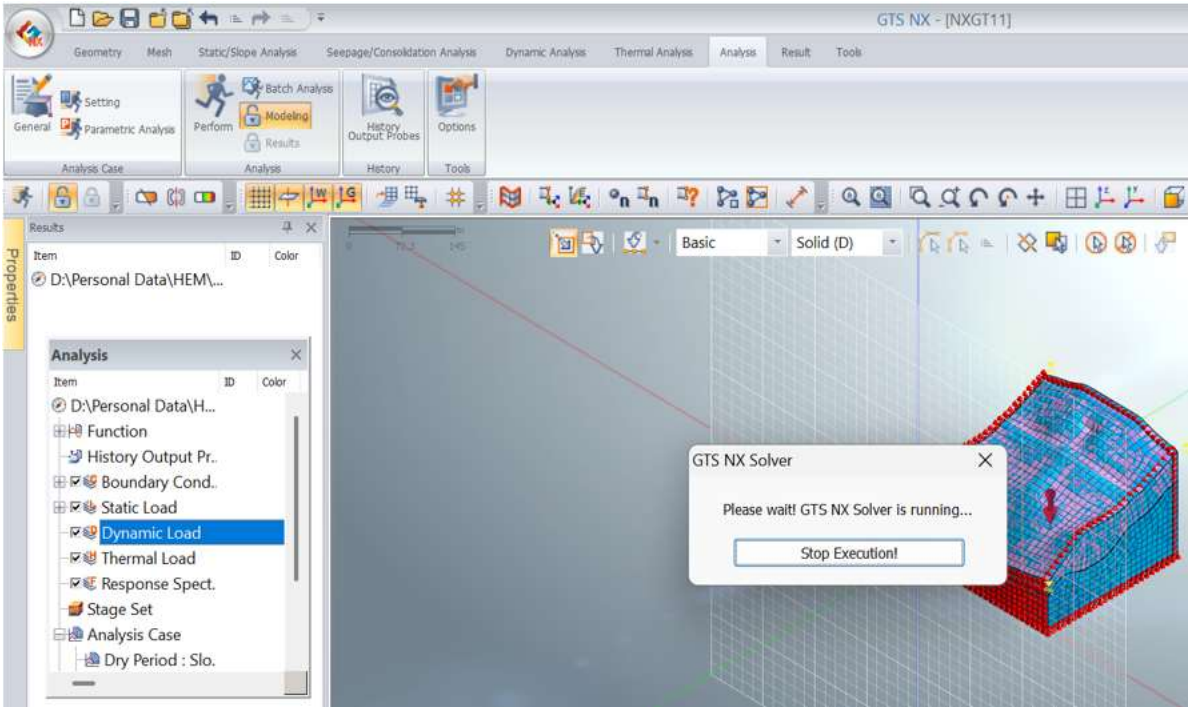

Figure 3- 12 Software in the analysis

3.5 MODELING OF PERMANENT DEFORMATION, SEIMIC ANALYSIS IN GTS NX

A two-dimensional finite element model was developed to analyze the slope stability of a landslide-prone section located in the southern region of Rwanda. The modeling process began with the acquisition of topographic data extracted from real Digital Elevation Models (DEMs) of Rwanda. These contour lines were used to construct the geometric profile of the slope in AutoCAD, ensuring accurate representation of the terrain geometry and dimensions.

The slope inclination was measured in the field using a clinometer, and it was found to range between 33° and 42°, indicating a steep and potentially unstable terrain. The model geometry shown in figure 3.8 was then imported into MIDAS GTS NX for further analysis.

Ground conditions and material properties, including unit weight, cohesion, and friction angle, were defined based on the results obtained from field investigations and laboratory tests conducted on soil samples from the site. These parameters were essential for simulating realistic slope behavior.

The numerical analysis considered both the stable and failure states of the slope. This involved conducting simulations under different loading conditions, including self-weight, seismic loading, and rainfall infiltration, to understand the potential failure mechanisms and post-

deformation behavior. The Shear Strength Reduction (SSR) technique was used to determine the Factor of Safety (FoS), while deformation analysis was carried out to evaluate displacement patterns under critical conditions.

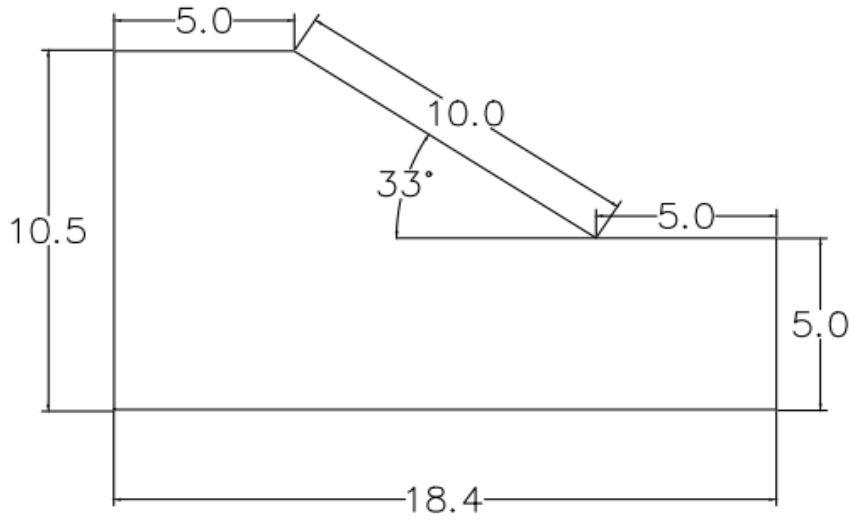

Figure 3- 13 The 2D model dimension in meter used in slope stability modeling

3.5.1 Seismic Slope Stability Analysis Using Pseudo-Static Method

A pseudo-static analysis was performed in MIDAS GTS NX to evaluate the effect of seismic loading on slope stability. This method converts dynamic earthquake forces into equivalent static horizontal loads using Peak Ground Acceleration (PGA). It is suitable for areas with limited seismic records. PGA values were selected based on regional seismic hazard data. A horizontal seismic coefficient (k_h) was applied to the slope model. The slope geometry and material properties were based on site investigations. The Shear Strength Reduction (SSR) method was used to compute the safety factor under seismic loading. This analysis helped identify critical failure conditions. Results supported the evaluation of earthquake-induced slope instability.

3.5.2 Definition of Seismic Coefficient

The pseudo-static horizontal force was modeled using the seismic coefficient k_h, kv, which is directly proportional to the site-specific PGA value. According to the National Risk Atlas of Rwanda (RHA & MIDIMAR, 2015), the Huye–Nyamagabe region is classified within a moderate seismic zone, with PGA values ranging between 0.10g and 0.16g, depending on the return period and hazard level (Affairs, 2015).

Three representative PGA values in table 3.4 were selected for analysis, each value was applied as a horizontal body force acting in the downslope direction, representing the inertia force developed during an earthquake event.:

Table 3- 4 the selected PGA and its horizontal acceleration

SN	Seismic coefficient K_h, kv	PGA	Horizontal acceleration(m/s^2)
A	0.05	0.05g	0.49
B	0.10	0.10g	098

3.5.3 Seismic Load Application in GTS NX

For each seismic case, a separate static load set was created and defined as a body force in the X-direction. The magnitude of the body force was calculated as:

$F_{seismic} = K_h . g = PGA \times 9.81\ m/s^2$ ……3.12

Three separate analysis cases were defined: PGA_0.10g, PGA_0.16g and PGA_0.20g, each case included the same slope geometry, mesh, boundary conditions, and material properties, with the only variation being the applied horizontal seismic coefficient the ground acceleration table used in analysis is in the appendix-6 the figure 3.9 shows the application of constraint and seismic and figure 3.10 shows the seismic loaded in the software under analysis.

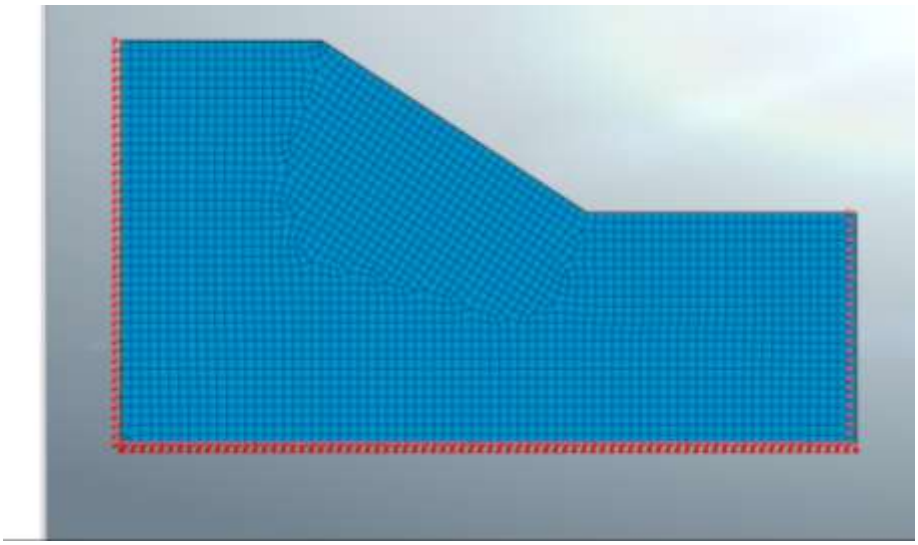

Figure 3- 14 Constraint application modeling seismic load

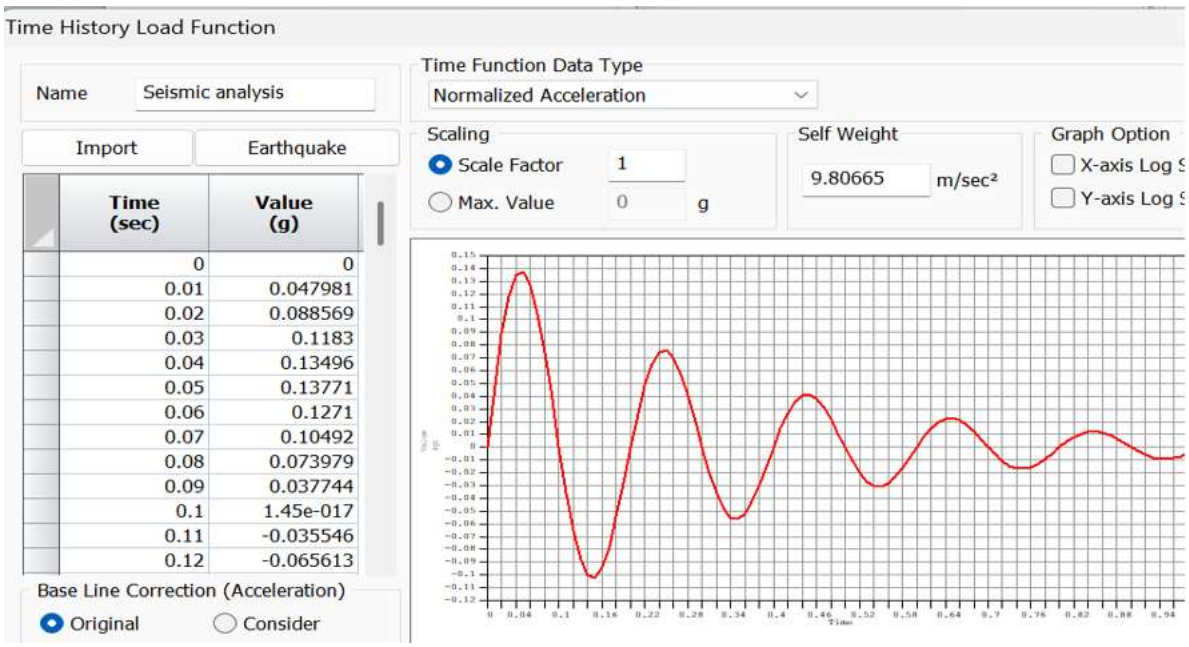

Figure 3- 15 seismic analysis of earthquakes in modeling

The total displacement under seismic loading was assessed for various PGA levels, as shown in Figure 3.13, the displacement corresponding to PGA 0.10g was relatively low. When the PGA increased to 0.16g (Figure 3.12), a noticeable increase in displacement occurred. The maximum displacement was recorded at PGA 0.20g, as illustrated in Figure 3.11, indicating a progressive loss in slope stability with increasing ground motion intensity.

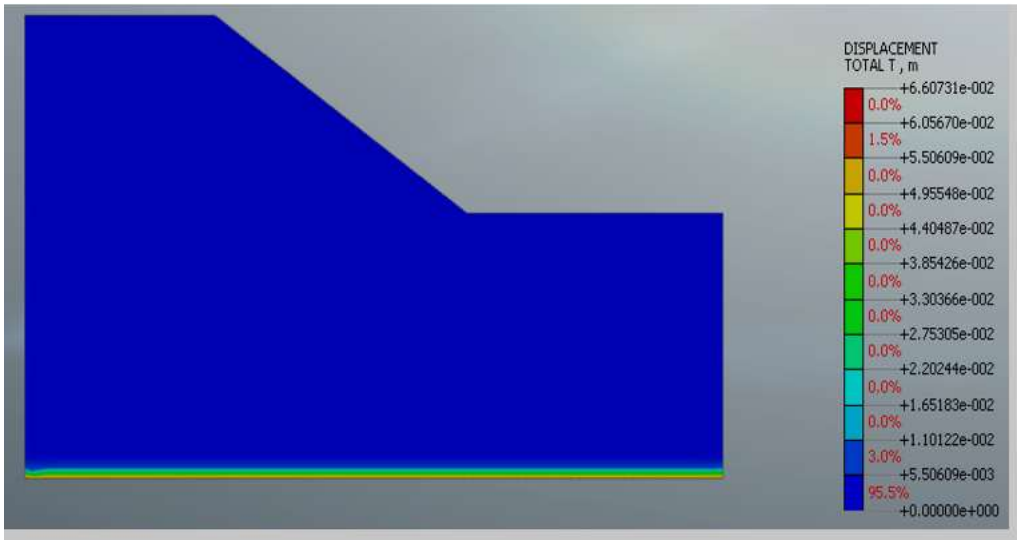

Figure 3- 16 Total displacement on the PGA of 0.20g

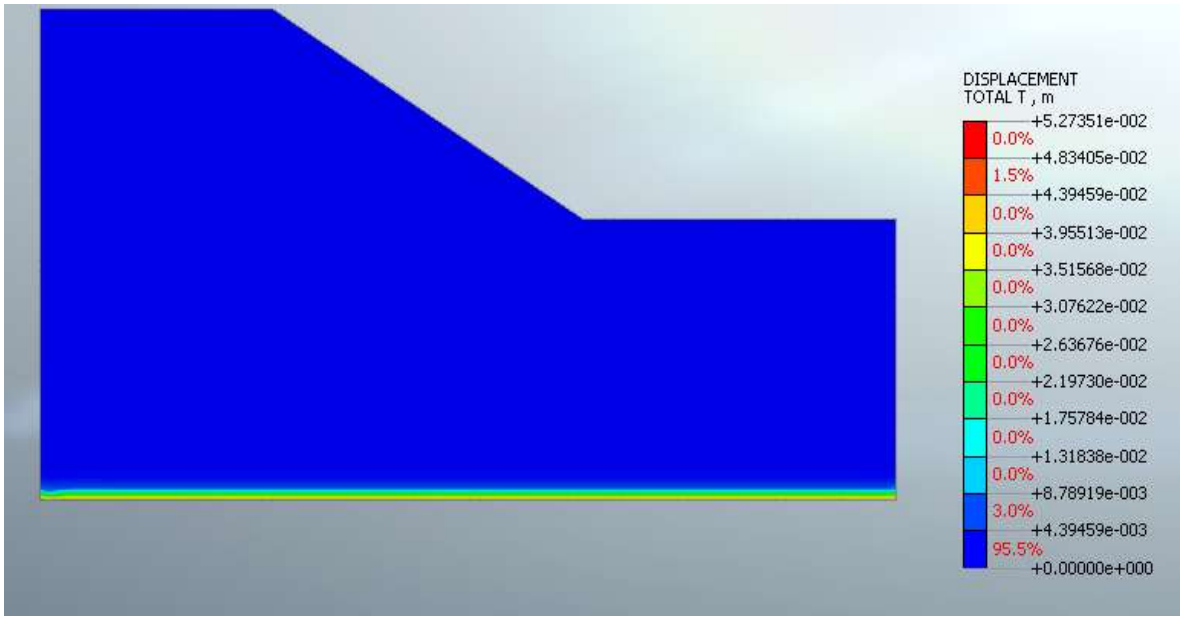

Figure 3- 17 Total displacement on PGA of 0.16g

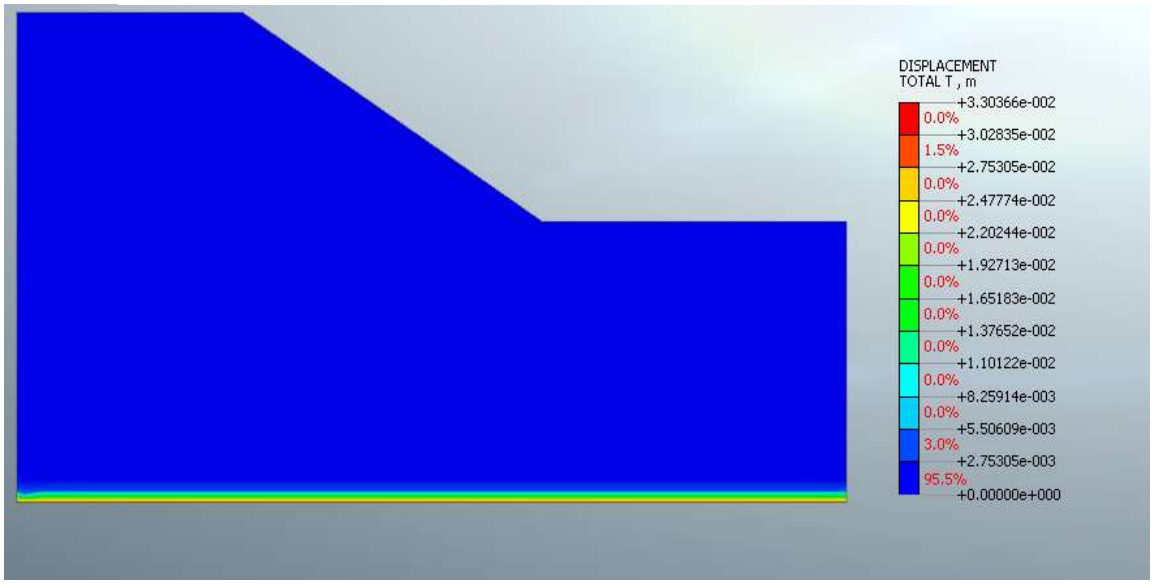

Figure 3- 18 Total displacement on PGA of 0.10g

3.6 SLOPE STABILIZATION

3.6.1 Stabilization by using Geogrid in Midas GTS Nx

This method was applied in the modeling of a road embankment, where geogrid reinforcement was introduced to enhance slope stability by increasing the Factor of Safety

3.6.1.1. Model Setup:

A 2D slope geometry was created and soil materials were defined using the Mohr-Coulomb

model. Geogrid layers were inserted as horizontal lines within the fill zone and modeled as truss elements with appropriate tensile stiffness.

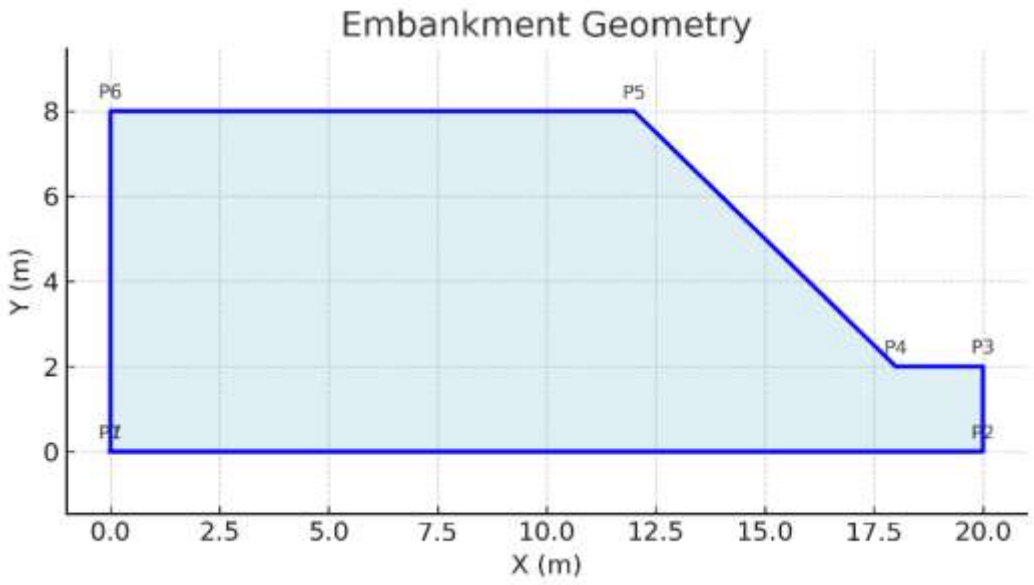

Figure 3- 19 Embankment 2D modeling on the failure area

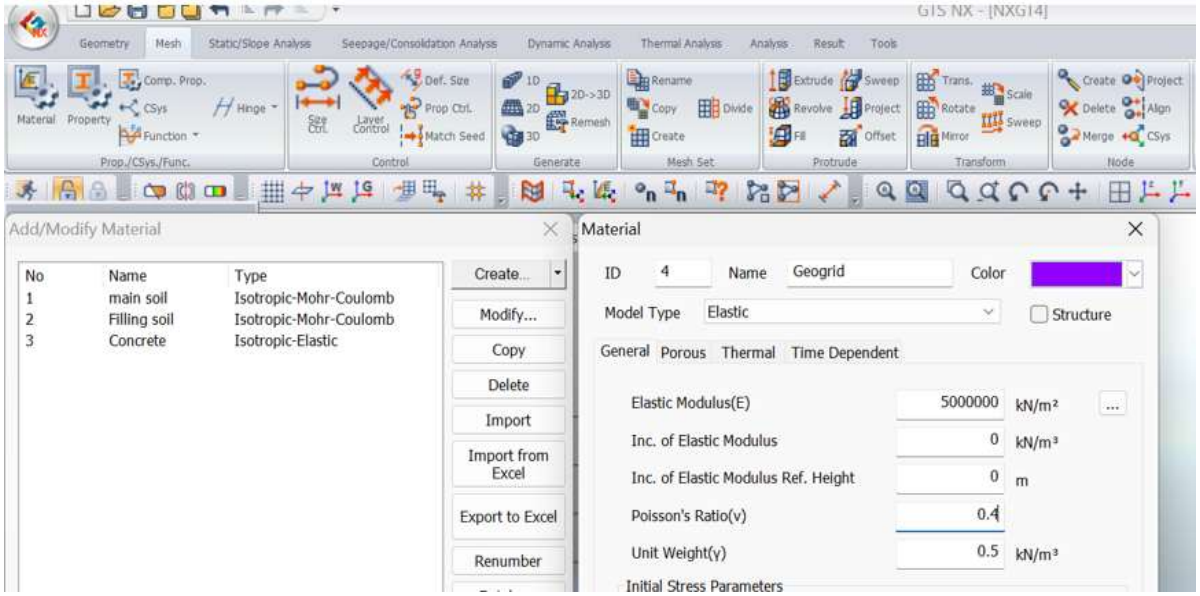

Figure 3- 20 Inserting, concrete wall and geogrid properties

3.6.1.2. Interface and Meshing:

To assess the stability of the road embankment, a 2D slope model was developed in MIDAS GTS NX using the Mohr-Coulomb failure criterion. The fill soil was assigned a cohesion of 10 kPa and a friction angle of 25°, as outlined in Table 4.3. Geogrid reinforcement was modeled

as truss elements with high tensile stiffness (EA = 2000 kN/m), inserted at vertical intervals of 2.0 m. Each geogrid layer extended 6.0 meters into the slope from a concrete anchoring wall defined with a unit weight of 24 kN/m³. Soil–geogrid interaction was simulated using Goodman contact interfaces. A mesh size of 0.5 m was adopted, with local refinement around reinforcement zones. The Shear Strength Reduction Method (SSR) was used to compute the Factor of Safety and visualize potential failure surfaces.

3.6.1.3. Analysis and Evaluation:

The slope stability was assessed using the Shear Strength Reduction Method (SSR) to compute The Factor of Safety and the failure surface were evaluated with geogrid reinforcement. The slope stability was assessed under multiple conditions both without stabilization and with stabilization to compare the effectiveness of the reinforcement system in analysis the rainfall of 0.291 kN/m² was insert as per figure 3.21.

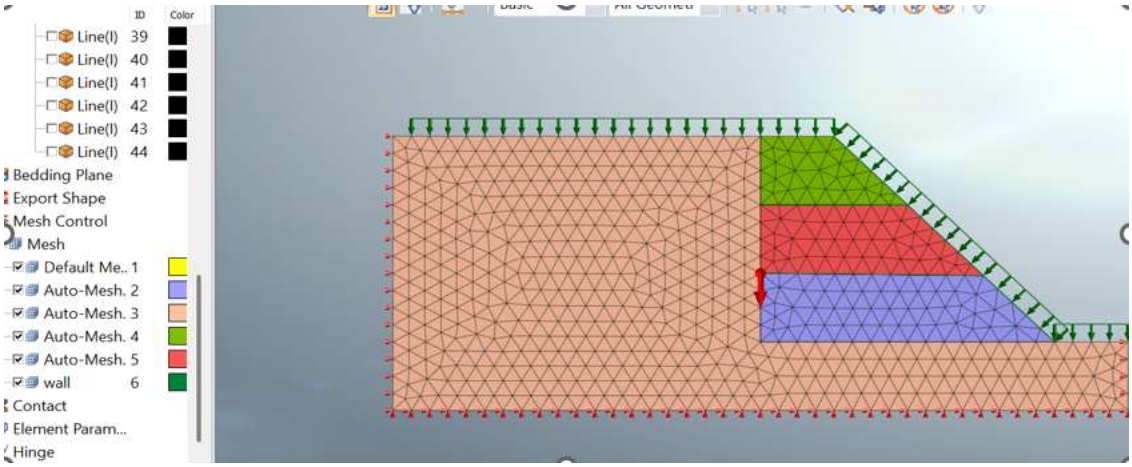

Figure 3- 21 meshing the model on inserted material of figure 3.20

3.6.2 Stabilization by using terraced slope technique

• Go to Structure → Create → Geometry → Create Line

• Draw the stepped profile using coordinate points. For example, to create 5 steps each 2 m high and 4 m wide the figure 3-22 was used, P1= (0.00, 8.00) , P2 = (4.00, 8.00) , P3 : (4.00, 6.00), P4 : (8.00, 6.00) , P5 : (8.00, 4.00) , P6 : (12.00, 4.00) , P7 : (12.00, 2.00) , P8 : (16.00, 2.00) P9 : (16.00, 0.00) , P10 : (20.00, 0.00) .

:

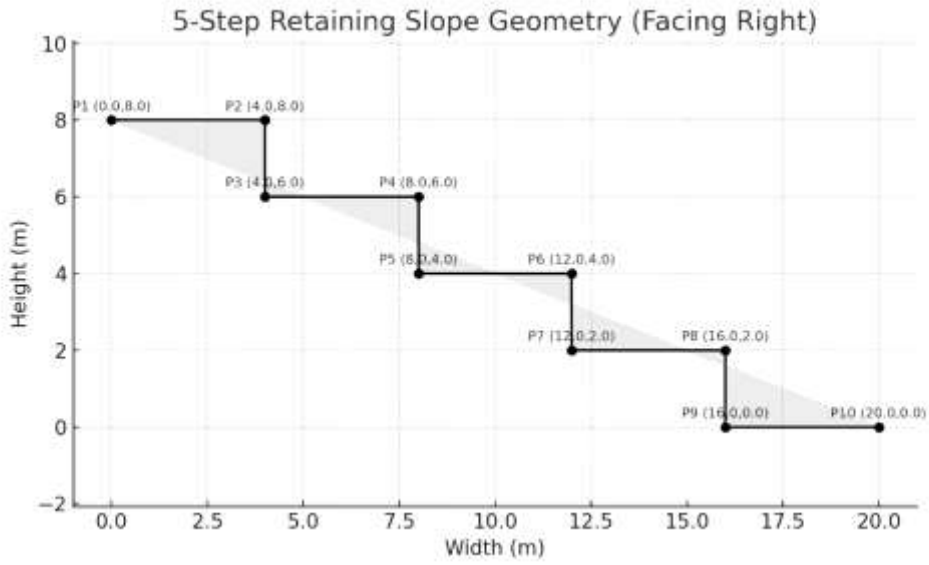

Figure 3- 22 the geometry of bench terraces the used in modelling

GTS NX, the slope profile was generated by defining geometry points and connecting them using polylines to represent the terrain accurately. Figures 3-23 and 3-24 illustrate the developed mesh with a uniform spacing of 0.4 m, ensuring precise discretization of the model. The self-weight of the soil was automatically applied as part of the gravitational loading conditions. Additionally, a rainfall-induced pressure of 0.291 kN/m² was incorporated to simulate the effect of infiltration on slope stability. These conditions were carefully integrated into the numerical model to represent real field scenarios. The mesh density and applied loads were optimized to achieve accurate and reliable analysis results. This setup forms the foundation for evaluating slope performance under combined self-weight and rainfall effects.

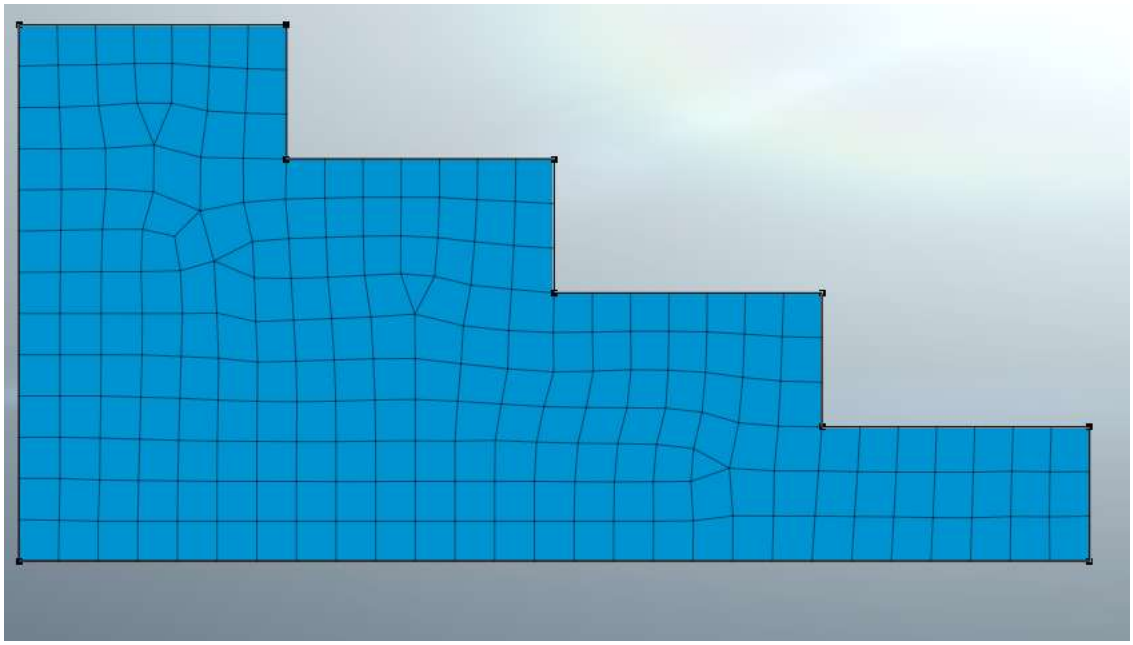

Figure 3- 23 The mesh generated in modeling

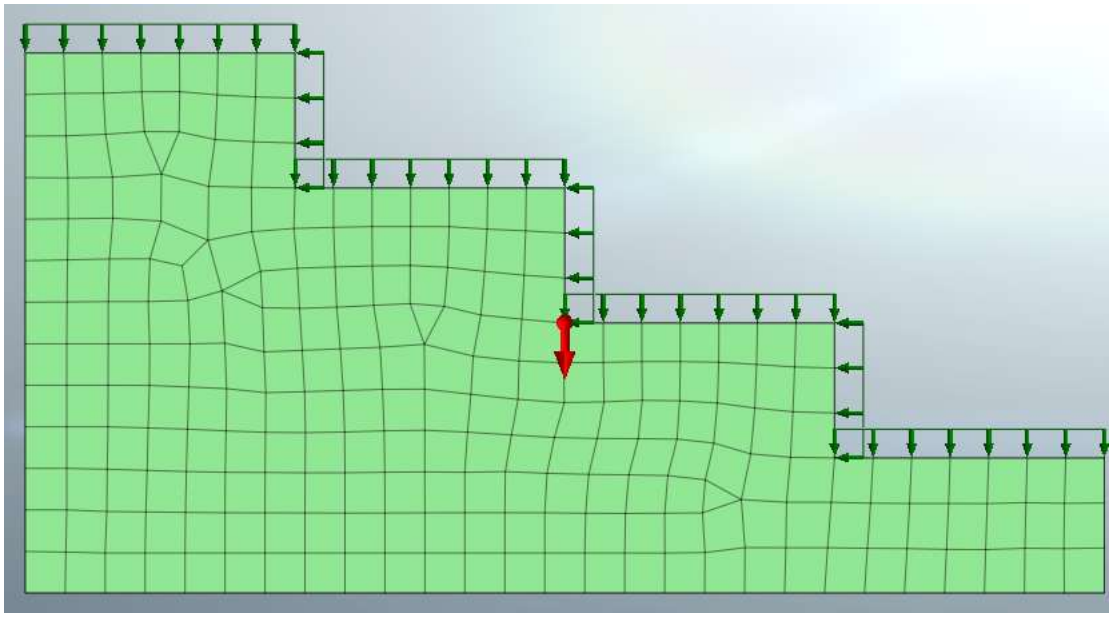

Figure 3- 24 Application of rain fall and self-weight of soil

CHAP IV. RESULTS AND ANALYSIS

4.1 SUMMARY OF FIELD AND LABORATORY TEST RESULTS

Soil Identification, Consistency, and Classification

To understand the engineering behavior of the subsoil, various field and laboratory tests were conducted on samples collected from trial pits along the study area and some referred from boreholes done in southern province projects. These tests aimed to determine the basic physical and index properties of the soils, which are essential for geotechnical classification, analysis, and design.

The **sieve analysis** was carried out to determine the grain size distribution of the soil samples, allowing for the classification of soils as coarse-grained or fine-grained, and helping to infer permeability and drainage characteristics. This test is critical for identifying whether the soil is gravelly, sandy, silty, or clayey in nature.

In addition, **Atterberg limits tests** namely, the liquid limit (LL), plastic limit (PL), and plasticity index (PI) were performed to evaluate the consistency and plasticity characteristics of fine-grained soils. These indices provide insight into the soil's behavior under varying moisture conditions and help identify its sensitivity to changes in water content, which is crucial for slope stability assessments.

Using the results of these tests, the soil samples were classified according to the **Unified Soil Classification System (USCS)**. This system enables the standardized description of soils based on their particle size distribution and plasticity properties. The classification provides a consistent framework to interpret the geotechnical behavior of soils, especially in terms of shear strength, compressibility, and drainage potential.

The results are presented in Tables 4.1 and 4.3, offering a comprehensive summary of the soil types identified at various depths, along with their respective Atterberg limits and grain size distribution. Notably, the data in Table 4.3 was sourced from a separate geotechnical

investigation conducted by another company operating in the surrounding area, as indicated in the table.

Table 4- 1 The summarized table of tested pits Results

Description	S1	S2	S3
Direct shear test results			
Unit Weight (γ), kN/m³	17.8	17.6	16.8
Cohesion (C), kN/m^2	15.4	28.2	30
Frictional Angle (φ), degree	28.6	28	26.2
Nature moisture content			
Moisture content, %	24.65	25.4	31.66
Proctor Test			
OPM (Optimum moisture content) ,%	17.2	15.8	17.2
Maximum dry density(g/cm^3)	1.65	1.7	1.64
specific gravity test results			
specific gravity test results	2.62	2.6	2.58
sieve analysis test results			
Aggregates, %	0	0	0
Sand, %	38.5	20.9	26.1
Silts, %	14.6	18.1	18.5
clay, %	47	61	55.4
Atterberg limits Tests			
LL (liquid limit), %	62.58	49.89	63.46
PL (plastic limits), %	31.1	26	33.5
Unified soil classification system (USCS)	CH: Fat clay	CL: Lean clay	CH: Fat clay

Through field observation of the existing slope and analysis of disturbed (slided) soil samples, the results summarized in Table 4.2 were obtained. The slope profile was composed of three distinct layers: a subgrade layer consisting of natural in-situ material, a subbase layer made of lateritic soil, and a base course comprising granular material. The pavement surface was finished with a bituminous layer. Imported fill material shall conform to ASTM C136 graduation requirements, with 100% passing the 75 mm sieve, 50–100% passing the 4.75 mm (No. 4) sieve,

and a maximum of 35% passing the 0.075 mm (No. 200) sieve. The material shall have a maximum Liquid Limit (LL) of 35%, a maximum Plasticity Index (PI) of 15%, and a Group Index (GI) not exceeding 10.

Table 4- 2 Subgrade existing embanked material characterization

Description	**Sample test**	**Standard specification**
Direct shear test results		
Unit Weight (γ), kN/m³	1.76	
Cohesion (C), kN/m^2	19	
Frictional Angle (φ), degree	28.7	
CBR Test		
CBR values, %	8.2	
Proctor test		
OPM (Optimum moisture content), %	18	
Maximum dry density(g/cm^3)	1.628	
sieve analysis test results		
Aggregates, %	4.43	
Sand, %	42.5	
Silts, %	17.7	
clay, %	39.8	
Atterberg limits Tests		
LL (liquid limit), %	44.8	Max, 35
PL (plastic limits), %	15.2	
PI (Plastic index)	30	Max,15
Unified soil classification system (USCS)	CL – Inorganic clay of low to medium plasticity	

Table 4- 3 Borehole done at Rwanda south provide in soil exploration done by Geo Consult Ltd

BH	Depth (m)	LL (%)	PL (%)	PI (%)	CBR (%)	Sand (%)	Silt (%)	USCS	SC Class
BH 1	1.00-2.00	49.85	22.07	27.78	3.5	39	57.5	CL: Sandy lean CLAY	SC3
BH 1	3.95-6.50				0	69.3	30.7	SC: Clayey SAND	SC3
BH 1	6.50-7.50				9.6	69	21.4	SC: Clayey SAND	SC3
BH 1	7.95-13.8				3.5	39	57.5	CL: Sandy lean CLAY	SC3
BH 1	15.2-16.4				0.1	41.3	58.6	CL: Sandy lean CLAY	SC3
BH 2	1.45-3.95				17.5	34.8	47.7	SM: Silty SAND with gravel	SC3
BH 2	8.45-9.50				3.1	68.5	28.4	SM: Silty SAND	SC3
BH 3	2.20-3.90	52.16	27.9	24.27	1	23.8	75.2	CH: Fat CLAY with sand	SC4
BH 3	5.50-6.00	44.44	23.72	20.72	0	41.5	58.5	CL: Sandy lean CLAY	SC3
BH 3	8.50-9.50				0	43.9	56.1	CL: Sandy lean CLAY	SC3
BH 3	9.95-12.5				0	87.2	12.8	SC: Clayey SAND	SC3
BH 3	13.5-14.0				3.1	68.5	28.4	SC: Clayey SAND	SC3
BH 3	14.0-14.5				9.6	69	21.4	SC: Clayey SAND	SC3

Table 4- 4 The DCP test done on the real site and interpretation to shear parameters

Depth (m)	CBR (%)	Cohesion (kPa)	Friction Angle (°)	Modulus E (MPa)	DCPI (mm/blow)
0	23.57	7.07	22.36	125.22	17.06
1	20.26	6.08	22.03	117.69	13.04
2	36.23	10.87	23.62	171.81	7.64
3	41.77	12.53	24.18	190.90	6.24
4	63.43	19.03	26.34	249.04	4.50
5	93.43	28.03	29.34	320.99	3.21
6	93.43	28.03	29.34	320.99	3.21

4.2 SLOPE STABILITY ANALYSIS RESULTS

GTS NX uses the Finite Element Method (FEM) to perform slope stability analysis; it applies the Shear Strength Reduction (SSR) method to calculate the Factor of Safety (FoS). The SSR method reduces cohesion (c) and friction angle (φ) until failure occurs, this technique provides a global FoS and visualizes potential failure surfaces, in this study, slope stability was analyzed in 3D using the actual terrain model. Figure 4.1 presents the total displacement distribution in the slope, Figure 4.2 shows the strain in the Z-direction during loading, Figure 4.3 summarizes the stress, displacement, and strain results. These outputs confirm the model's ability to capture realistic slope behavior.

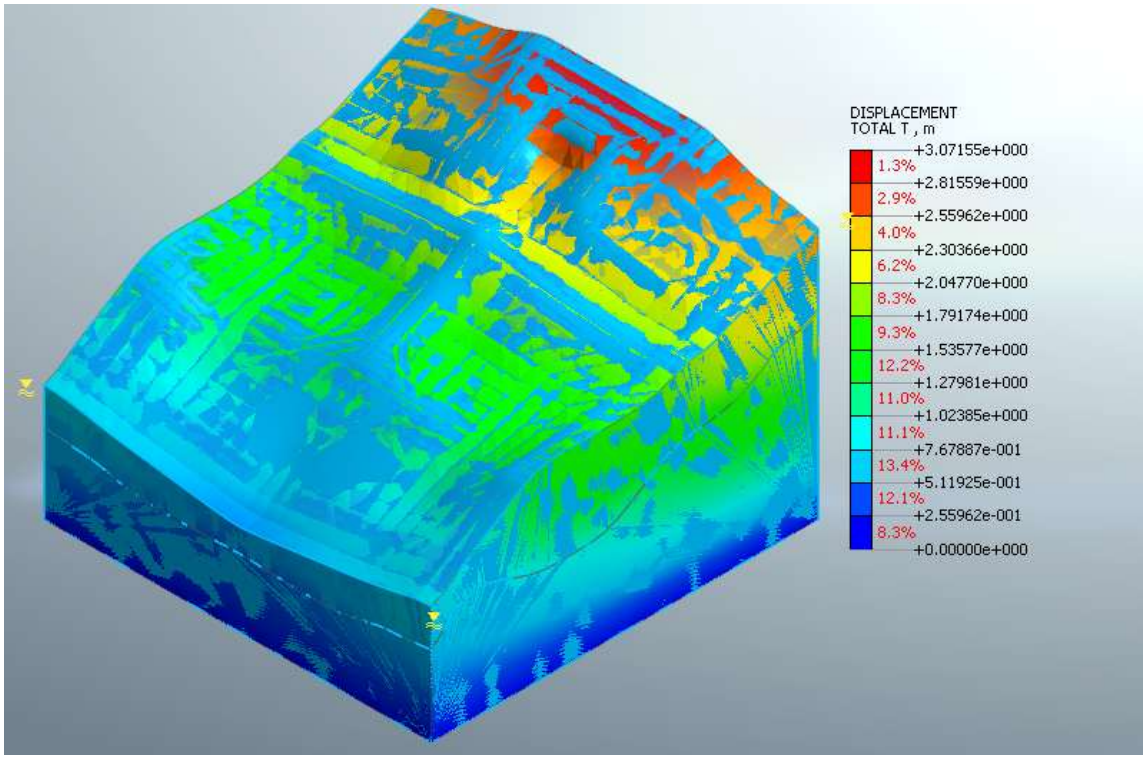

Figure 4- 1 The total displacement

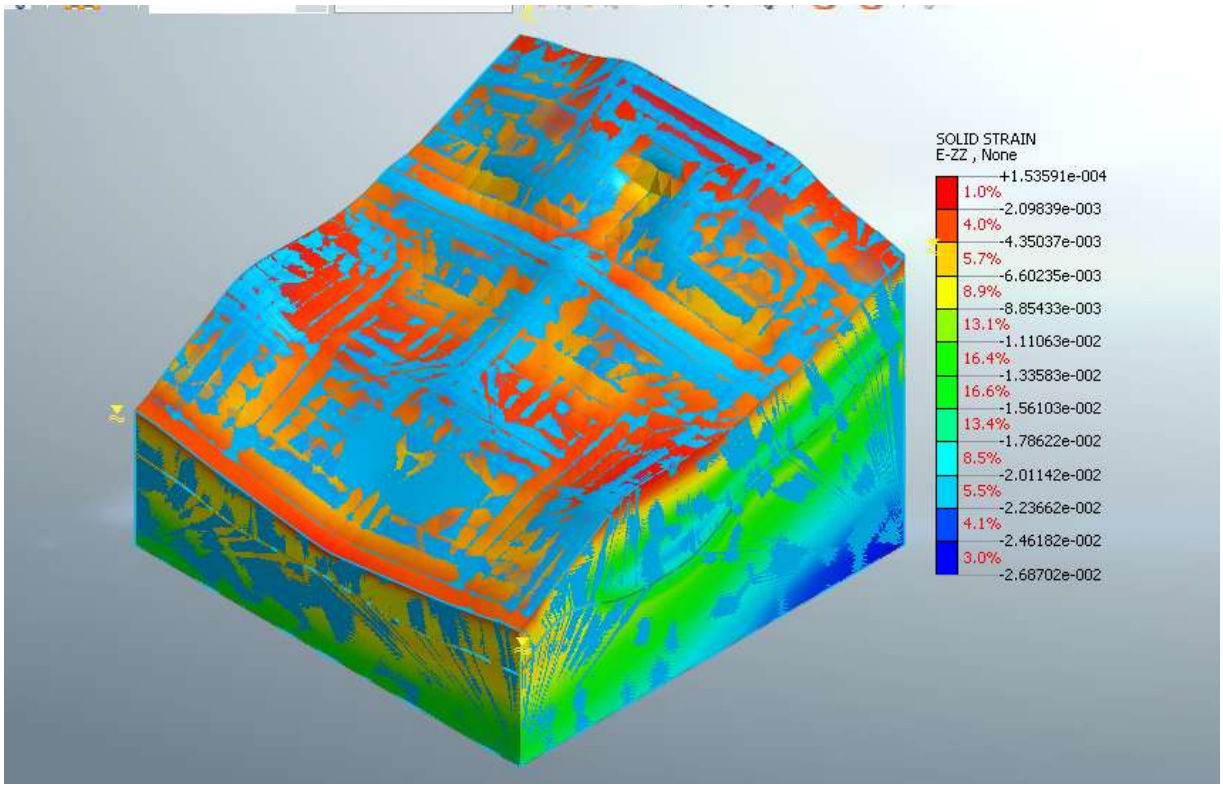

Figure 4- 2 Total strain in E-ZZ direction

Table 4- 5 Summarized Results of on modelling of 3d terrain

Result Type	Max Value	Min Value
Displacement Total (m)	3.07155	0
Solid Stress S-XX (kN/m²)	1057.2	-1224.48
Solid Stress S-YY (kN/m²)	1299.94	-1224.07
Solid Stress S-ZZ (kN/m²)	800.93	-2841.66
Solid Strain E-XX	0.00165	-0.00197
Solid Strain E-YY	0.00365	-0.00798
Solid Strain E-ZZ	0.00153	-0.02687

The strength reduction analysis produced a Factor of Safety (FOS) of 1.064 shown in figure 4.3**,** indicating the slope is marginally stable and highly susceptible to failure, especially during the rainy period. According to standard geotechnical criteria, a minimum FOS of 1.3 is typically required for safe slope performance, which is not met in this scenario. Therefore, slope stabilization measures are recommended.

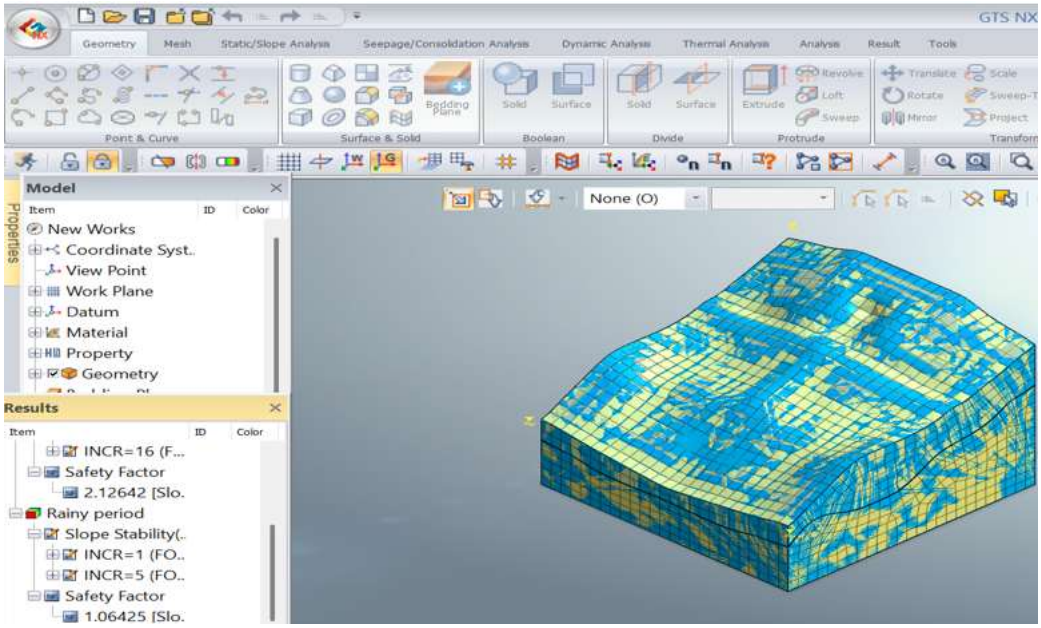

Figure 4- 3 the safety factor obtained on the real terrain

4.3 SEISMIC ANALYSIS AND DEFORMATION ANALYSIS.

Table 4.6 presents the Peak Ground Acceleration (PGA) values alongside the corresponding displacements obtained from the analysis. Similarly, Figure 3.4 demonstrates that as acceleration increases, displacement also increases. In Figure 4.5, the relative displacement is

shown to grow with increasing PGA; however, the displacement remains nearly constant between 0.16g and 0.20g, indicating a possible plateau effect.

Table 4- 6 PGA and max displacement

PGA (g)	Max Displacement (m)
0.1	0.039
0.16	0.0527
0.2	0.0667

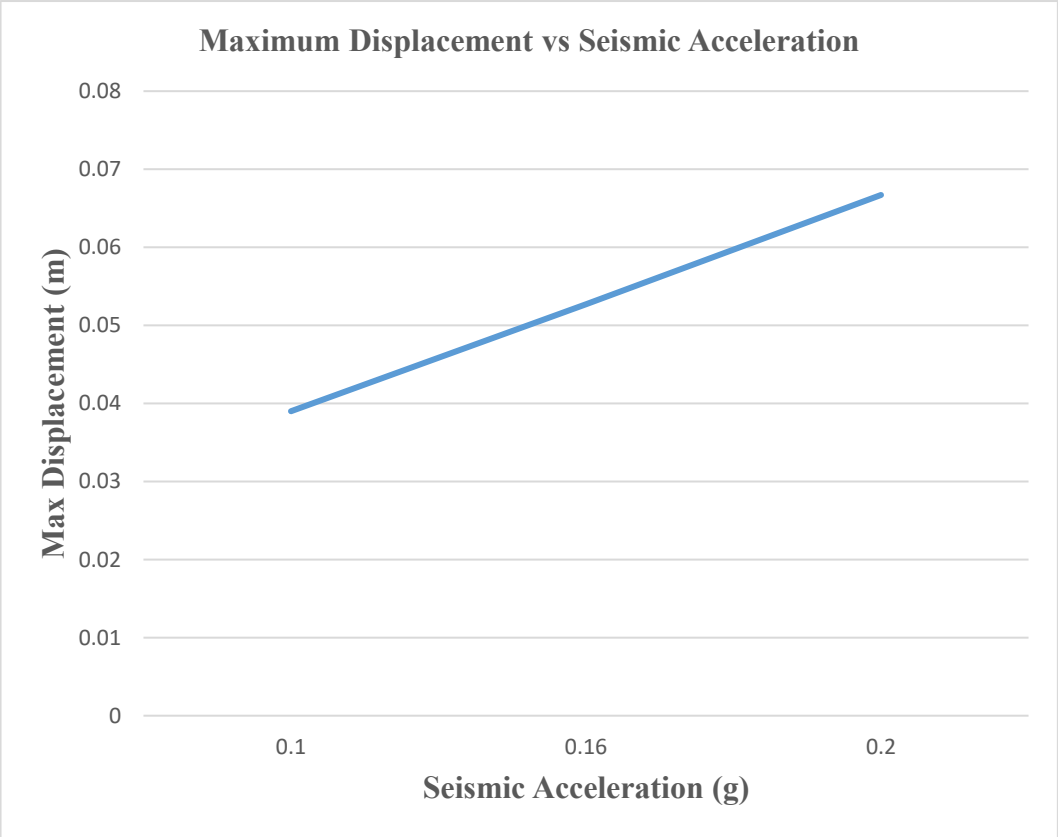

Figure 4- 4 Maximum displacement vs seismic acceleration

Table 4- 7 Summarized table of strain and stress and displacement obtained on different PGA

PGA (g)	Max Displacement (m)	Max Relative Displacement (m)	Max Acceleration (m/s²)	Max Plane Strain Force XX (kN/m)	Max Plane Strain Stress S-XX (kN/m²)
0.1	0.0298	0.0476	0.98	0.744	0.47
0.16	0.0476	0.0595	1.323	0.939	0.66
0.2	0.0595	0.0595	1.654	0.939	0.66

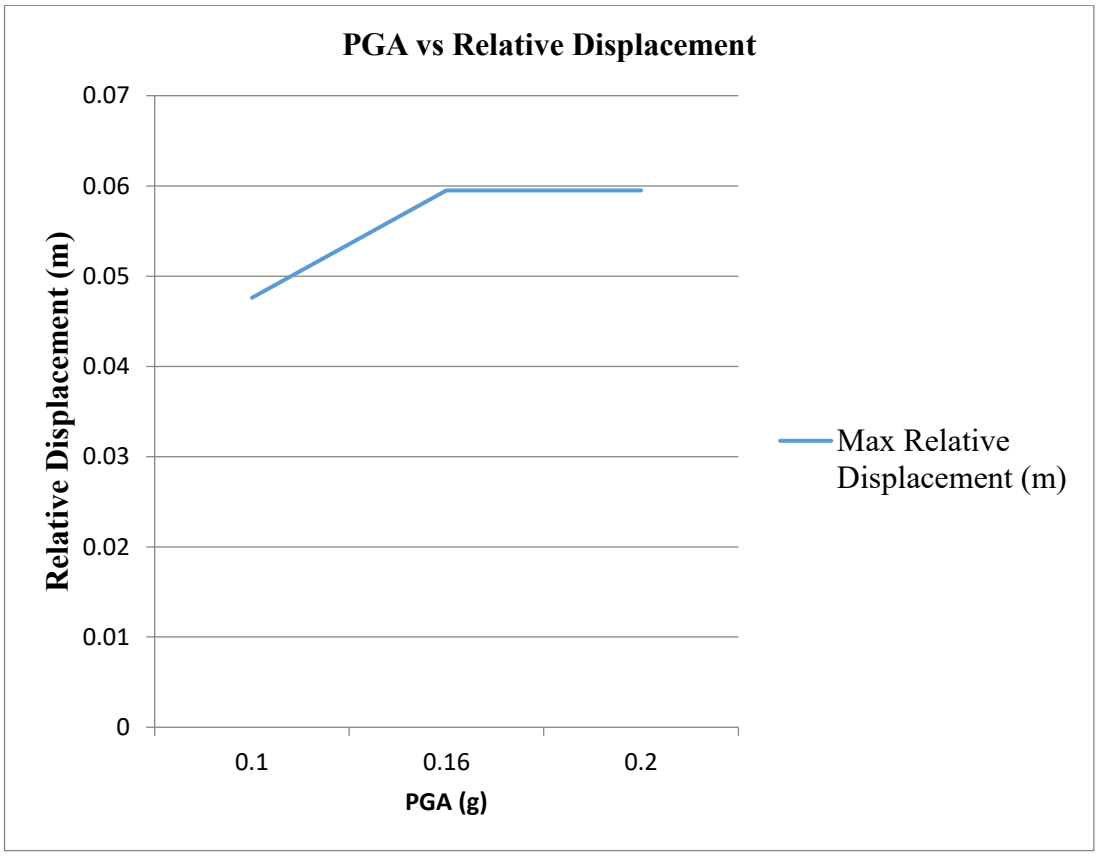

Figure 4- 5 PGA VS Relative displacement

Figure 4.6 illustrates the maximum acceleration values applied during the analysis, corresponding to each specified PGA level. Figure 4.7 demonstrates a clear trend of increasing

displacement as the PGA values rise, highlighting the direct relationship between seismic intensity and slope response.

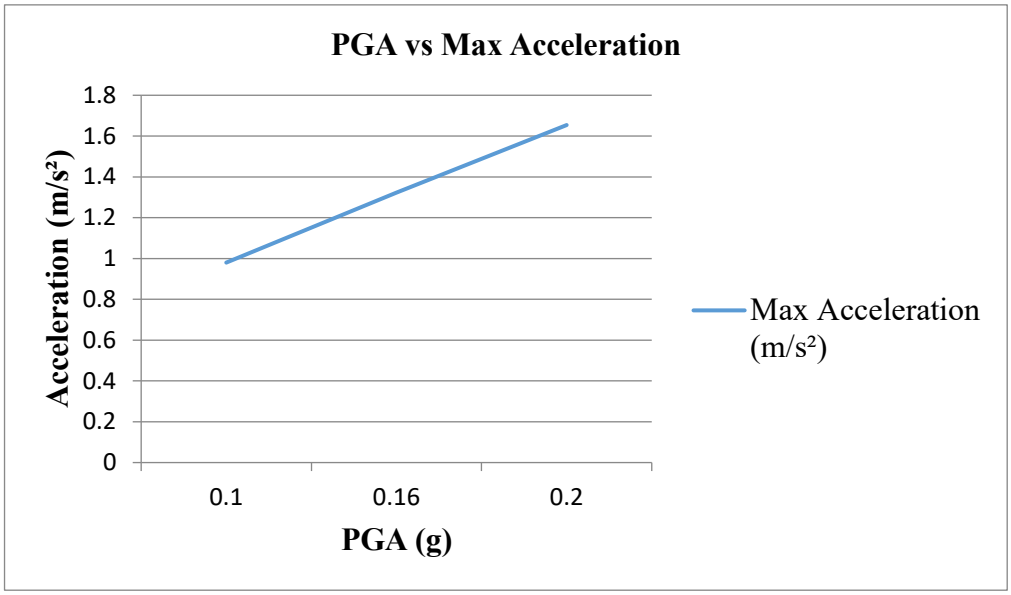

Figure 4- 6 PGA VS Max Acceleration

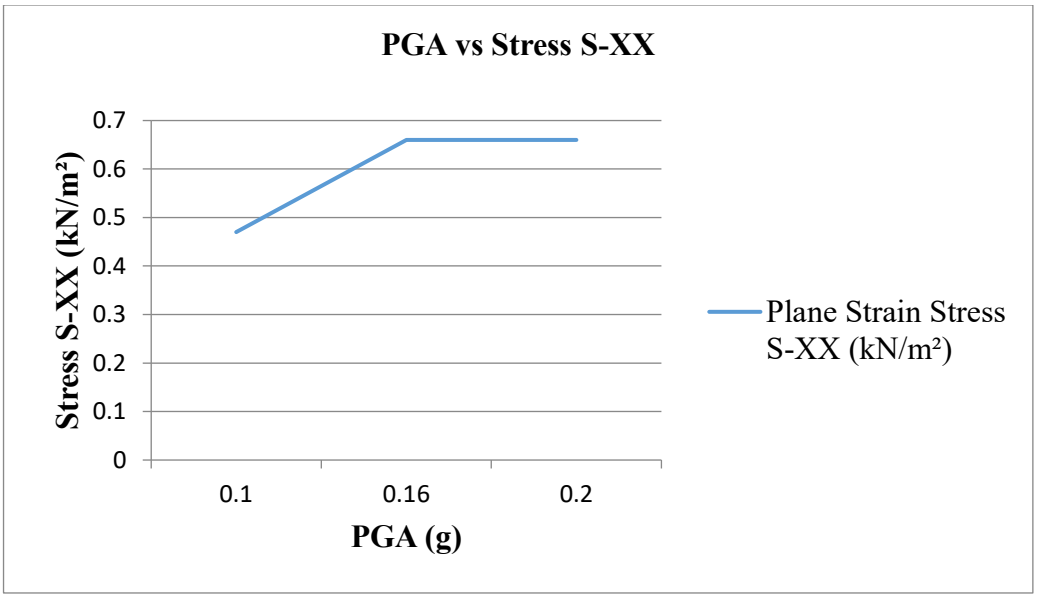

Figure 4- 7 PGA Vs stress in X-axis direction

4.4 STABILIZATION OF SOIL RESULTS

4.4.1 Stabilization by using terraced slope technique

In the stabilization analysis using the terraced slope technique, the slope geometry was modified by creating a series of horizontal benches along the inclined surface to reduce the overall slope height and distribute the driving forces. This approach effectively minimized the potential for deep-seated failure by interrupting the continuous failure plane and reducing the surcharge acting on lower slope sections. The analysis revealed a notable improvement in the Factor of Safety compared to the untreated slope, indicating enhanced global stability. Displacement contours also showed a significant reduction in lateral and vertical movements, confirming the terracing's effectiveness in controlling deformation. This technique proved particularly beneficial for slopes with weak geological layers, such as weathered soil and rock, common along the Huye–Nyamagabe corridor figure 4.10 shows FoS obtained of 3.14.

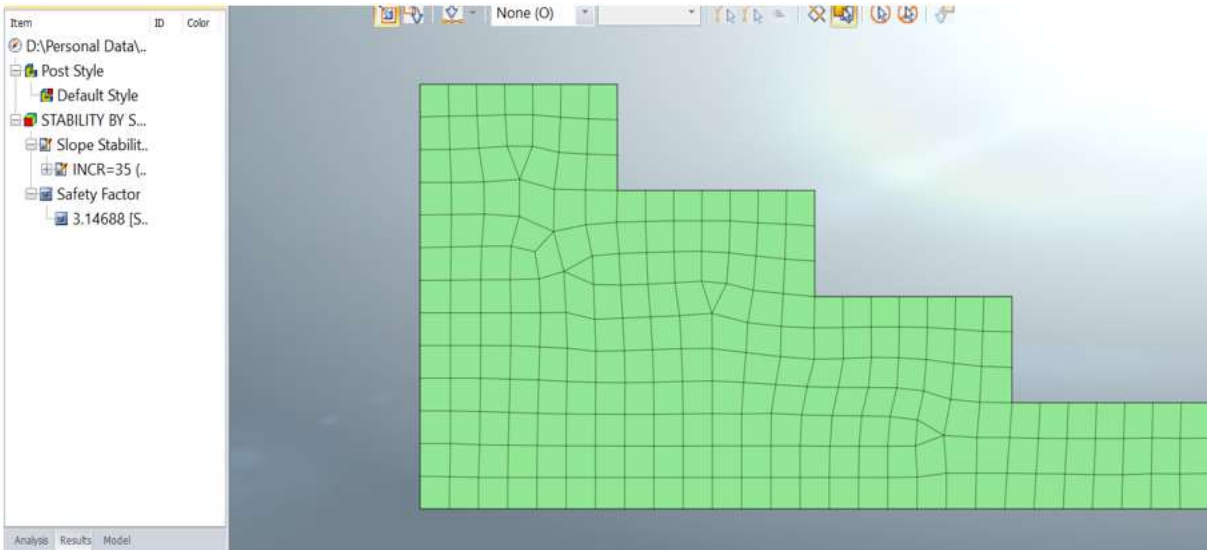

Figure 4- 8 obtained safety factor on bench terrace analysis

4.4.2 Geogrid stabilization results analysis

This section presents the comparative analysis of slope stability for an embankment structure under different stabilization conditions. The assessment is based on the Factor of Safety (FOS) and maximum displacement results obtained from numerical simulations in MIDAS GTS NX. Stabilization techniques considered include geogrid reinforcement, retaining wall, and their combination. The results are visualized through charts and interpreted for their engineering significance.

4.4.2.1. Factor of Safety (FOS) Comparison

Figure 4.11 shows the variation of Factor of Safety under four conditions: without stabilization, with wall, with geogrid, and with both wall and geogrid. The lowest FOS of 1.1625 is observed in the case of no stabilization, indicating potential instability check the figure 4.13. Use of a retaining wall improves the FOS to 2.2625, while geogrid alone achieves 2.1938. The combined effect yields the highest FOS of 2.2656, demonstrating the efficiency of reinforcement.

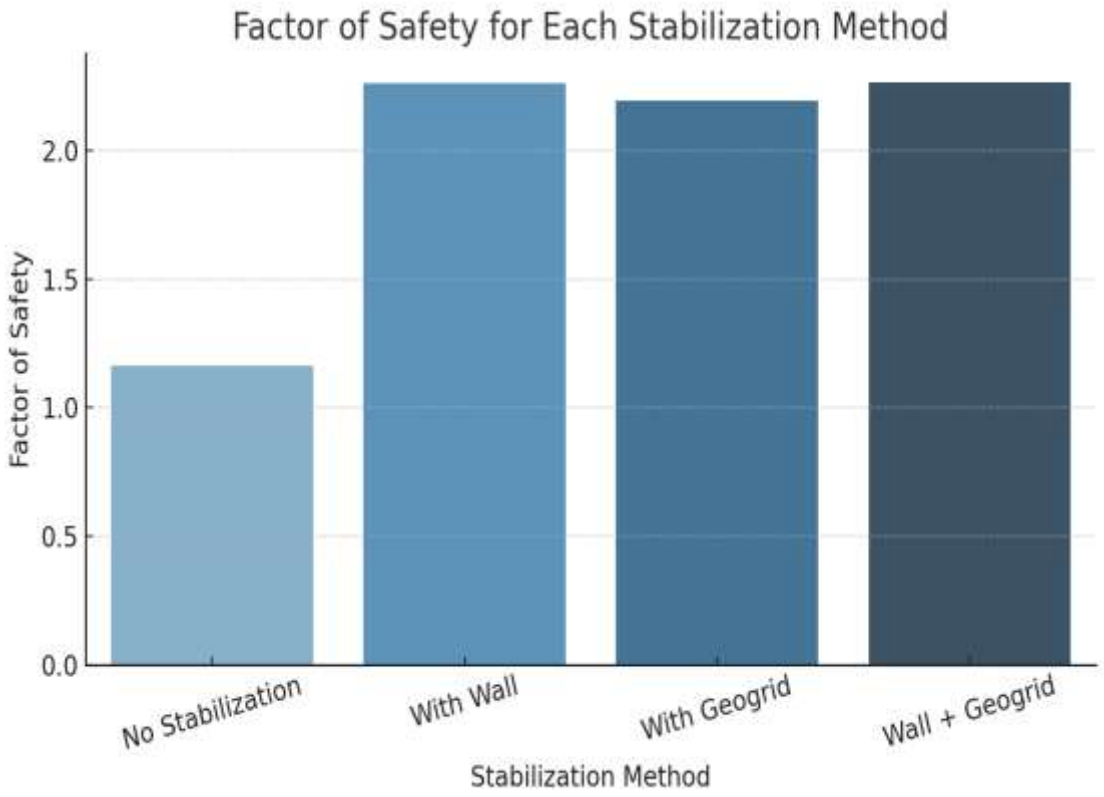

Figure 4- 9 Fator of safety vs stabilization method

4.4.2.2. Maximum Displacement Comparison

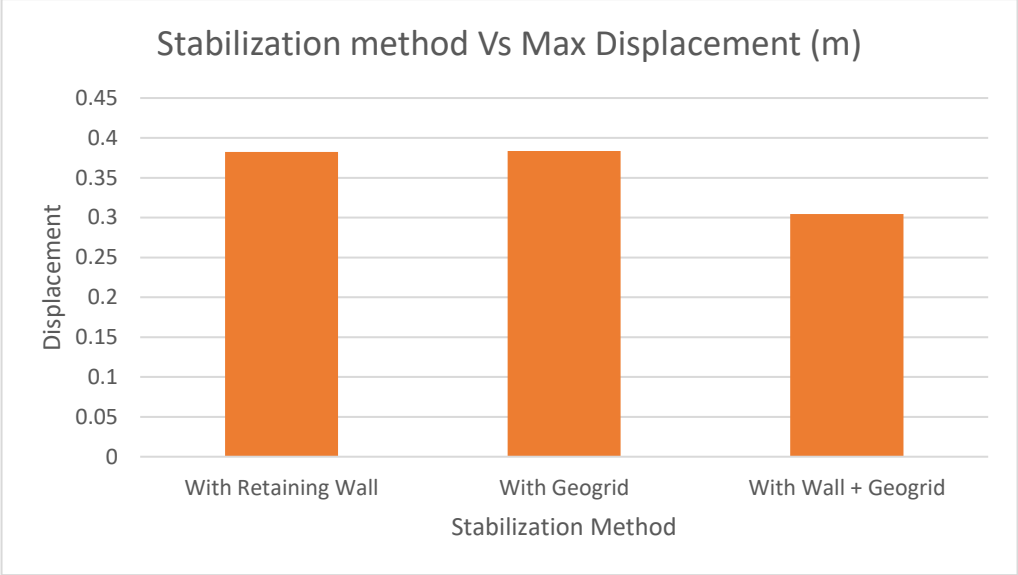

Figure 4- 10 maximum displacement vs method of stabilization

Figure 4.12 illustrates the maximum displacement observed under various conditions. The highest displacement of 0.7206 m was recorded for the unsterilized embankment, indicating significant deformation and slope instability. With the introduction of stabilization techniques, displacement decreased notably. The lowest displacement, measured at 0.3045 m, was achieved when both retaining wall and geogrid were employed, demonstrating enhanced structural performance and stability.

Figure 4.13 presents the analysis of the road embankment fill material, where the initial Factor of Safety (FoS) was determined to be 1.16, which falls below the recommended minimum of 1.3 for stable slopes. However, after applying geogrid reinforcement, the FoS improved significantly to 2.2, confirming the effectiveness of the stabilization.

Figure 4.14 further depicts the deformation pattern of the slope, highlighting the zones of maximum displacement under the analyzed conditions

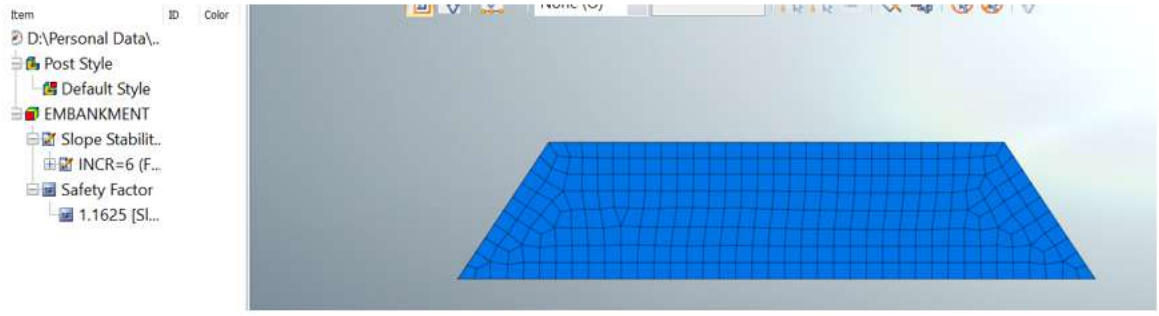

Figure 4- 11 unstabized filling material on road

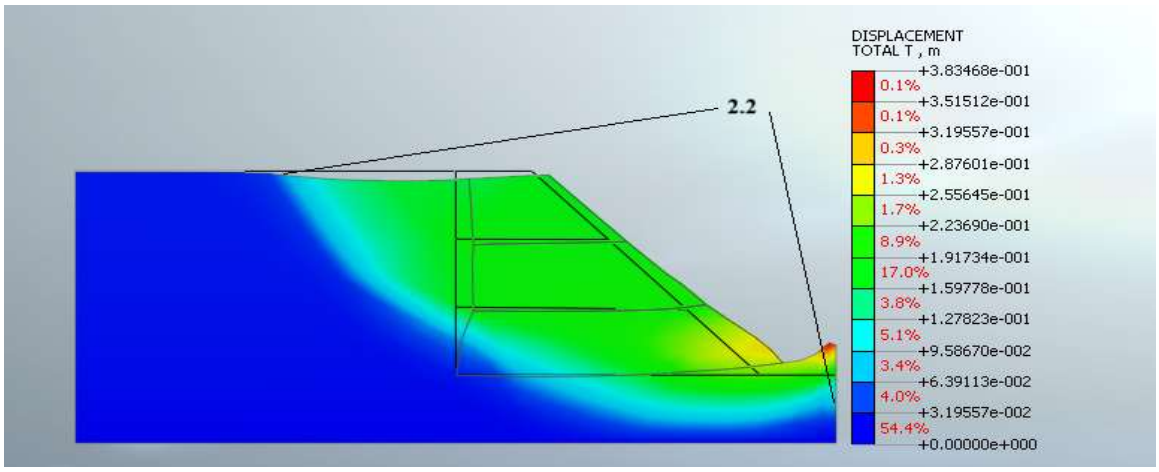

Figure 4- 12 displacement/deformation demonstrated on the model

4.4.3. Discussion

The untreated slope exhibited a critically low Factor of Safety (FoS) of 1.06, indicating a high risk of failure. Displacement analysis further confirms the effectiveness of stabilization techniques, showing a significant reduction in deformations from 0.7206 m in the untreated slope to 0.3823 m, 0.3835 m, and 0.3045 m for the retaining wall, geogrid reinforcement, and their combined application, respectively. Furthermore, for the embankment slope, the FoS improved markedly from 1.16 to 2.2 after stabilization. These results highlight the crucial role of stabilization methods in enhancing slope stability and safety, particularly for steeper

gradients. Table 4.9 provides the standard specifications and applications of various stabilization techniques.

Table 4- 8 Displacement standard with specifications

Standard / Guideline	Typical Allowable Displacement	Application
FHWA (USA)	< 0.3 – 0.5 m	Roadway embankments
Eurocode 7	Depends on serviceability, typically < 0.5 m	General geotechnical design
IS 14496 (India)	< 0.2 m for critical structures	Slopes and embankments
BS 8006 (UK)	Limits vary based on risk, often < 0.5 m	Reinforced earth slopes
FHWA NHI-05-123	Max 1 m for very large, non-critical slopes	Landslide risk mitigation

CHAPTER FIVE: CONCLUSION AND RECOMMENDATIONS

5.1 CONCLUSION

This study focused on the geotechnical characterization and evaluation of factors influencing slope failure along the Huye–Nyamagabe road, employing laboratory testing, in-situ investigations, and advanced finite element modeling using MIDAS GTS NX. The following key conclusions were drawn:

- The slope is predominantly composed of weak geomaterials, such as weathered soil and weathered rock, which exhibit low cohesion and friction angle values. These geotechnical properties significantly contribute to the area's vulnerability to slope failure.

- Under static loading conditions, the slope was found to be marginally stable, with a Factor of Safety (FoS) of approximately 1.06, indicating a high risk of failure in the absence of reinforcement measures.

- Seismic loading had a pronounced impact on slope behavior. As Peak Ground Acceleration (PGA) increased from 0.10g to 0.20g, both lateral displacements and deformation magnitudes increased, resulting in a marked reduction in slope safety margins.

- Permanent deformation analysis revealed the development of plastic strain zones, especially at the toe of the slope and along material interface boundaries, indicating these as potential failure initiation zones.

- The combination of steep slope geometry, prolonged rainfall infiltration, and regional seismic activity creates a compound hazard, significantly increasing the landslide risk in the studied corridor.

- Finite Element Modeling (FEM) using GTS NX proved effective in capturing realistic slope behavior, highlighting the importance of site-specific numerical modeling and the need for continuous geotechnical monitoring for sustainable slope management and design optimization.

5.2 RECOMMENDATIONS

Based on the analysis, laboratory findings, and numerical modeling results, the following engineering recommendations are proposed to improve slope stability and mitigate failure risks:

- Surface and Subsurface Drainage
  Implement surface catch drains and subsurface drainage systems (e.g., perforated pipes, trench drains) to minimize water infiltration and reduce pore water pressure buildup within the slope mass.

- Vegetative Protection
  Encourage the use of vegetation cover and bioengineering methods on exposed slopes to reduce surface erosion and enhance near-surface soil cohesion.

- Slope Geometry Modification
  Where feasible, adjust slope profiles through benching or flattening to decrease gravitational driving forces and enhance the Factor of Safety in high-risk zones.

- Monitoring and Early Warning Systems
  Install geotechnical monitoring instruments such as inclinometers, piezometers, and total station systems to detect slope movements, pore water pressure changes, and other failure indicators in real time.

- Seismic Design Integration
  Incorporate seismic parameters and dynamic analysis into slope design to ensure performance under earthquake loading. Slope stabilization strategies should explicitly account for the regional seismic hazard profile.

- Site-Specific Modeling and Data Validation
  Ensure that numerical models are consistently updated and validated using reliable field investigation data. Periodic recalibration using real-time monitoring results is essential for accurate forecasting and risk management.

REFERENCE

RWANDA TRANSPORT DEVELOPMENT AGENCY (RTDA). (2022). FEEDER ROADS DEVELOPMENT PROJECT (FRDP). kigali: RWANDA TRANSPORT DEVELOPMENT AGENCY (RTDA).

Affairs, M. o. (2015). THE NATIONAL RISK ATLAS OF RWANDA. kigali: MIDIMAR.

Alexandria. (September 1986). Soil Mechanics. virginia: NAVAL FACILITIES ENGINEERING COMMAND PUBLICATIONS TRANSMITTAL.

Arjun Tirkey, B. Y. (2023). STABILITY ANALYSIS OF OVERBURDEN DUMP SLOPE . International Research Journal of Modernization in Engineering Technology and Science , 4.

B.NADI, F. (2014). SEISMIC PERFORMANCE OF SLOPES IN PSEUDO-STATIC DESIGNS WITH DIFFERENT SAFETY FACTORS. researchgate, 12.

Boruah, P. P. (27 June 2024). researchgate. A Systematic Review on Slope Stability and Deformation Analysis Subjected to Rainfall and Earthquake, 1-16.

C.VENKATRAMAIAH. (2006). GEOTECHNICAL ENGINEERING. NEW DELHI: New Age International (P) Ltd.

charfeldine, M. (2015). Slope stability analysis report. reseachgate, 9.

DAS, B. M. (2010). Principles of Geotechnical Engineering. Stamford: Cengage Learning Customer & Sales Support,.

Editorial, K. (2020, 10 21). KIGALI TODAY. Retrieved from KIGALITODY.COM: https://www.kigalitoday.com/amakuru/amakuru-mu-rwanda/article/umuhanda-kigali-karongi-nyamasheke-rusizi-nturi-nyabagendwa

Engineers®, U. A. (2003). Engineering and Design SLOPE STABILITY. Washington,: DEPARTMENT OF THE ARMY U.S. Army Corps of Engineers .

Griffiths, D. V. (1999). Slope Stability Analysis by Finite Elements.

HAN, T. N. (2021). THE EFFECTS OF SOIL STRENGTH AND SLOPE GEOMETRY PARAMETERS ON SLOPE STABILITY.

IT, M. (2023). GTS NX User Manual. Retrieved from MIDAS Information Technology Co., Ltd: https://www.midasuser.com/GTSNX

J. Michael Duncan, S. G. (2014). Soil Strength and Slope Stability. canada: John Wiley & Sons, Inc., Hoboken, New Jersey.

Kleyn, E. G. (1983). The Application of the Pavement DCP to Determine. Trondheim, Norway.: Proceedings of the International.

LANE, D. V. (1999). Slope stability analysis by finite elements. GeÂotechnique 49, 14.

LARSSON, L. (2018). Slope Stability Evaluation from a Risk Management Perspective. Stockholm: KTH Royal Institute of Technology.

Livneh, M. (1987). The Use of the Dynamic Cone Penetrometer for the Design of Road. Transportation Research Record.

Look, B. G. (2007). Handbook of Geotechnical Investigation and Design Tables. London: Taylor & Francis Group, .

manual, N. G. (2014). SLOPE STABILITY ANALYSIS. newyork.

MININFRA. (2018). DISASTER EFFECTS SITUATION REPORT FROM 3 TO 22 MAY 2023. KIGALI: 2018.

Nikolaides, A. (2015). Highway Engineering Pavements, Materials and Control of Quality. us: Taylor & Francis Group, LLC.

NKURUNZIZA, M. (2024, January 11). News times. Retrieved from The ews times: https://www.newtimes.co.rw/article/13796/news/environment/what-next-after-heavy-rain-

NX, G. (2020). 3D Slope Stability . Beiging: GTS Nx.

NX, G. (2020). SD SLOPE STABILTY. GTS NX TEAM.

ongcheezen. (2005). slope stability analysis. UNIMAS.

Partha Pratim Boruah, J. T. (2024). A Systematic Review on Slope Stability and Deformation Analysis Subjected to Rainfall and Earthquake. Geotechnical Engineering Journal of the SEAGS & AGSSEA, 14.

Partha Pratim Boruah, V. R. (2025). A Parametric Study of a Vulnerable Slope Subjected to Rainfall Infiltration and Earthquakes in Arunachal Pradesh India . Reseachgate, 5.

REMA. (2018). Landslide Risks Assessment and Mitigation in Four Urban Sub-Catchments in Rwanda. KIGALI: REMA.

Shiferaw, H. M. (2021). Study on the influence of slope height and angle on the factor of safety and shape of failure of slopes based on strength reduction method of analysis. Beni-Suef University Journal of Basic and Applied Sciences, 5.

SHLASH, A. (2020). COMPARATIVE STUDY OF SLOPE STABILITY BY GEOTECHNICAL SOFTWARE PROGRAMS. NICOSIA.

APPENDIX-1: DCP TEST RESULTS

The DCP test was conducted on-site to investigate subsurface conditions. CBR values were calculated, and the shear strength parameters were interpreted accordingly the below are six point that done on the site .

CLIENT: Student project(Eric:221028015) **PROJECT : Slope stability analysis** **Project location : Huye-Nymagabe Road**						**TESTING DATE:** 26/05/2024 **POINT Number :** 1st Point		
Point number : 1								
Depth (m)	Cumulative Blows	ΔBlows	Penetration (mm)	DCPI (mm/blow)	CBR (%)	Cohesion (kPa)	Friction Angle (°)	Modulus E (MPa)
0.1	10	10	100		563.33	169.00	76.33	1013.91
0.2	22	12	100	8.33	27.76	8.33	22.78	147.66
0.3	35	13	100	7.69	30.73	9.22	23.07	157.58
0.4	51	16	100	6.25	40.00	12.00	24.00	186.55
0.5	68	17	100	5.88	43.20	12.96	24.32	195.98
0.6	80	12	100	8.33	27.76	8.33	22.78	147.66
0.7	86	6	100	16.67	11.51	3.45	21.15	84.06
0.8	88	2	100	50.00	2.85	0.86	20.29	34.42
0.9	91	3	100	33.33	4.77	1.43	20.48	47.85
1	95	4	100	25.00	6.88	2.06	20.69	60.46
1.1	99	4	100	25.00	6.88	2.06	20.69	60.46
1.2	106	7	100	14.29	14.00	4.20	21.40	95.28
1.3	118	12	100	8.33	27.76	8.33	22.78	147.66
1.4	131	13	100	7.69	30.73	9.22	23.07	157.58
1.5	143	12	100	8.33	27.76	8.33	22.78	147.66

1.6	154	11	100	9.09	24.85	7.46	22.49	137.57
1.7	161	7	100	14.29	14.00	4.20	21.40	95.28
1.8	173	12	100	8.33	27.76	8.33	22.78	147.66
1.9	183	10	100	10.00	22.02	6.61	22.20	127.32
2	191	8	100	12.50	16.58	4.98	21.66	106.20
2.1	201	10	100	10.00	22.02	6.61	22.20	127.32
2.2	212	11	100	9.09	24.85	7.46	22.49	137.57
2.3	224	12	100	8.33	27.76	8.33	22.78	147.66
2.4	234	10	100	10.00	22.02	6.61	22.20	127.32
2.5	250	16	100	6.25	40.00	12.00	24.00	186.55
2.6	270	20	100	5.00	53.10	15.93	25.31	223.65
2.7	290	20	100	5.00	53.10	15.93	25.31	223.65
2.8	309	19	100	5.26	49.75	14.93	24.98	214.52
2.9	329	20	100	5.00	53.10	15.93	25.31	223.65
3	347	18	100	5.56	46.45	13.93	24.64	205.30
3.1	368	21	100	4.76	56.49	16.95	25.65	232.70
3.2	386	18	100	5.56	46.45	13.93	24.64	205.30
3.3	403	17	100	5.88	43.20	12.96	24.32	195.98
3.4	419	16	100	6.25	40.00	12.00	24.00	186.55
3.5	436	17	100	5.88	43.20	12.96	24.32	195.98
3.6	448	12	100	8.33	27.76	8.33	22.78	147.66
3.7	460	12	100	8.33	27.76	8.33	22.78	147.66
3.8	478	18	100	5.56	46.45	13.93	24.64	205.30
3.9	494	16	100	6.25	40.00	12.00	24.00	186.55
4	514	20	100	5.00	53.10	15.93	25.31	223.65
4.1	535	21	100	4.76	56.49	16.95	25.65	232.70
4.2	555	20	100	5.00	53.10	15.93	25.31	223.65
4.3	576	21	100	4.76	56.49	16.95	25.65	232.70
4.4	597	21	100	4.76	56.49	16.95	25.65	232.70
4.5	616	19	100	5.26	49.75	14.93	24.98	214.52
4.6	635	19	100	5.26	49.75	14.93	24.98	214.52

4.7	665	30	100	3.33	88.86	26.66	28.89	310.96
4.8	694	29	100	3.45	85.12	25.54	28.51	302.50
4.9	723	29	100	3.45	85.12	25.54	28.51	302.50
5	752	29	100	3.45	85.12	25.54	28.51	302.50
5.1	782	30	100	3.33	88.86	26.66	28.89	310.96
5.2	812	30	100	3.33	88.86	26.66	28.89	310.96
5.3	844	32	100	3.13	96.45	28.94	29.65	327.70
5.4	875	31	100	3.23	92.64	27.79	29.26	319.35
5.5	907	32	100	3.13	96.45	28.94	29.65	327.70
5.6	940	33	100	3.03	100.30	30.09	30.03	336.00
5.7	972	32	100	3.13	96.45	28.94	29.65	327.70
5.8	1003	31	100	3.23	92.64	27.79	29.26	319.35
5.9	1035	32	100	3.13	96.45	28.94	29.65	327.70

CLIENT: Student project(Eric:221028015) **PROJECT : Slope stability analysis** **Project location : Huye-Nymagabe Road**	**TESTING DATE:** 26/05/2024 **POINT Number :** 3rd Point

Point number : 2

Depth (m)	Cumulative Blows	ΔBlows	Penetration (mm)	DCPI (mm/blow)	CBR (%)	Cohesion (kPa)	Friction Angle (°)	Modulus E (MPa)
0.1	6	6	100		563.33	169.00	76.33	1013.91
0.2	16	10	100	10.00	22.02	6.61	22.20	127.32
0.3	27	11	100	9.09	24.85	7.46	22.49	137.57
0.4	34	7	100	14.29	14.00	4.20	21.40	95.28
0.5	38	4	100	25.00	6.88	2.06	20.69	60.46
0.6	41	3	100	33.33	4.77	1.43	20.48	47.85

0.7	47	6	100	16.67	11.51	3.45	21.15	84.06
0.8	51	4	100	25.00	6.88	2.06	20.69	60.46
0.9	54	3	100	33.33	4.77	1.43	20.48	47.85
1	60	6	100	16.67	11.51	3.45	21.15	84.06
1.1	67	7	100	14.29	14.00	4.20	21.40	95.28
1.2	76	9	100	11.11	19.26	5.78	21.93	116.87
1.3	87	11	100	9.09	24.85	7.46	22.49	137.57
1.4	100	13	100	7.69	30.73	9.22	23.07	157.58
1.5	114	14	100	7.14	33.76	10.13	23.38	167.37
1.6	126	12	100	8.33	27.76	8.33	22.78	147.66
1.7	138	12	100	8.33	27.76	8.33	22.78	147.66
1.8	150	12	100	8.33	27.76	8.33	22.78	147.66
1.9	161	11	100	9.09	24.85	7.46	22.49	137.57
2	171	10	100	10.00	22.02	6.61	22.20	127.32
2.1	183	12	100	8.33	27.76	8.33	22.78	147.66
2.2	194	11	100	9.09	24.85	7.46	22.49	137.57
2.3	203	9	100	11.11	19.26	5.78	21.93	116.87
2.4	212	9	100	11.11	19.26	5.78	21.93	116.87
2.5	223	11	100	9.09	24.85	7.46	22.49	137.57
2.6	234	11	100	9.09	24.85	7.46	22.49	137.57
2.7	240	6	100	16.67	11.51	3.45	21.15	84.06
2.8	247	7	100	14.29	14.00	4.20	21.40	95.28
2.9	257	10	100	10.00	22.02	6.61	22.20	127.32
3	263	6	100	16.67	11.51	3.45	21.15	84.06
3.1	269	6	100	16.67	11.51	3.45	21.15	84.06
3.2	275	6	100	16.67	11.51	3.45	21.15	84.06
3.3	280	5	100	20.00	9.13	2.74	20.91	72.48
3.4	286	6	100	16.67	11.51	3.45	21.15	84.06
3.5	290	4	100	25.00	6.88	2.06	20.69	60.46
3.6	294	4	100	25.00	6.88	2.06	20.69	60.46
3.7	299	5	100	20.00	9.13	2.74	20.91	72.48

3.8	306	7	100	14.29	14.00	4.20	21.40	95.28
3.9	316	10	100	10.00	22.02	6.61	22.20	127.32
4	328	12	100	8.33	27.76	8.33	22.78	147.66
4.1	341	13	100	7.69	30.73	9.22	23.07	157.58
4.2	354	13	100	7.69	30.73	9.22	23.07	157.58
4.3	368	14	100	7.14	33.76	10.13	23.38	167.37
4.4	383	15	100	6.67	36.85	11.05	23.68	177.02
4.5	399	16	100	6.25	40.00	12.00	24.00	186.55
4.6	424	25	100	4.00	70.50	21.15	27.05	268.13
4.7	448	24	100	4.17	66.93	20.08	26.69	259.38
4.8	472	24	100	4.17	66.93	20.08	26.69	259.38
4.9	497	25	100	4.00	70.50	21.15	27.05	268.13
5	522	25	100	4.00	70.50	21.15	27.05	268.13
5.1	548	26	100	3.85	74.10	22.23	27.41	276.81
5.2	575	27	100	3.70	77.73	23.32	27.77	285.43
5.3	603	28	100	3.57	81.41	24.42	28.14	294.00
5.4	632	29	100	3.45	85.12	25.54	28.51	302.50
5.5	662	30	100	3.33	88.86	26.66	28.89	310.96
5.6	693	31	100	3.23	92.64	27.79	29.26	319.35
5.7	725	32	100	3.13	96.45	28.94	29.65	327.70
5.8	758	33	100	3.03	100.30	30.09	30.03	336.00
5.9	791	33	100	3.03	100.30	30.09	30.03	336.00
6	825	34	100	2.94	104.17	31.25	30.42	344.26
6.1	860	35	100	2.86	108.08	32.42	30.81	352.46
6.2	895	35	100	2.86	108.08	32.42	30.81	352.46
6.3	931	36	100	2.78	112.02	33.61	31.20	360.63

6.4	968	37	100	2.70	115.98	34.80	31.60	368.75
6.5	1005	37	100	2.70	115.98	34.80	31.60	368.75
6.6	1037	32	100	3.13	96.45	28.94	29.65	327.70
6.7	1071	34	100	2.94	104.17	31.25	30.42	344.26
6.8	1104	33	100	3.03	100.30	30.09	30.03	336.00
6.9	1140	36	100	2.78	112.02	33.61	31.20	360.63

CLIENT: Student project(Eric:221028015)	**TESTING DATE:** 26/05/2024
PROJECT : Slope stability analysis	**POINT Number :** 3rd Point
Project location : Huye-Nymagabe Road	

Point number : 3								
Depth (m)	Cumulative Blows	ΔBlows	Penetration (mm)	DCPI (mm/blow)	CBR (%)	Cohesion (kPa)	Friction Angle (°)	Modulus E (MPa)
0.1	6	6	100					
0.2	16	10	100	10.00	22.02	6.61	22.20	127.32
0.3	27	11	100	9.09	24.85	7.46	22.49	137.57
0.4	34	7	100	14.29	14.00	4.20	21.40	95.28
0.5	38	4	100	25.00	6.88	2.06	20.69	60.46
0.6	41	3	100	33.33	4.77	1.43	20.48	47.85

0.7	47	6	100	16.67	11.51	3.45	21.15	84.06
0.8	51	4	100	25.00	6.88	2.06	20.69	60.46
0.9	54	3	100	33.33	4.77	1.43	20.48	47.85
1	60	6	100	16.67	11.51	3.45	21.15	84.06
1.1	67	7	100	14.29	14.00	4.20	21.40	95.28
1.2	76	9	100	11.11	19.26	5.78	21.93	116.87
1.3	87	11	100	9.09	24.85	7.46	22.49	137.57
1.4	100	13	100	7.69	30.73	9.22	23.07	157.58
1.5	114	14	100	7.14	33.76	10.13	23.38	167.37
1.6	126	12	100	8.33	27.76	8.33	22.78	147.66
1.7	138	12	100	8.33	27.76	8.33	22.78	147.66
1.8	150	12	100	8.33	27.76	8.33	22.78	147.66
1.9	161	11	100	9.09	24.85	7.46	22.49	137.57
2	171	10	100	10.00	22.02	6.61	22.20	127.32
2.1	183	12	100	8.33	27.76	8.33	22.78	147.66
2.2	194	11	100	9.09	24.85	7.46	22.49	137.57
2.3	203	9	100	11.11	19.26	5.78	21.93	116.87
2.4	212	9	100	11.11	19.26	5.78	21.93	116.87
2.5	223	11	100	9.09	24.85	7.46	22.49	137.57
2.6	234	11	100	9.09	24.85	7.46	22.49	137.57
2.7	240	6	100	16.67	11.51	3.45	21.15	84.06
2.8	247	7	100	14.29	14.00	4.20	21.40	95.28
2.9	257	10	100	10.00	22.02	6.61	22.20	127.32
3	263	6	100	16.67	11.51	3.45	21.15	84.06
3.1	269	6	100	16.67	11.51	3.45	21.15	84.06
3.2	275	6	100	16.67	11.51	3.45	21.15	84.06
3.3	280	5	100	20.00	9.13	2.74	20.91	72.48
3.4	286	6	100	16.67	11.51	3.45	21.15	84.06
3.5	290	4	100	25.00	6.88	2.06	20.69	60.46
3.6	294	4	100	25.00	6.88	2.06	20.69	60.46
3.7	299	5	100	20.00	9.13	2.74	20.91	72.48

3.8	306	7	100	14.29	14.00	4.20	21.40	95.28
3.9	316	10	100	10.00	22.02	6.61	22.20	127.32
4	328	12	100	8.33	27.76	8.33	22.78	147.66
4.1	341	13	100	7.69	30.73	9.22	23.07	157.58
4.2	354	13	100	7.69	30.73	9.22	23.07	157.58
4.3	368	14	100	7.14	33.76	10.13	23.38	167.37
4.4	383	15	100	6.67	36.85	11.05	23.68	177.02
4.5	399	16	100	6.25	40.00	12.00	24.00	186.55
4.6	415	16	100	6.25	40.00	12.00	24.00	186.55
4.7	434	19	100	5.26	49.75	14.93	24.98	214.52
4.8	460	26	100	3.85	74.10	22.23	27.41	276.81
4.9	486	26	100	3.85	74.10	22.23	27.41	276.81
5	518	32	100	3.13	96.45	28.94	29.65	327.70
5.1	553	35	100	2.86	108.08	32.42	30.81	352.46
5.2	590	37	100	2.70	115.98	34.80	31.60	368.75
5.3	626	36	100	2.78	112.02	33.61	31.20	360.63
5.4	662	36	100	2.78	112.02	33.61	31.20	360.63
5.5	692	30	100	3.33	88.86	26.66	28.89	310.96
5.6	724	32	100	3.13	96.45	28.94	29.65	327.70
5.7	755	31	100	3.23	92.64	27.79	29.26	319.35
5.8	787	32	100	3.13	96.45	28.94	29.65	327.70
5.9	820	33	100	3.03	100.30	30.09	30.03	336.00
6	854	34	100	2.94	104.17	31.25	30.42	344.26
6.1	884	30	100	3.33	88.86	26.66	28.89	310.96
6.2	919	35	100	2.86	108.08	32.42	30.81	352.46

6.3	957	38	100	2.63	119.98	35.99	32.00	376.83
6.4	995	38	100	2.63	119.98	35.99	32.00	376.83
6.5	1027	32	100	3.13	96.45	28.94	29.65	327.70
6.6	1062	35	100	2.86	108.08	32.42	30.81	352.46
6.7	1094	32	100	3.13	96.45	28.94	29.65	327.70
6.8	1128	34	100	2.94	104.17	31.25	30.42	344.26
6.9	1162	34	100	2.94	104.17	31.25	30.42	344.26

CLIENT: Student project(Eric:221028015) **PROJECT : Slope stability analysis** **Project location : Huye-Nymagabe Road**	**TESTING DATE:** 26/05/2024 **POINT Number :** 4th Point

Point number : 5								
Depth (m)	Cumulative Blows	ΔBlows	Penetration (mm)	DCPI (mm/blow)	CBR (%)	Cohesion (kPa)	Friction Angle (°)	Modulus E (MPa)
0.1	17	17	100		563.33	169.00	76.33	1013.91
0.2	33	16	100	6.25	40.00	12.00	24.00	186.55
0.3	51	18	100	5.56	46.45	13.93	24.64	205.30
0.4	70	19	100	5.26	49.75	14.93	24.98	214.52
0.5	88	18	100	5.56	46.45	13.93	24.64	205.30
0.6	101	13	100	7.69	30.73	9.22	23.07	157.58
0.7	109	8	100	12.50	16.58	4.98	21.66	106.20
0.8	117	8	100	12.50	16.58	4.98	21.66	106.20

0.9	125	8	100	12.50	16.58	4.98	21.66	106.20
1	132	7	100	14.29	14.00	4.20	21.40	95.28
1.1	138	6	100	16.67	11.51	3.45	21.15	84.06
1.2	142	4	100	25.00	6.88	2.06	20.69	60.46
1.3	148	6	100	16.67	11.51	3.45	21.15	84.06
1.4	156	8	100	12.50	16.58	4.98	21.66	106.20
1.5	163	7	100	14.29	14.00	4.20	21.40	95.28
1.6	171	8	100	12.50	16.58	4.98	21.66	106.20
1.7	181	10	100	10.00	22.02	6.61	22.20	127.32
1.8	191	10	100	10.00	22.02	6.61	22.20	127.32
1.9	201	10	100	10.00	22.02	6.61	22.20	127.32
2	212	11	100	9.09	24.85	7.46	22.49	137.57
2.1	222	10	100	10.00	22.02	6.61	22.20	127.32
2.2	232	10	100	10.00	22.02	6.61	22.20	127.32
2.3	242	10	100	10.00	22.02	6.61	22.20	127.32
2.4	250	8	100	12.50	16.58	4.98	21.66	106.20
2.5	260	10	100	10.00	22.02	6.61	22.20	127.32
2.6	270	10	100	10.00	22.02	6.61	22.20	127.32
2.7	284	14	100	7.14	33.76	10.13	23.38	167.37
2.8	301	17	100	5.88	43.20	12.96	24.32	195.98
2.9	320	19	100	5.26	49.75	14.93	24.98	214.52
3	339	19	100	5.26	49.75	14.93	24.98	214.52
3.1	353	14	100	7.14	33.76	10.13	23.38	167.37
3.2	369	16	100	6.25	40.00	12.00	24.00	186.55
3.3	389	20	100	5.00	53.10	15.93	25.31	223.65
3.4	415	26	100	3.85	74.10	22.23	27.41	276.81
3.5	433	18	100	5.56	46.45	13.93	24.64	205.30
3.6	449	16	100	6.25	40.00	12.00	24.00	186.55
3.7	469	20	100	5.00	53.10	15.93	25.31	223.65
3.8	488	19	100	5.26	49.75	14.93	24.98	214.52
3.9	507	19	100	5.26	49.75	14.93	24.98	214.52

4	528	21	100	4.76	56.49	16.95	25.65	232.70
4.1	546	18	100	5.56	46.45	13.93	24.64	205.30
4.2	566	20	100	5.00	53.10	15.93	25.31	223.65
4.3	585	19	100	5.26	49.75	14.93	24.98	214.52
4.4	603	18	100	5.56	46.45	13.93	24.64	205.30
4.5	627	24	100	4.17	66.93	20.08	26.69	259.38
4.6	652	25	100	4.00	70.50	21.15	27.05	268.13
4.7	678	26	100	3.85	74.10	22.23	27.41	276.81
4.8	708	30	100	3.33	88.86	26.66	28.89	310.96
4.9	740	32	100	3.13	96.45	28.94	29.65	327.70
5	773	33	100	3.03	100.30	30.09	30.03	336.00
5.1	806	33	100	3.03	100.30	30.09	30.03	336.00
5.2	840	34	100	2.94	104.17	31.25	30.42	344.26
5.3	875	35	100	2.86	108.08	32.42	30.81	352.46
5.4	909	34	100	2.94	104.17	31.25	30.42	344.26
5.5	943	34	100	2.94	104.17	31.25	30.42	344.26
5.6	979	36	100	2.78	112.02	33.61	31.20	360.63
5.7	1015	36	100	2.78	112.02	33.61	31.20	360.63
5.8	1051	36	100	2.78	112.02	33.61	31.20	360.63
5.9	1088	37	100	2.70	115.98	34.80	31.60	368.75
6	1124	36	100	2.78	112.02	33.61	31.20	360.63

6.1	1159	35	100	2.86	108.08	32.42	30.81	352.46
6.2	1195	36	100	2.78	112.02	33.61	31.20	360.63
6.3	1231	36	100	2.78	112.02	33.61	31.20	360.63
6.4	1267	36	100	2.78	112.02	33.61	31.20	360.63
6.5	1303	36	100	2.78	112.02	33.61	31.20	360.63

CLIENT: Student project(Eric:221028015) **PROJECT : Slope stability analysis** **Project location : Huye-Nymagabe Road**	**TESTING DATE:** 26/05/2024 **POINT Number : 5th Point**

Point number : 6

Depth (m)	Cumulative Blows	ΔBlows	Penetration (mm)	DCPI (mm/blow)	CBR (%)	Cohesion (kPa)	Friction Angle (°)	Modulus E (MPa)
0.1	5	5	100		563.33	169.00	76.33	1013.91
0.2	17	12	100	8.33	27.76	8.33	22.78	147.66
0.3	32	15	100	6.67	36.85	11.05	23.68	177.02
0.4	40	8	100	12.50	16.58	4.98	21.66	106.20
0.5	48	8	100	12.50	16.58	4.98	21.66	106.20
0.6	56	8	100	12.50	16.58	4.98	21.66	106.20
0.7	63	7	100	14.29	14.00	4.20	21.40	95.28
0.8	68	5	100	20.00	9.13	2.74	20.91	72.48
0.9	74	6	100	16.67	11.51	3.45	21.15	84.06
1	82	8	100	12.50	16.58	4.98	21.66	106.20

1.1	90	8	100	12.50	16.58	4.98	21.66	106.20
1.2	98	8	100	12.50	16.58	4.98	21.66	106.20
1.3	106	8	100	12.50	16.58	4.98	21.66	106.20
1.4	113	7	100	14.29	14.00	4.20	21.40	95.28
1.5	121	8	100	12.50	16.58	4.98	21.66	106.20
1.6	133	12	100	8.33	27.76	8.33	22.78	147.66
1.7	145	12	100	8.33	27.76	8.33	22.78	147.66
1.8	163	18	100	5.56	46.45	13.93	24.64	205.30
1.9	181	18	100	5.56	46.45	13.93	24.64	205.30
2	196	15	100	6.67	36.85	11.05	23.68	177.02
2.1	212	16	100	6.25	40.00	12.00	24.00	186.55
2.2	229	17	100	5.88	43.20	12.96	24.32	195.98
2.3	243	14	100	7.14	33.76	10.13	23.38	167.37
2.4	258	15	100	6.67	36.85	11.05	23.68	177.02
2.5	273	15	100	6.67	36.85	11.05	23.68	177.02

CLIENT: Student project(Eric:221028015) **PROJECT : Slope stability analysis** **Project location : Huye-Nymagabe Road**								**TESTING DATE:** 26/05/2024 **POINT Number :** 6th Point
Point number : 7								
Depth (m)	Cumulative Blows	ΔBlows	Penetration (mm)	DCPI (mm/blow)	CBR (%)	Cohesion (kPa)	Friction Angle (°)	Modulus E (MPa)
0.1	10	10	100		563.33	169.00	76.33	1013.91
0.2	20	10	100	10.00	22.02	6.61	22.20	127.32
0.3	33	13	100	7.69	30.73	9.22	23.07	157.58
0.4	61	28	100	3.57	81.41	24.42	28.14	294.00
0.5	68	7	100	14.29	14.00	4.20	21.40	95.28

0.6	72	4	100	25.00	6.88	2.06	20.69	60.46
0.7	75	3	100	33.33	4.77	1.43	20.48	47.85
0.8	79	4	100	25.00	6.88	2.06	20.69	60.46
0.9	84	5	100	20.00	9.13	2.74	20.91	72.48
1	94	10	100	10.00	22.02	6.61	22.20	127.32
1.1	107	13	100	7.69	30.73	9.22	23.07	157.58
1.2	119	12	100	8.33	27.76	8.33	22.78	147.66
1.3	134	15	100	6.67	36.85	11.05	23.68	177.02
1.4	142	8	100	12.50	16.58	4.98	21.66	106.20
1.5	153	11	100	9.09	24.85	7.46	22.49	137.57
1.6	163	10	100	10.00	22.02	6.61	22.20	127.32
1.7	173	10	100	10.00	22.02	6.61	22.20	127.32
1.8	184	11	100	9.09	24.85	7.46	22.49	137.57
1.9	197	13	100	7.69	30.73	9.22	23.07	157.58
2	210	13	100	7.69	30.73	9.22	23.07	157.58
2.1	221	11	100	9.09	24.85	7.46	22.49	137.57
2.2	233	12	100	8.33	27.76	8.33	22.78	147.66
2.3	252	19	100	5.26	49.75	14.93	24.98	214.52
2.4	264	12	100	8.33	27.76	8.33	22.78	147.66
2.5	279	15	100	6.67	36.85	11.05	23.68	177.02
2.6	296	17	100	5.88	43.20	12.96	24.32	195.98
2.7	315	19	100	5.26	49.75	14.93	24.98	214.52
2.8	335	20	100	5.00	53.10	15.93	25.31	223.65
2.9	353	18	100	5.56	46.45	13.93	24.64	205.30
3	367	14	100	7.14	33.76	10.13	23.38	167.37
3.1	385	18	100	5.56	46.45	13.93	24.64	205.30
3.2	402	17	100	5.88	43.20	12.96	24.32	195.98
3.3	419	17	100	5.88	43.20	12.96	24.32	195.98
3.4	432	13	100	7.69	30.73	9.22	23.07	157.58
3.5	446	14	100	7.14	33.76	10.13	23.38	167.37
3.6	460	14	100	7.14	33.76	10.13	23.38	167.37

3.7	470	10	100	10.00	22.02	6.61	22.20	127.32
3.8	484	14	100	7.14	33.76	10.13	23.38	167.37
3.9	503	19	100	5.26	49.75	14.93	24.98	214.52
4	525	22	100	4.55	59.93	17.98	25.99	241.67
4.1	547	22	100	4.55	59.93	17.98	25.99	241.67
4.2	570	23	100	4.35	63.41	19.02	26.34	250.56
4.3	593	23	100	4.35	63.41	19.02	26.34	250.56
4.4	616	23	100	4.35	63.41	19.02	26.34	250.56
4.5	633	17	100	5.88	43.20	12.96	24.32	195.98
4.6	653	20	100	5.00	53.10	15.93	25.31	223.65
4.7	675	22	100	4.55	59.93	17.98	25.99	241.67
4.8	698	23	100	4.35	63.41	19.02	26.34	250.56
4.9	724	26	100	3.85	74.10	22.23	27.41	276.81
5	749	25	100	4.00	70.50	21.15	27.05	268.13
5.1	776	27	100	3.70	77.73	23.32	27.77	285.43
5.2	804	28	100	3.57	81.41	24.42	28.14	294.00
5.3	833	29	100	3.45	85.12	25.54	28.51	302.50
5.4	863	30	100	3.33	88.86	26.66	28.89	310.96
5.5	894	31	100	3.23	92.64	27.79	29.26	319.35
5.6	927	33	100	3.03	100.30	30.09	30.03	336.00
5.7	959	32	100	3.13	96.45	28.94	29.65	327.70
5.8	991	32	100	3.13	96.45	28.94	29.65	327.70
5.9	1024	33	100	3.03	100.30	30.09	30.03	336.00
6	1058	34	100	2.94	104.17	31.25	30.42	344.26
6.1	1092	34	100	2.94	104.17	31.25	30.42	344.26
6.2	1126	34	100	2.94	104.17	31.25	30.42	344.26

6.3	1161	35	100	2.86	108.08	32.42	30.81	352.46
6.4	1196	35	100	2.86	108.08	32.42	30.81	352.46
6.5	1232	36	100	2.78	112.02	33.61	31.20	360.63

APPENDIX-2: CLASSIFICATION TESTS RESULTS

Classification tests sieve analysis and Atterberg limit both performed on disturbed sample.

RWANDA POLYTECHNIC

IPRC HUYE
Integrated Polytechnic Regional College

P.o.Box 575 HUYE-Rwanda
Tel:+250255119248
Email: info@iprchuye.rp.ac.rw
www.iprchuye.rp.ac.rw

DETERMINATION OF ATTERBERG LIMITS
Test method BS 1377 : 1990 : Part 2 : Clause 4.5 , 5 and 6.5
TEST DATA AND REPORT

Client:	*Eric*
Project name/ location	*slope stability analysis*
Sampling depth(m)/Coordinates	*2.45-2.85*
Source of sample/Sample description	*n/a -P1*
Sampling date	*28/09/2024*
Test date	*5/10/2024*

TEST DATA

LIQUIDITY LIMITS (WL)

Number of Blows	17	21	27	33
can N°	A	B	C	D
Wet Weight + Can (g)	56.55	60.34	53.83	56.44
Dry Weight + can (g)	48.61	51.19	47.53	40.82
Weight of Water (g)	7.94	9.14	6.31	15.62
Weight of the can (g)	36.98	37.17	37.10	13.10
Weight of wet soil (g)	19.57	23.17	16.73	43.35
Weight of Dry Soil (g)	11.63	14.02	10.42	27.73
Moisture Content (%)	68.2	65.2	60.5	56.3

PLASTIC LIMIT (Wp)

Wet Weight + can (g)	32.1	31.5	Average:
Dry Weight + can (g)	27.6	27.2	27.3595
Weight of the can (g)	13.1	13.1	13.104
Weight of Dry Soil (g)	14.5	14.0	14.2555
Weight of wet soil (g)	19.1	18.3	18.696
Weight of Water (g)	4.6	4.3	4.4405
Moisture Content (%)	31.44	30.85	**31.14**

SHRINKAGE LIMIT

Original length of the specimen, Lo,mm	140
length of the oven-dry specimen,LD,mm	124
Percentage passing 425 µm sieve	**64.65**
Percentage linear shrinkage: $\frac{L_0 - L_D}{L_0} \times 100$	**11.43**

TEST REPORT

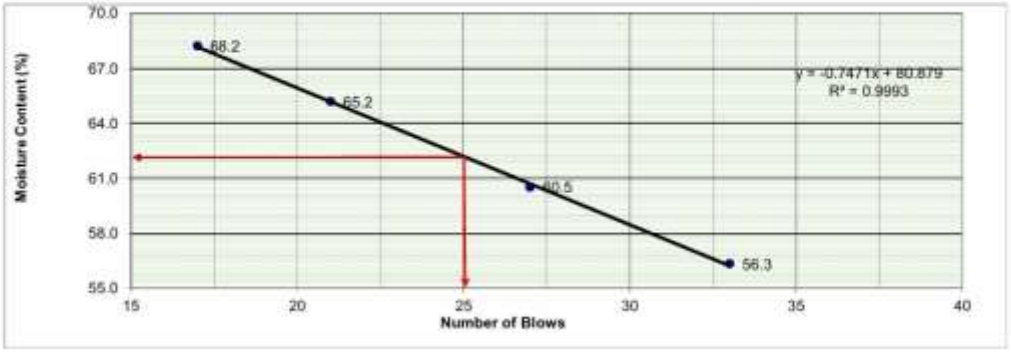

TEST SUMMARY

Liquidity Limit (WL) =	62.58	Plasticity Limit (Wp) =	31.1	Plasticity Index (Ip) =	31

Plasticity chart for the classification of fine soils and the finer part of coarse soils

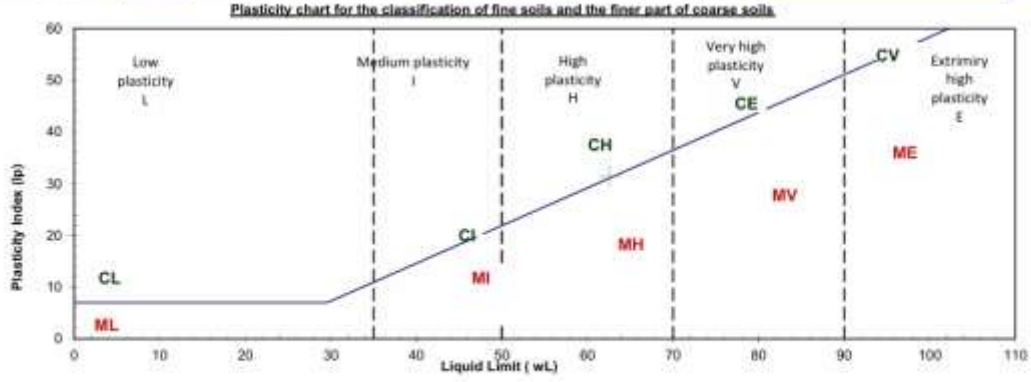

Done by:
Eng.NIYIGENA Eric
Laboratory Technician

RWANDA POLYTECHNIC

IPRC HUYE
Integrated Polytechnic Regional College

P.o.Box 575 HUYE-Rwanda
Tel:+250255119248
Email: info@iprchuye.rp.ac.rw
www.iprchuye.rp.ac.rw

DETERMINATION OF ATTERBERG LIMITS
Test method BS 1377 : 1990 : Part 2 : Clause 4.5 , 5 and 6.5
TEST DATA AND REPORT

Client:	*Eric*
Project name/ location	*slope stability analysis*
Sampling depth(m)/Coordinates	*2.45-2.85*
Source of sample/Sample description	*n/a -P2*
Sampling date	*28/09/2024*
Test date	*5/10/2024*

TEST DATA

LIQUIDITY LIMITS (WL)

Number of Blows	16	21	27	33
can N°	A	B	C	D
Wet Weight + Can (g)	64.54	62.25	54.66	38.40
Dry Weight + can (g)	53.26	52.36	48.06	28.99
Weight of Water (g)	11.28	9.89	6.60	9.41
Weight of the can (g)	36.98	37.17	37.10	13.10
Weight of wet soil (g)	27.56	25.08	17.55	25.31
Weight of Dry Soil (g)	16.28	15.19	10.95	15.90
Moisture Content (%)	69.3	65.1	60.2	59.2

PLASTIC LIMIT (Wp)

Wet Weight + can (g)	33.5	33.5	Average:
Dry Weight + can (g)	28.5	28.3	28.3595
Weight of the can (g)	13.1	13.1	13.104
Weight of Dry Soil (g)	15.4	15.1	15.2555
Weight of wet soil (g)	20.4	20.3	20.362
Weight of Water (g)	5.0	5.2	5.1065
Moisture Content (%)	32.40	34.56	33.48

SHRINKAGE LIMIT

Original length of the specimen, Lo,mm	140
length of the oven-dry specimen,LD,mm	126
Percentage passing 425 µm sieve	68.72
Percentage linear shrinkage $(1-\frac{LD}{LO})X\ 100$	10.00

TEST REPORT

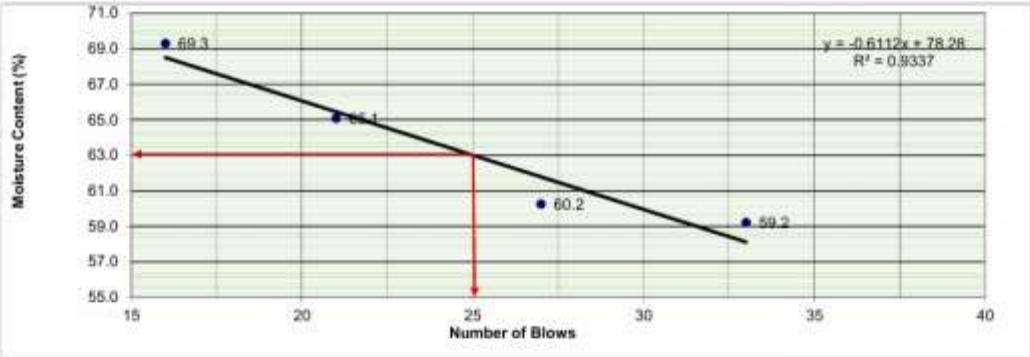

TEST SUMMARY

Liquidity Limit (WL) =	63.46	Plasticity Limit (Wp) =	33.5	Plasticity Index (Ip) =	30

Plasticity chart for the classification of fine soils and the finer part of coarse soils

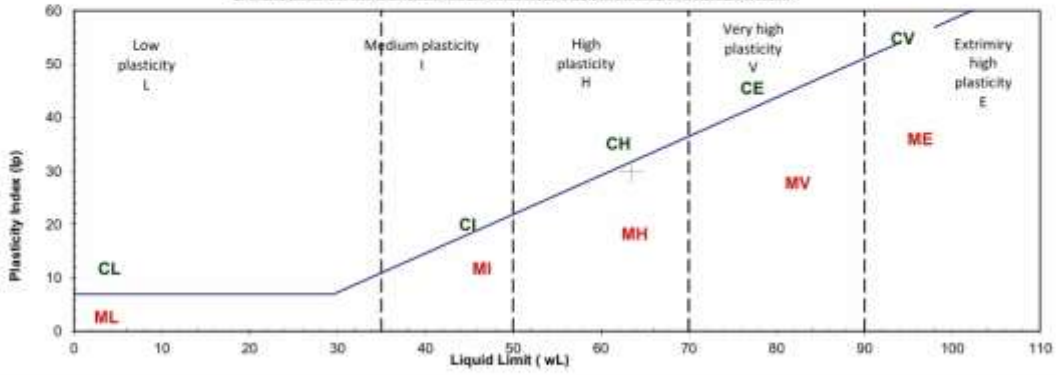

Done by:
Eng.NIYIGENA Eric
Laboratory Technician

RWANDA POLYTECHNIC

IPRC HUYE
Integrated Polytechnic Regional College

P.o.Box 575 HUYE-Rwanda
Tel:+250255119248
Email: info@iprchuye.rp.ac.rw
www.iprchuye.rp.ac.rw

DETERMINATION OF ATTERBERG LIMITS

Test method BS 1377 : 1990 : Part 2 : Clause 4.5 , 5 and 6.5

TEST DATA AND REPORT

Client:	*Eric*
Project name/ location	*slope stability analysis*
Sampling depth(m)/Coordinates	*2.45-2.85*
Source of sample/Sample description	*n/a -P3*
Sampling date	*28/09/2024*
Test date	*5/10/2024*

TEST DATA

LIQUIDITY LIMITS (WL)

Number of Blows	16	21	27	33
can N°	A	B	C	D
Wet Weight + Can (g)	54.46	67.56	50.43	56.44
Dry Weight + can (g)	48.34	57.36	46.06	42.72
Weight of Water (g)	6.12	10.19	4.38	13.72
Weight of the can (g)	36.98	37.17	37.10	13.10
Weight of wet soil (g)	17.48	30.39	13.33	43.35
Weight of Dry Soil (g)	11.36	20.19	8.95	29.63
Moisture Content (%)	53.9	50.5	48.9	46.3

PLASTIC LIMIT (Wp)

Wet Weight + can (g)	32.4	31.5	Average:
Dry Weight + can (g)	28.4	27.8	28.0595
Weight of the can (g)	13.1	13.1	13.104
Weight of Dry Soil (g)	15.3	14.6	14.9555
Weight of wet soil (g)	19.3	18.3	18.842
Weight of Water (g)	4.0	3.7	3.8865
Moisture Content (%)	26.47	25.48	25.98

SHRINKAGE LIMIT

Original length of the specimen, Lo,mm	140
length of the oven-dry specimen,LD,mm	128
Percentage passing 425 µm sieve	63.71
Percentage linear shrinkage: $\left(1-\frac{LD}{LO}\right)LF\ 100$	8.57

TEST REPORT

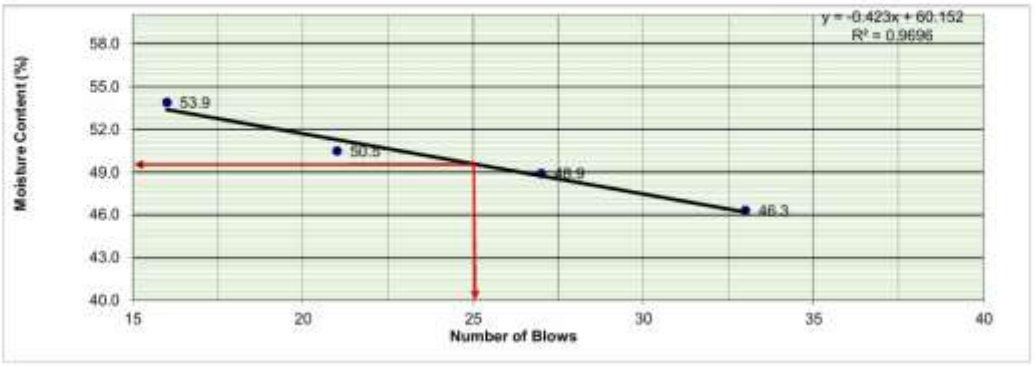

TEST SUMMARY

Liquidity Limit (WL) =	49.89	Plasticity Limit (Wp) =	26.0	Plasticity Index (Ip) =	24

Plasticity chart for the classification of fine soils and the finer part of coarse soils

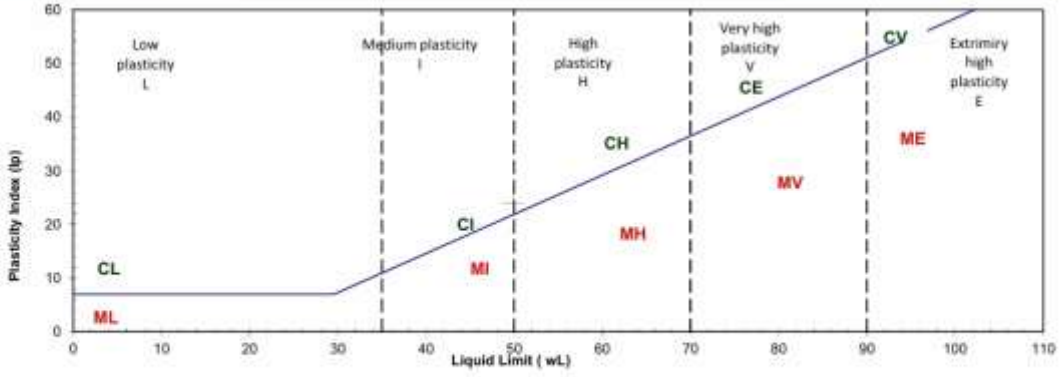

Done by:
Eng.NIYIGENA Eric
Laboratory Technician

Civil Engineering Laboratory
Determination of particles size distribution
Wet sieving method - tested in accordance with BS 1377-2:1990: Clause 9 (procedure 9.2.4)

Client: Student project(Eric:221028015)			**Sampling date:**09/01/2025
Project name: Slope stability analysis			**Testing date:**18-20/01/2025
Source of sample/Location: Pit-1			**Weight After washing (g)** 157.6
Initial weight (g):	388.6		
Ref: Test Civ_Lab_250108_002			**Retaining Wall N°:** 1

Sieve Size(mm)	Weight of empty sieve(g)	Weight of sieve +retained sample (g)	Partial Retained (g)	Cum Retained (g)	% Retained	% Of passing
50.000	1183.2	1183.2	0	0	0.00	100.00
37.500	1513.4	1513.4	0	0	0.00	100.00
28.000	1143.2	1143.2	0	0	0.00	100.00
20.000	1037.2	1037.2	0	0	0.00	100.00
14.000	1130.0	1130.0	0.0	0.0	0.00	100.00
10.000	1216.8	1216.8	0.0	0.0	0.00	100.00
6.300	1128.8	1128.8	0.0	0.0	0.00	100.00
4.750	1124.6	1124.6	0.0	0.0	0.00	100.00
3.350	417.0	427.8	10.8	10.8	2.78	97.22
2.000	529.0	541.8	12.8	23.6	6.07	93.93
1.180	527.4	535.4	8.0	31.6	8.13	91.87
0.600	513.2	520.0	6.8	38.4	9.88	90.12
0.425	434.6	439.6	5.0	43.4	11.17	88.83
0.300	422.6	438.4	15.8	59.2	15.23	84.77
0.212	412.6	424.8	12.2	71.4	18.37	81.63
0.150	436.4	459.8	23.4	94.8	24.40	75.60
0.075	554	608.6	54.6	149.4	38.45	61.55
0.050					32.00	68.00
0.020					34.00	66.00
0.010					38.00	62.00
0.005					40.00	60.00
0.002					53.00	47.00
0.001					54.00	46.00

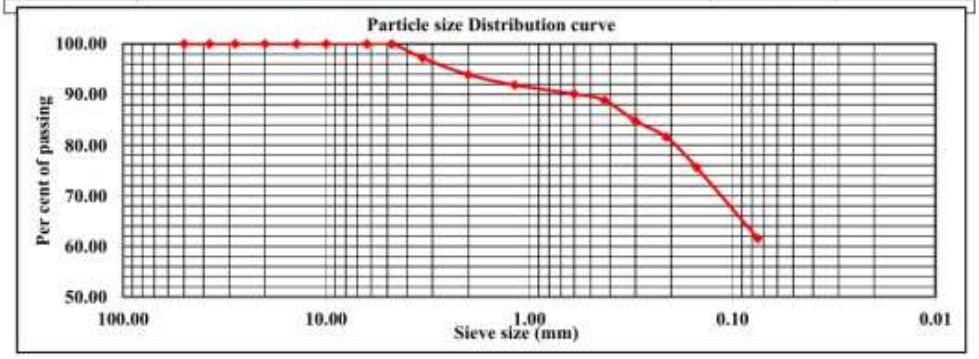

Note: 1.Material passes on 75 µm sieve size is greater than 10 % hydrometer method recommended.

Done by:

Eng.NIYIGENA Eric

Civil Engineering Laboratory
Determination of particles size distribution
Wet sieving method - tested in accordance with BS 1377-2:1990: Clause 9 (procedure 9.2.4)

Client: Student project(Eric:221028015)			**Sampling date:**09/01/2025
Project name: Slope stability analysis			**Testing date:**18-20/01/2025
Source of sample/Location: Pit-1			**Weight After washing (g)** 157.6
Initial weight (g):	388.6		
Ref: Test Civ_Lab_250108_002			**Retaining Wall N°:** 1

Sieve Size(mm)	Weight of empty sieve(g)	Weight of sieve +retained sample (g)	Partial Retained (g)	Cum Retained (g)	% Retained	% Of passing
50.000	1183.2	1183.2	0	0	0.00	100.00
37.500	1513.4	1513.4	0	0	0.00	100.00
28.000	1143.2	1143.2	0	0	0.00	100.00
20.000	1037.2	1037.2	0	0	0.00	100.00
14.000	1130.0	1130.0	0.0	0.0	0.00	100.00
10.000	1216.8	1216.8	0.0	0.0	0.00	100.00
6.300	1128.8	1128.8	0.0	0.0	0.00	100.00
4.750	1124.6	1124.6	0.0	0.0	0.00	100.00
3.350	417.0	427.8	10.8	10.8	2.78	97.22
2.000	529.0	541.8	12.8	23.6	6.07	93.93
1.180	527.4	535.4	8.0	31.6	8.13	91.87
0.600	513.2	520.0	6.8	38.4	9.88	90.12
0.425	434.6	439.6	5.0	43.4	11.17	88.83
0.300	422.6	438.4	15.8	59.2	15.23	84.77
0.212	412.6	424.8	12.2	71.4	18.37	81.63
0.150	436.4	459.8	23.4	94.8	24.40	75.60
0.075	554	608.6	54.6	149.4	38.45	61.55
0.050					32.00	68.00
0.020					34.00	66.00
0.010					38.00	62.00
0.005					40.00	60.00
0.002					53.00	47.00
0.001					54.00	46.00

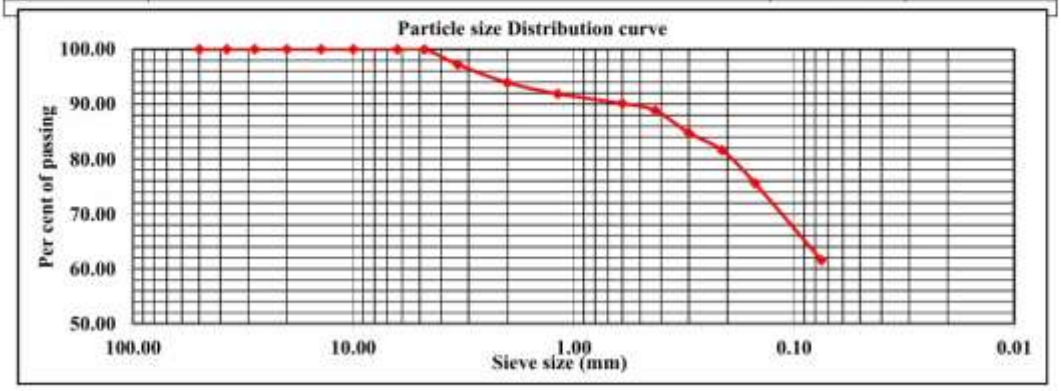

Note: 1.Material passes on 75 µm sieve size is greater than 10 % hydrometer method recommended.

Done by:

Eng.NIYIGENA Eric

Civil Engineering Laboratory
Determination of particles size distribution
Wet sieving method - tested in accordance with BS 1377-2:1990: Clause 9 (procedure 9.2.4)

Client: Student project(Eric:221028015)			**Sampling date:**09/01/2025
Project name: Climete Resilient Schools Project			**Testing date:**18-20/01/2025
Source of sample/Location: Pit-3			**Weight After washing (g)** 104.2
Initial weight (g):	351.4		
Ref: Test Civ_Lab_250108_002			**Retaining Wall N°:** 5

Sieve Size(mm)	Weight of empty sieve(g)	Weight of sieve +retained sample (g)	Partial Retained (g)	Cum Retained (g)	% Retained	% Of passing
50.000	1183.2	1183.2	0	0	0.00	100.00
37.500	1513.4	1513.4	0	0	0.00	100.00
28.000	1143.2	1143.2	0	0	0.00	100.00
20.000	1037.2	1037.2	0	0	0.00	100.00
14.000	1130.0	1130.0	0.0	0.0	0.00	100.00
10.000	1216.8	1216.8	0.0	0.0	0.00	100.00
6.300	1128.8	1128.8	0.0	0.0	0.00	100.00
4.750	1124.6	1124.6	0.0	0.0	0.00	100.00
3.350	417.0	417.4	0.4	0.4	0.11	99.89
2.000	529.0	532.8	3.8	4.2	1.20	98.80
1.180	527.4	530.0	2.6	6.8	1.94	98.06
0.600	513.2	512.2	-1.0	5.8	1.65	98.35
0.425	434.6	437.0	2.4	8.2	2.33	97.67
0.300	422.6	435.2	12.6	20.8	5.92	94.08
0.212	412.6	422.4	9.8	30.6	8.71	91.29
0.150	436.4	454.0	17.6	48.2	13.72	86.28
0.075	554	597.6	43.6	91.8	26.12	73.88
0.050					28.00	72.00
0.020					32.30	67.70
0.010					35.80	64.20
0.005					43.30	56.70
0.002					44.60	55.40
0.001					47.30	52.70

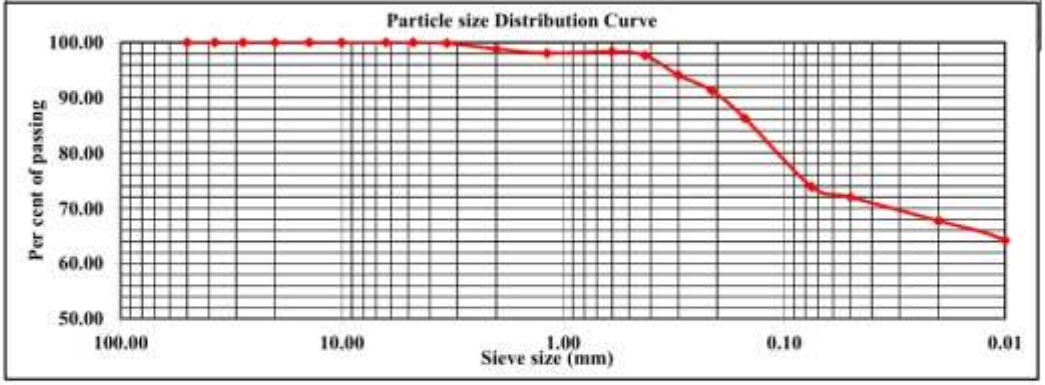

Note: 1.Material passes on 75 µm sieve size is greater than 10 % hydrometer method recommended.

Done by:

Eng.NIYIGENA Eric

APPENDIX-3 SHEAR TEST REULTS

RWANDA POLYTECHNIC

HUYE COLLEGE

DETERMINATION OF SHEAR STRENGTH BY DIRECT SHEAR (in the small shearbox apparatus)
Set of single stage tests - tested in accordance with BS 1377:1990:Part 7: Clause 4 (procedure 4.5.4)
TEST REPORT - SUMMARY

Project location	*Huye Nyamagabe Road*		
Project reference	*Eric (221028015)*	Sample depth (m)	*2.00*
Borehole number	*Pit-3*	Sample type	*Compacted cohesionless*
Sample number	*Slope stability analysis*	Specimen orientation	*Vertical*
Sample description	*UNDISTURBED SAMPLE*		

Particle density (Mg/m³)	*2.65 (Assumed)*	Specimens tested dry

INITIAL CONDITIONS	Specimen 1	Specimen 2	Specimen 3
Specimen depth (m)	*0.20*	*0.20*	*0.20*
Height (mm)	*20.0*	*20.0*	*20.0*
-			
Diameter (mm)	*60.0*	*60.0*	*60.0*
Area (mm²)	*2827.4*	*2827.4*	*2827.4*
Moisture content (measured) (%)	*26*	*26*	*26*
Moisture content (trimmings) (%)	*10*	*10*	*10*
Bulk density (Mg/m³)	*1.66*	*1.66*	*1.66*
Dry density (Mg/m³)	*1.32*	*1.32*	*1.32*
Voids ratio	*1.003*	*1.003*	*1.003*
Degree of saturation (%)	*68*	*68*	*68*

Voids ratio at the end of consolidation	*0.930*	*0.572*	*0.815*

SHEARING			
Rate of displacement (mm/min)	*0.600000*	*0.600000*	*0.600000*
Conditions at peak shear stress			
Normal stress (kPa)	*25*	*50*	*100*
Shear stress (kPa)	*35*	*50*	*87*
Horizontal displacement (mm)	*3.86*	*4.14*	*5.66*
Vertical deformation (mm)	*0.513*	*0.026*	*0.460*

Apparent cohesion (kPa)	*16.6*
Angle of shearing resistance (°)	*34.9*

Comments / variations from procedures:

Tested	*N.E & M.G*	Checked	*N.S*	Approved	*T.B*
Date	*24/01/2025*	Date	*24/01/2025*	Date	*24/01/2025*

DETERMINATION OF SHEAR STRENGTH BY DIRECT SHEAR (in the small shearbox apparatus)
Set of single stage tests - tested in accordance with BS 1377:1990:Part 7: Clause 4 (procedure 4.5.4)
TEST REPORT - SUMMARY

Project location	*Huye Nyamagabe Road*		
Project reference	*Eric (221028015)*	Sample depth (m)	*2.00*
Borehole number	*Pit-2*	Sample type	*Compacted cohesionless*
Sample number	*Slope stability analysis*	Specimen orientation	*Vertical*
Sample description	*UNDISTURBED SAMPLE*		
Particle density (Mg/m³)	*2.65 (Assumed)*		Specimens tested dry

INITIAL CONDITIONS	Specimen 1	Specimen 2	Specimen 3
Specimen depth (m)	*0.20*	*0.20*	*0.20*
Height (mm)	*20.0*	*20.0*	*20.0*
Diameter (mm)	*60.0*	*60.0*	*60.0*
Area (mm²)	*2827.4*	*2827.4*	*2827.4*
Moisture content (measured) (%)	*26*	*26*	*26*
Moisture content (trimmings) (%)	*10*	*10*	*10*
Bulk density (Mg/m³)	*1.66*	*1.66*	*1.66*
Dry density (Mg/m³)	*1.32*	*1.32*	*1.32*
Voids ratio	*1.003*	*1.003*	*1.003*
Degree of saturation (%)	*68*	*68*	*68*

Voids ratio at the end of consolidation	*0.930*	*0.572*	*0.815*

SHEARING			
Rate of displacement (mm/min)	*0.600000*	*0.600000*	*0.600000*
Conditions at peak shear stress			
Normal stress (kPa)	*25*	*50*	*100*
Shear stress (kPa)	*54*	*71*	*123*
Horizontal displacement (mm)	*12.30*	*11.03*	*8.91*
Vertical deformation (mm)	*-1.159*	*-0.722*	*-0.659*

Apparent cohesion (kPa)	*28.2*
Angle of shearing resistance (°)	*43.0*

Comments / variations from procedures:

Tested	*N.E & M.G*	Checked	*N.S*	Approved	*T.B*
Date	*24/01/2025*	Date	*24/01/2025*	Date	*24/01/2025*

DETERMINATION OF SHEAR STRENGTH BY DIRECT SHEAR (in the small shearbox apparatus)
Set of single stage tests - tested in accordance with BS 1377:1990:Part 7: Clause 4 (procedure 4.5.4)
TEST REPORT - SUMMARY

Project location	*Huye Nyamagabe Road*		
Project reference	*Eric (221028015)*	Sample depth (m)	*2.00*
Borehole number	*Pit-1*	Sample type	*Compacted cohesionless*
Sample number	*Slope stability analysis*	Specimen orientation	*Vertical*
Sample description	*UNDISTURBED SAMPLE*		
Particle density (Mg/m³)	*2.65 (Assumed)*		Specimens tested dry

INITIAL CONDITIONS	Specimen 1	Specimen 2	Specimen 3
Specimen depth (m)	*0.20*	*0.20*	*0.20*
Height (mm)	*20.0*	*20.0*	*20.0*
Diameter (mm)	*60.0*	*60.0*	*60.0*
Area (mm²)	*2827.4*	*2827.4*	*2827.4*
Moisture content (measured) (%)	*26*	*26*	*26*
Moisture content (trimmings) (%)	*12*	*12*	*12*
Bulk density (Mg/m³)	*1.68*	*1.68*	*1.68*
Dry density (Mg/m³)	*1.34*	*1.34*	*1.34*
Voids ratio	*0.982*	*0.982*	*0.982*
Degree of saturation (%)	*69*	*69*	*69*

Voids ratio at the end of consolidation	*0.910*	*0.594*	*0.860*

SHEARING			
Rate of displacement (mm/min)	*0.600000*	*0.600000*	*0.600000*
Conditions at peak shear stress			
Normal stress (kPa)	*25*	*50*	*100*
Shear stress (kPa)	*35*	*50*	*87*
Horizontal displacement (mm)	*3.86*	*4.14*	*5.66*
Vertical deformation (mm)	*0.513*	*0.026*	*0.460*

Apparent cohesion (kPa)	*15.4*
Angle of shearing resistance (°)	*35.5*

Comments / variations from procedures:

Tested	*N.E & M.G*	Checked	*N.S*	Approved	*T.B*
Date	*24/01/2025*	Date	*24/01/2025*	Date	*24/01/2025*

APPENDIX-4 NATURE MOISTURE CONTENT RESULTS

RWANDA POLYTECHNIC

HUYE COLLEGE

CIVL ENGINEERING LABORATORY
DETERMINATION OF NATURE MOISTURE CONTENT
TEST METHOD: TESTED IN ACCORDING TO BS 812-109:1990

Project	Slope stability analysis
Client	Student project(Eric:221028015)
Source of sample/ Depth(m)	TP3
Sample date	26/03/2024
Sample description	N/A
Test date	28/03/2024

REF: Test Civil Lab_22122_004

SAMPLE NAME	S1	S2	S3
can N°	**R**	**TT**	**KK**
Weight of Tray (g)	912.2	752.2	710.6
Wet Weight + Tray (g)	1276.6	1477.8	1450.6
Dry Weight + Tray (g)	1186.5	1314.4	1266.7
Weight of Water (g)	90.1	163.4	183.9
Weight of wet soil (g)	364.4	725.6	740.0
Weight of Dry Soil (g)	274.3	562.2	556.1
Moisture Content (%)	32.85	29.06	33.07
AVERAGE Moisture Content(%)	**31.66**		

Operated by:

Eng.NIYIGENA Eric

Laboratory Technician

RWANDA POLYTECHNIC

HUYE COLLEGE

CIVL ENGINEERING LABORATORY
DETERMINATION OF NATURE MOISTURE CONTENT
TEST METHOD: TESTED IN ACCORDING TO BS 812-109:1990

Project	Slope stability analysis
Client	Student project(Eric:221028015)
Source of sample/ Depth(m)	TP1
Sample date	26/03/2024
Sample description	N/A
Test date	28/03/2024

REF: Test Civil Lab_22122_004

SAMPLE NAME	S1	S2	S3
can N°	**R**	**TT**	**KK**
Weight of Tray (g)	903.2	741.6	740.2
Wet Weight + Tray (g)	1255.8	1465.2	1409.8
Dry Weight + Tray (g)	1174.5	1322.6	1290.4
Weight of Water (g)	81.3	142.6	119.4
Weight of wet soil (g)	352.6	723.6	669.6
Weight of Dry Soil (g)	271.3	581	550.2
Moisture Content (%)	29.97	24.54	21.70
AVERAGE Moisture Content(%)	**25.40**		

Operated by:

Eng.NIYIGENA Eric

Laboratory Technician

RWANDA POLYTECHNIC

HUYE COLLEGE

CIVL ENGINEERING LABORATORY

DETERMINATION OF NATURE MOISTURE CONTENT

TEST METHOD: TESTED IN ACCORDING TO BS 812-109:1990

Project	Slope stability analysis
Client	Student project(Eric:221028015)
Source of sample/ Depth(m)	TP1
Sample date	26/03/2024
Sample description	N/A
Test date	28/03/2024

REF: Test Civil Lab_22122_004

SAMPLE NAME	S1	S2	S3
can N°	**23**	**EE**	**E5**
Weight of Tray (g)	912.2	752.2	710.6
Wet Weight + Tray (g)	1280.6	1456.2	1445
Dry Weight + Tray (g)	1209.6	1322.6	1290.4
Weight of Water (g)	71	133.6	154.6
Weight of wet soil (g)	368.4	704	734.4
Weight of Dry Soil (g)	297.4	570.4	579.8
Moisture Content (%)	23.87	23.42	26.66
AVERAGE Moisture Content(%)	**24.65**		

Operated by:

Eng.NIYIGENA Eric

Laboratory Technician

APPENDIX-5 SLIDED SIDE PHOTOS FILLED MATERAIL WAS TAKEN

APPENDIX-6 SEISMIC ANALYSIS ANALYSED TABLES

Process of Scaling Seismic Acceleration Time History

To perform dynamic seismic analysis in MIDAS GTS NX, an acceleration time history representing ground shaking is required. Typically, this input is provided in a normalized form, where the maximum acceleration is scaled to 1g. This normalization allows for easy scaling to any desired Peak Ground Acceleration (PGA).

Step 1: Normalize the Original Acceleration Time History

Given an original acceleration time history, each value is divided by the maximum absolute value to obtain the normalized acceleration. This ensures that the peak of the acceleration time series equals 1g.

Formula:

abnormalized(t) = a_original(t) / max(|a_original(t)|)

Step 2: Scale the Normalized Time History to Desired PGA

Once the normalized acceleration data is obtained, it is scaled to the target PGA by multiplying each normalized value by the desired PGA.

Formula:

a scaled(t) = PGA_target × a_normalized(t)

Where:

- a_scaled(t): Scaled acceleration at time t (in g)
- PGA_target: Target Peak Ground Acceleration (e.g., 0.10g, 0.16g, 0.20g)
- a_normalized(t): Normalized acceleration value at time t (unitless)

PGA:0.2g			PGA:0.1g			PGA:0.16g	
Time (sec)	Value (g)		Time (sec)	Value (g)		Time (sec)	Value (g)
0	0		0	0		0	0
0.01	0.059977		0.01	0.029988		0.01	0.047981
0.02	0.110711		0.02	0.055356		0.02	0.088569
0.03	0.147877		0.03	0.073939		0.03	0.118302
0.04	0.168702		0.04	0.084351		0.04	0.134962
0.05	0.172142		0.05	0.086071		0.05	0.137713
0.06	0.158878		0.06	0.079439		0.06	0.127102
0.07	0.131155		0.07	0.065578		0.07	0.104924
0.08	0.092474		0.08	0.046237		0.08	0.073979
0.09	0.047179		0.09	0.02359		0.09	0.037744
0.1	1.81E-17		0.1	9.06E-18		0.1	1.45E-17
0.11	-0.04443		0.11	-0.02222		0.11	-0.03555
0.12	-0.08202		0.12	-0.04101		0.12	-0.06561
0.13	-0.10955		0.13	-0.05478		0.13	-0.08764
0.14	-0.12498		0.14	-0.06249		0.14	-0.09998
0.15	-0.12753		0.15	-0.06376		0.15	-0.10202
0.16	-0.1177		0.16	-0.05885		0.16	-0.09416
0.17	-0.09716		0.17	-0.04858		0.17	-0.07773
0.18	-0.06851		0.18	-0.03425		0.18	-0.0548

0.19	-0.03495		0.19	-0.01748		0.19	-0.02796
0.2	-2.69E-17		0.2	-1.34E-17		0.2	-2.15E-17
0.21	0.032916		0.21	0.016458		0.21	0.026333
0.22	0.06076		0.22	0.03038		0.22	0.048608
0.23	0.081157		0.23	0.040578		0.23	0.064925
0.24	0.092586		0.24	0.046293		0.24	0.074069
0.25	0.094473		0.25	0.047237		0.25	0.075579
0.26	0.087194		0.26	0.043597		0.26	0.069755
0.27	0.07198		0.27	0.03599		0.27	0.057584
0.28	0.050751		0.28	0.025375		0.28	0.0406
0.29	0.025893		0.29	0.012946		0.29	0.020714
0.3	2.99E-17		0.3	1.49E-17		0.3	2.39E-17
0.31	-0.02438		0.31	-0.01219		0.31	-0.01951
0.32	-0.04501		0.32	-0.02251		0.32	-0.03601
0.33	-0.06012		0.33	-0.03006		0.33	-0.0481
0.34	-0.06859		0.34	-0.03429		0.34	-0.05487
0.35	-0.06999		0.35	-0.03499		0.35	-0.05599
0.36	-0.06459		0.36	-0.0323		0.36	-0.05168
0.37	-0.05332		0.37	-0.02666		0.37	-0.04266
0.38	-0.0376		0.38	-0.0188		0.38	-0.03008
0.39	-0.01918		0.39	-0.00959		0.39	-0.01535
0.4	-2.95E-17		0.4	-1.48E-17		0.4	-2.36E-17
0.41	0.018065		0.41	0.009032		0.41	0.014452
0.42	0.033346		0.42	0.016673		0.42	0.026676
0.43	0.04454		0.43	0.02227		0.43	0.035632
0.44	0.050812		0.44	0.025406		0.44	0.04065
0.45	0.051848		0.45	0.025924		0.45	0.041478
0.46	0.047853		0.46	0.023927		0.46	0.038282
0.47	0.039503		0.47	0.019752		0.47	0.031603

0.48	0.027853		0.48	0.013926		0.48	0.022282
0.49	0.01421		0.49	0.007105		0.49	0.011368
0.5	2.74E-17		0.5	1.37E-17		0.5	2.19E-17
0.51	-0.01338		0.51	-0.00669		0.51	-0.01071
0.52	-0.0247		0.52	-0.01235		0.52	-0.01976
0.53	-0.033		0.53	-0.0165		0.53	-0.0264
0.54	-0.03764		0.54	-0.01882		0.54	-0.03011
0.55	-0.03841		0.55	-0.0192		0.55	-0.03073
0.56	-0.03545		0.56	-0.01773		0.56	-0.02836
0.57	-0.02926		0.57	-0.01463		0.57	-0.02341
0.58	-0.02063		0.58	-0.01032		0.58	-0.01651
0.59	-0.01053		0.59	-0.00526		0.59	-0.00842
0.6	-2.43E-17		0.6	-1.21E-17		0.6	-1.94E-17
0.61	0.009914		0.61	0.004957		0.61	0.007931
0.62	0.0183		0.62	0.00915		0.62	0.01464
0.63	0.024444		0.63	0.012222		0.63	0.019555
0.64	0.027886		0.64	0.013943		0.64	0.022309
0.65	0.028455		0.65	0.014227		0.65	0.022764
0.66	0.026262		0.66	0.013131		0.66	0.02101
0.67	0.02168		0.67	0.01084		0.67	0.017344
0.68	0.015286		0.68	0.007643		0.68	0.012229
0.69	0.007799		0.69	0.003899		0.69	0.006239
0.7	-6.60E-17		0.7	-3.30E-17		0.7	-5.28E-17
0.71	-0.00734		0.71	-0.00367		0.71	-0.00588
0.72	-0.01356		0.72	-0.00678		0.72	-0.01085
0.73	-0.01811		0.73	-0.00905		0.73	-0.01449
0.74	-0.02066		0.74	-0.01033		0.74	-0.01653
0.75	-0.02108		0.75	-0.01054		0.75	-0.01686
0.76	-0.01946		0.76	-0.00973		0.76	-0.01556

0.77	-0.01606		0.77	-0.00803		0.77	-0.01285
0.78	-0.01132		0.78	-0.00566		0.78	-0.00906
0.79	-0.00578		0.79	-0.00289		0.79	-0.00462
0.8	-1.78E-17		0.8	-8.88E-18		0.8	-1.42E-17
0.81	0.005441		0.81	0.00272		0.81	0.004353
0.82	0.010043		0.82	0.005022		0.82	0.008035
0.83	0.013415		0.83	0.006708		0.83	0.010732
0.84	0.015304		0.84	0.007652		0.84	0.012243
0.85	0.015616		0.85	0.007808		0.85	0.012493
0.86	0.014413		0.86	0.007207		0.86	0.01153
0.87	0.011898		0.87	0.005949		0.87	0.009519
0.88	0.008389		0.88	0.004195		0.88	0.006711
0.89	0.00428		0.89	0.00214		0.89	0.003424
0.9	1.49E-17		0.9	7.44E-18		0.9	1.19E-17
0.91	-0.00403		0.91	-0.00202		0.91	-0.00322
0.92	-0.00744		0.92	-0.00372		0.92	-0.00595
0.93	-0.00994		0.93	-0.00497		0.93	-0.00795
0.94	-0.01134		0.94	-0.00567		0.94	-0.00907
0.95	-0.01157		0.95	-0.00578		0.95	-0.00926
0.96	-0.01068		0.96	-0.00534		0.96	-0.00854
0.97	-0.00881		0.97	-0.00441		0.97	-0.00705
0.98	-0.00621		0.98	-0.00311		0.98	-0.00497
0.99	-0.00317		0.99	-0.00159		0.99	-0.00254
1	-1.22E-17		1	-6.10E-18		1	-9.76E-18